UNIVERSITÀ DEGLI STUDI DEL MOLISE

NEUROMED I.R.C.C.S. ISTITUTO NEUROLOGICO MEDITERRANEO

PHD IN TRANSLATIONAL AND CLINICAL MEDICINE

XXXII° CYCLE

SCIENTIFIC DISCIPLINARY SECTOR: MED/50 SCIENZE TECNICHE MEDICHE APPLICATE

CARBON NANOTUBE BASED MICROELECTRODE ARRAYS FOR LONG-TERM ELECTROCORTICOGRAPHIC RECORDINGS

Phd Candidate:

Luigi PAVONE

Supervisor: Chiar.mo Prof.

Daniela CARNEVALE

PhD Coordinator: Chiar.mo

Prof. Marco Sarchiapone

DOTTORATO IN MEDICINA TRASLAZIONALE E CLINICA

XXXII° CICLO

SETTORE SCIENTIFICO DISCIPLINARE: MED/50 SCIENZE TECNICHE MEDICHE APPLICATE

GRIGLIE DI ELETTRODI IN NANOTUBI DI CARBONIO PER REGISTRAZIONI ELETTROCORTICOGRAFICHE A LUNGO TERMINE

Phd Candidate:

Luigi PAVONE

Supervisor: Chiar.mo Prof.

Daniela CARNEVALE

PhD Coordinator: Chiar.mo

Prof. Marco Sarchiapone

A mio padre Nicolino

Acknowledgements.

I would like to thank first Prof. Slavianka Moyanova, who shared with me most of the activity and the experiments carried out during my PhD project, for her valuable scientific support.

I would like to thank my supervisor, Prof. Daniela Carnevale, and all my colleagues in Neuromed, where this project was realized, I would also like to thank my colleagues from ENEA – Centro Ricerche Casaccia and from the NAST Centre of Tor Vergata University for the productive collaboration.

Finally, I would like to thank my girlfriend Eva, my mother Giuliana and my family for their support and their love.

Ringraziamenti

Ringrazio innanzitutto la Prof.ssa Slavianka Moyanova, con cui ho condiviso gran parte delle attività e gli esperimenti che hanno portato alla redazione di questo lavoro di tesi, per il suo prezioso lavoro di supporto e coordinamento scientifico.

Ringrazio il mio relatore, la Prof.ssa Daniela Carnevale, e tutti i colleghi dell'IRCCS Neuromed, dove questo progetto è stato realizzato, i colleghi dell'ENEA Centro Ricerche Casaccia e del centro NAST dell'Università di Tor Vergata per la proficua collaborazione.

Ringrazio la mia fidanzata Eva, mia mamma Giuliana e la mia famiglia per la loro vicinanza e il loro supporto.

ABSTRACT (English)

The development of array of electrodes able to safely record brain electrical activity, with no side effects for the patient, is a critical issue in the developing of brain computer interface (BCI) devices and in long-term recordings. Commercially available electrode arrays commonly used in a clinical setting have some limitations which limited their use in chronic applications and therefore for prolonged time intervals. In particular, such grids have inappropriate long-term electrical stability, poor biocompatibility with brain tissue and inadequate flexibility to accurately adhere with brain surface, which is irregular and curvilinear. The availability of sensors able to overcome these limitations could offer very interesting opportunities for the developing of BCI devices to help patients with severe neurodegenerative diseases, in particular to restore functions irremediably compromised by the disease itself. In the last decades, many studies have been performed and many are the technologies that have been proposed for this purpose, but without achieving resounding success. Aiming at developing simple technologies for the developing of flexible and stretchable electronic devices, elementary bidimensional circuitry made of single wall carbon nanotube (SWCNT) based conductors, self-grafted on different polymer films, could represent a very promising alternative for the developing of reliable neural interfaces for BCI applications. This study reports in-vivo and ex-vivo characterization of new electrode arrays made of single-walled carbon nanotubes (SWCNT) embedded in medium-density polyethylene (MD-PE) films. In particular, the long-term electrical stability, the flexibility and the biocompatibility of these electrodes have been evaluated in a chronic setting.

The long-term electrical stability was evaluated through impedance measurement, the analysis of ElectroCorticoGraphic (ECoG) recorded in laboratory rats for a period of two months in an in-vivo experimental setting and the analysis of evoked synaptic potentials recorded in an ex-vivo experimental setting. The flexibility was evaluated through the comparison between ECoGs recorded from electrodes placed in the dorsal cortex with those recorded from electrodes placed in the lateral cortex and also through the mechanical characterization of the device. Finally, the biocompatibility was evaluated through the analysis of the immunohistochemical and histological profile of brain tissue after the explantation of the devices. The performance of the SWCNT-based grids have been compared with that of a similar grid having the same geometry and the same MD-PE film, but with electrodes made by platinum (Pt), which is one of the most used metal for electrodes in clinical practice. The SWCNT grids showed better performance compared with Pt grids, mainly for the immunohistochemical and histological profile and for the flexibility and stretchability properties. Furthermore, SWCNT grids provided good results in the recording of reliable evoked synaptic local field potentials in the ex-vivo experiments. The results demonstrate that the SWCNT grids embedded in MD-PE are suitable for manufacturing flexible devices for subdural ECoG recording and are promising candidates for long-term neural implants for epilepsy monitoring or neuroprosthetic BCI.

ABSTRACT (Italian)

Lo sviluppo di griglie di elettrodi in grado di registrare l'attività elettrica cerebrale in modo sicuro, senza indurre complicanze al paziente, rappresenta un punto cruciale nella creazione di dispositivi per applicazioni di brain computer interface (BCI) e nelle registrazioni a lungo termine. Le griglie di elettrodi disponibili in commercio comunemente usate per questi scopi presentano dei limiti che non ne consentono l'utilizzo in cronico, per intervalli temporali molto lunghi. In particolare, queste griglie hanno una stabilità elettrica a lungo termine insoddisfacente, sono caratterizzate da un basso livello di biocompatibilità con il tessuto cerebrale e non sono adeguatamente flessibili ed in grado di conformarsi perfettamente con la superficie cerebrale, caratterizzata da una superficie irregolare e curvilinea. La possibilità di disporre di sensoristica in grado di superare queste limitazioni, potrebbe offrire della prospettive molto interessanti per lo sviluppo di dispositivi di BCI per l'ausilio di pazienti affetti da gravi patologie neurodegenerative, in particolare per il ripristino di funzioni irrimediabilmente compromesse a seguito della patologia. Negli ultimi decenni, molti sono stati gli studi e le tecnologie proposte in tal senso, ma con modesto successo. In particolare, nell'ottica di sviluppare tecnologie semplici per la creazione di dispositivi elettronici flessibili ed estensibili, la realizzazione di circuiti bidimensionali a bassa complessità costituiti da conduttori basati su nano tubi di carbonio a parete singola (SWCNT) potrebbe rappresentare una linea di sviluppo molto promettente per la realizzazione di interfacce neurali affidabili per applicazioni di BCI. Questo lavoro presenta una caratterizzazione in-vivo ed ex-vivo di una griglia di elettrodi in SWCNT su film in

polietilene a media densità (MD-PE). In particolare, di queste griglie sono state analizzate la stabilità elettrica a lungo termine, la flessibilità e la biocompatibilità in in cronico. La stabilità elettrica a lungo termine è stata valutata mediante l'analisi delle impedenze degli elettrodi, l'analisi del segnale ElettroCorticoGrafico (ECoG) registrato per un periodo di due mesi durante gli esperimenti in-vivo su ratti da laboratorio e l'analisi dei potenziali evocati sinaptici registrati durante gli esperimento ex-vivo. La flessibilità è stata analizzata attraverso la comparazione dei segnali ECoG registrati dagli elettrodi posizionati sulla parte dorsale della corteccia e di quelli registrati dagli elettrodi posizionati sulla parte laterale della corteccia negli esperimenti in-vivo ed anche attraverso la caratterizzazione meccanica del dispositivo. Infine, la biocompatibilità è stata valutata attraverso analisi del profilo immuno-istochimico ed istologico del tessuto cerebrale post-mortem. Le prestazioni delle griglie sono state confrontate con quelle di griglie simili, aventi la stessa geometria, ma con elettrodi in Platino (Pt), uno dei metalli più utilizzati per la fabbricazione della maggior parte delle griglie di elettrodi presenti in commercio ed utilizzate nella pratica clinica. Le griglie SWCNT hanno mostrato delle perfomance migliori rispetto a quelle Pt, soprattutto in termini di profilo immuno-istochimico, istologico, e dal punto di vista della flessibilità e dell'estensibilità. Infine, gli elettrodi SWCNT hanno mostrato ottimi risultati nella registrazione di potenziali evocati sinaptici in setting ex-vivo. I risultati ottenuti mostrano come griglie SWCNT in film MD-PE possono essere utilizzati con ottimi risultati per lo sviluppo di dispositivi flessibili per la registrazione di segnali ECoG e potrebbero rappresentare un candidato ideale per lo sviluppo di interfacce neurali per applicazioni di neuroprotesica e BCI.

SUMMARY

LIST OF ACRONYMS

SWCNT: single walled carbon nanotube

ECoG: electrocorticogram/electrocorticography

BCI: brain computer interface

MD-PE: medium density polyethylene

MEAs : microelectrodes arrays

fMRI: functional Magnetic Resonance Imaging

rs-fMRI: resting-state fMRI

BOLD: blood oxygenation level dependent

RSNs: resting state networks

PET: positron emission tomography

fNIRS: functional near-infrared spectroscopy

oxy-Hb: oxyhemoglobine

deoxy-Hb: deoxyhemoglobine

EEG: electroencephalogram

EMG: electromyography

EOG: electrooculography

AP: action potential

MUA: multiunit activity

LFP: local field potential

MEG: magnetoencephalography

μECoG: micro-electrocorticogram

MEMS: microelectromechanical systems

SEM: scanning electron microscope

PEGPCL: poly(ethylene glycol)-poly(ε-caprolactone)

EFM: electrospun fiber mat

PCL: poly(ε-caprolactone)

LCD: liquid crystal displays

AMOLED: active-matrix organic light-emitting diodes

CES: cortical electrical stimulation

ITO: indium tin oxide

SIROF: sputtered iridium oxide film

FBR: foreign body response

CNS: central nervous system

GFAP: glial fibrillary acidic protein

iba1: ionized calcium-binding adapter molecule 1

SWDs: spike and wave discharges

WAG/Rij: Wistar Albino Glaxo from Rijswijk

MRI: Magnetic Resonance Imaging

SNR: signal to noise ratio

MWCNT: multi walled carbon nanotube

HiPco: high-pressure carbon monoxide

FEGSEM: field emission gun scanning electron microscopy

HD-PE: high-density poly-ethylene

PVC: poly-vinyl chloride

Video-EEG: video electroencephalography

ECG: electrocardiogram

PW: passive waking

SWS: slow wave sleep

REM: rapid eye movement

PLA: pulsed laser ablation

PLD: pulsed laser deposition

PA: poly-amide

FFT: fast Fourier transformation

CWT: continuous wavelet transform

PSD: power spectral density

Neun: neuronal nuclei

HFI : high frequency stimulation

TTX: tetrodotoxin

LIST OF FIGURES

CHAPTER 1

INTRODUCTION

1.1 THE SOURCE OF BRAIN ELECTRICAL ACTIVITY

The brain is the main organ of the central nervous system and neurons are its core components. Brain functions depend on the ability of neurons to transmit electrochemical signals to other cells, and to respond appropriately to electrochemical signals received from them. The electrical activity of neurons is modulated by different metabolic and biochemical processes, in particular by the interactions between neurotransmitters and receptors that take place at synapses [1]. A neuron is constituted by a cell body, the so called "soma", dendrites, and an axon (Figure 1). Dendrites are membranous tree-like projections arising from the body of the neuron, about 5–7 per neuron on average, and about 2μm in length [2] and represent the entry site of neural signals into neurons. The axon of a neuron arises from the cell body and extends to the region or regions of synaptic contact. Axons are specialized processes that are characterized by having an excitable membrane, a membrane that is capable of generating or propagating an action potential [3], so an axon can be intended as the transmission cable of electrical impulses from a neuron to another.

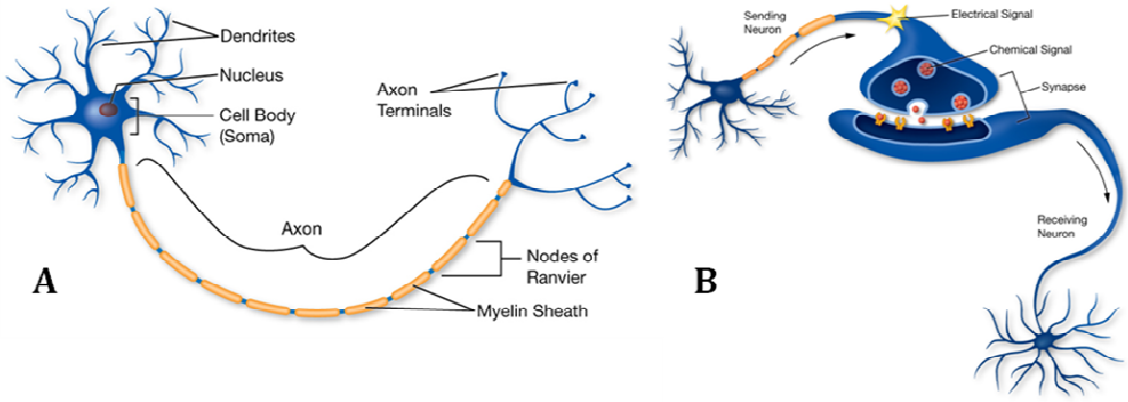

Figure 1: Structure of neuron (A) and of a synaptic connection (B). Figure taken from [4]

Neurons communicate by sending chemicals, called neurotransmitters, across the synaptic connections, between the axons and dendrites of adjacent neurons.

Neurons do not work in isolation, but they are organized into ensembles, called neural circuits, that process specific kinds of information. Such circuits are constituted by three functional classes of neurons: afferent neurons (which carry information from the periphery toward the brain or spinal cord), efferent neurons (which carry information away from the brain or spinal cord) and inter-neurons (which possess short axons and only participate in local aspects). The generation and the propagation of the electrical signals in neurons were very well mathematically explained in a pioneering work of Hodgkin and Huxley [5-7]. Neurons encode and transfer several types of different electrical signals. When they are at rest, they are able to generate a constant little voltage (from 40 to 90 mV) across their membranes, called the resting membrane potential, which vary based on the type of neuron. Neurons generate electrical signals in response of stimuli which produce a change in resting membrane potential. Activation of synapses generates synaptic potentials, which allow the transmission of information from one neuron to another. Although neurons and axons are capable of passively conducting electricity, their electrical properties are extremely poor. Despite these limitations, neurons are able to spread electrical signals over great distances, through the generation of electrical signals, called action potentials (also referred to as "spikes" or "impulses"). An action potential is the way through which a neuron transports electrical signals and consists of a change in the voltage across the membrane due to the flow of ions into and out of the neuron (Figure 2). The neuron with the resting potential difference is said to be polarized. When a passive current flows across the membrane, it

induces a depolarization. If the depolarized membrane potential passes a threshold (about -48 mV), the membrane potential is highly depolarized to generate a positive peak (spike). The intensity of the signal is determined by the number of action potentials generated per unit time, the so called firing rate. The polarization is followed by a repolarization process. The membrane potential drops quickly from the positive peak to a negative level, even lower than the resting potential. This phase is called hyperpolarization. After a few milliseconds the membrane potential returns to its resting level. During the time following the repolarization phase of the action potential, the voltage-gated Na+ channels are inactivated and unable to be opened, regardless of how much the membrane is depolarized. This is the absolute refractory period, which is followed by a short relative refractory period during which action potential can be generated but only with larger-than-normal depolarization. This limited rate of action potential generation determines the neurons frequency resolution. One way to elicit an action potential is to pass an electrical current across the membrane of the neuron. As we said before, passive current across the membrane caused by a synaptic or receptor stimulation does not travel far because the depolarization declines with distance, due to the leakage through the transmembrane ion channels. However, if this initial depolarization is strong enough to pass the threshold, an action potential will be triggered (usually initiated at the interface between the cell body and axon), which travel down the axon to depolarize new pieces of membrane to continue the process. The sequentially triggered action potentials relay the neuronal signal from the synapse or the receptor along the axon to its terminators, where the signal is passed on to other neurons.

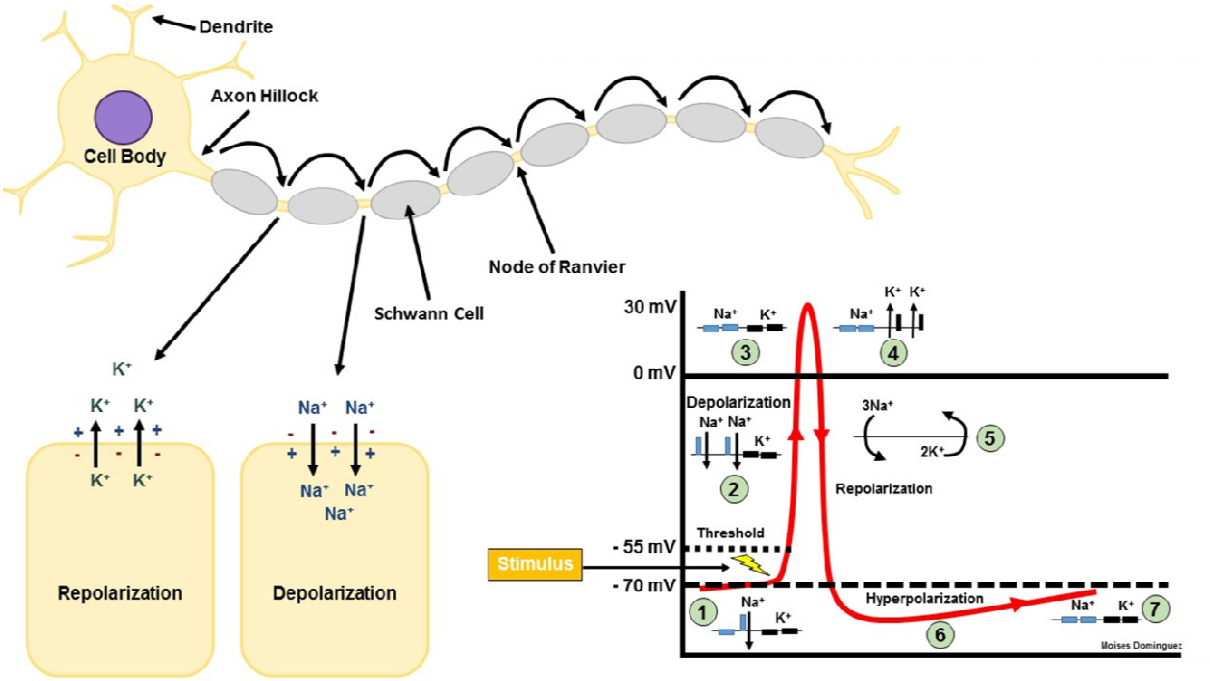

Figure 2: Mechanism of action potentials propagation in the neuron (from [8])

1.2 BRAIN SIGNALS RECORDING TECHNIQUES

The physiological mechanisms underlying brain electrical activity and the functional mapping of the brain can be obtained with electrophysiological recordings. They are usually grouped by two distinct approaches: invasive and non-invasive. The first category can be divided into intracellular, where sharp or patch electrodes positioned inside the cell are used, and extracellular recordings where microelectrodes arrays (MEAs) positioned near the cell of interest are used. However, it is important to point out the fact that the term "invasive", even though commonly used for these devices, possesses an inherent negative undertone. Nonetheless, many are of the opinion that even the so-called non-invasive procedures, can induce a so strong awkwardness, due to the process for fixing the electrode on the scalp or the long learning/calibration time, to be considered as much invasive as a surgery. In the next subparagraphs are listed most of the existing recording techniques, both invasive and non invasive.

1.2.1 FUNCTIONAL MAGNETIC RESONANCE IMAGING

Functional Magnetic Resonance Imaging (fMRI) is a neuroimaging method which allows to analyze regional, time-varying changes in brain metabolism [9-11]. These metabolic

changes can be induced by the execution of a specific motor or cognitive task or as a result of a stimulus (*task-related fMRI*) or the result of uncontrolled processes in the brain at rest, acquired in the absence of a stimulus or a task (*resting-state fMRI, rs-fMRI*). fMRI is widely used for its widespread availability, non-invasive nature (does not require injection of a radioisotope or other pharmacologic agent), and good spatial resolution. On the contrary, it has low temporal resolution (BOLD signal is slow), it is very expensive and technically complex.

fMRI measures the BOLD (Blood Oxygenation Level Dependent) response by tracking the changes in the blood flow indicated by the relative amounts of the different forms of hemoglobin. In particular, when a brain region's metabolic activity increase, its oxygen consumption increases and, to meet this increased demand, blood flow increases to the active area. fMRI can be used to produce activation maps showing which parts of the brain are involved in a certain process. In task-related fMRI, activation maps are produced by comparing BOLD level contrast between active periods, when the subject is performing a task or is receiving a particular stimulus, and rest periods (Figure 3). Rs-fMRI focuses on spontaneous, low frequency fluctuations (<0.1 Hz) in the BOLD signal. Application of this technique has allowed for the identification of various resting state networks (RSNs), or spatially distinct areas of the brain that demonstrate synchronous BOLD fluctuations at rest. This technique is based on the measurement of the correlation between the BOLD time course of a seed region (or a single voxel) and that of all other areas in the brain.

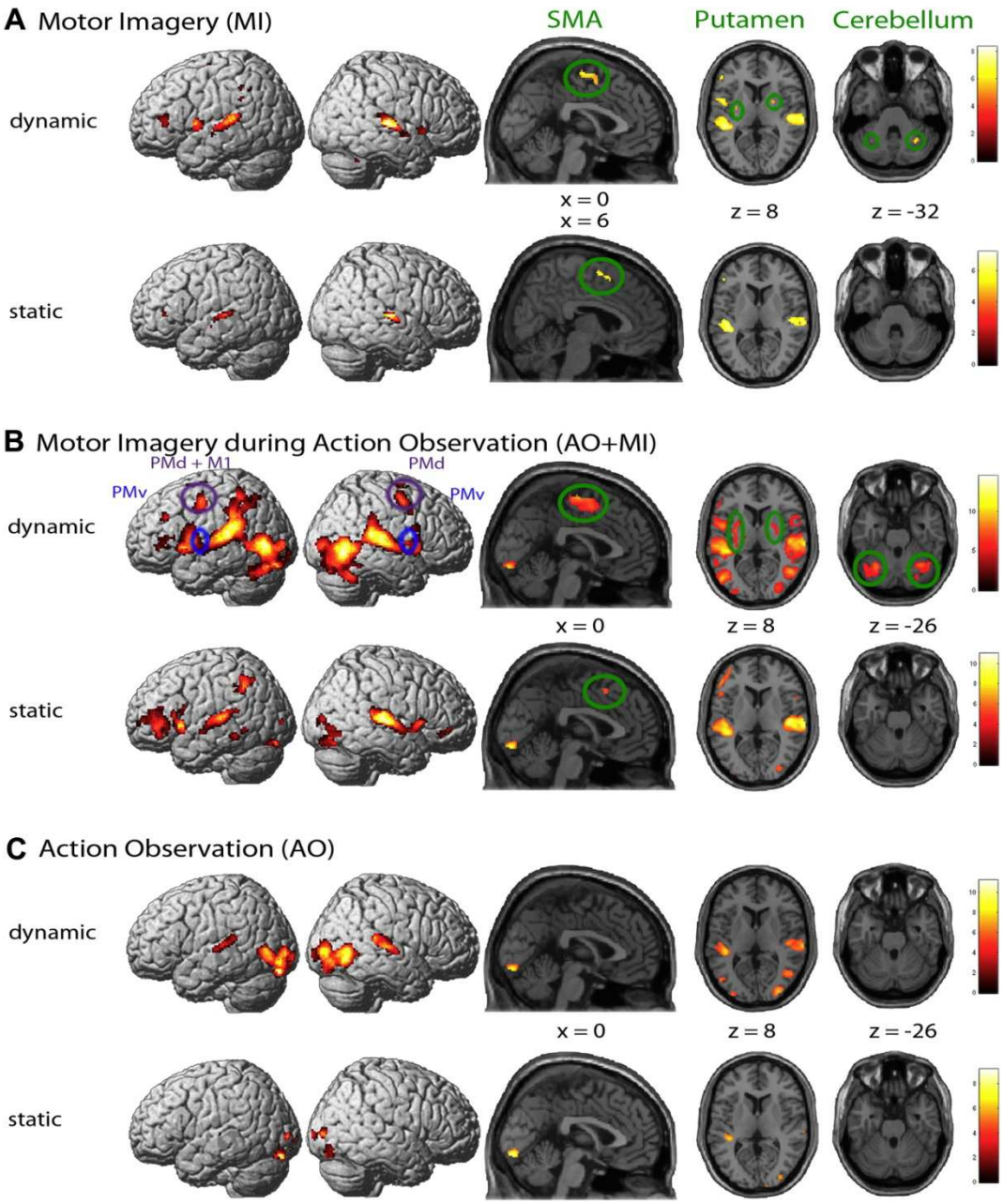

Figure 3: Example of task-related fMRI analysis (from [13]). The colored spots on the images represent the regions activated by the task specified in the title of the subgraphs A,B,C. The color bar indicates the intensity of the activation.

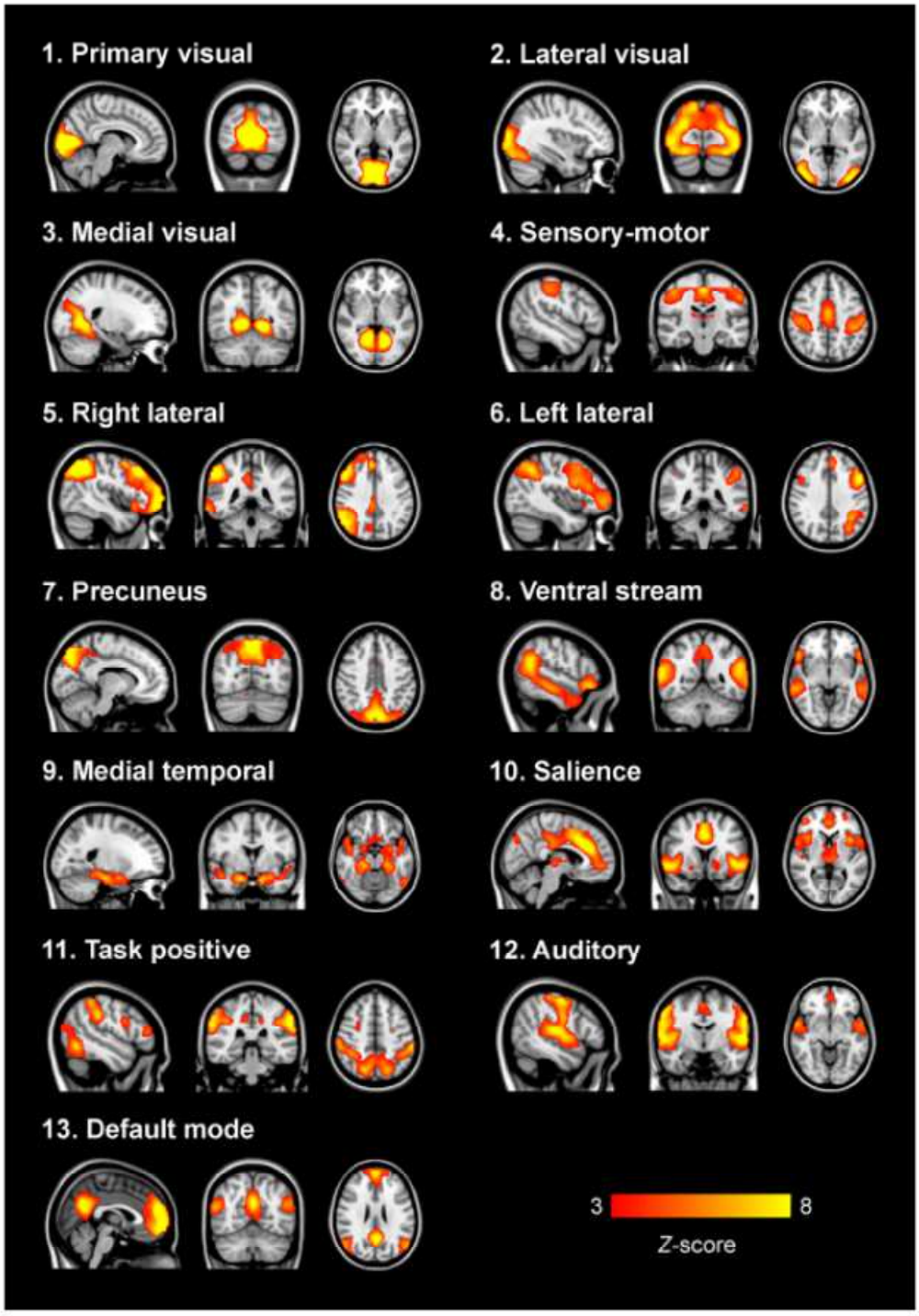

Figure 4: The most relevant RSNs. The left hemisphere of the brain corresponds to the right side in this image. (from [14])

1.2.2 POSITRON EMISSION TOMOGRAPHY

Positron Emission Tomography (PET) can produce images of chemical processes [15] and can also produce images of metabolic processes by detecting changes in blood flow [16]. Although PET is very slow in imaging chemical processes (i.e., requiring tens of minutes), it is substantially faster in imaging blood flow (i.e., <1 min). PET requires the injection of radioactive isotopes used have short half-lives and are administered at doses small enough to preclude harmful biological effects. After injection of the marker, the PET scanner starts to collect images by measuring radiation with a ring of detectors in the scanner. Whenever a radioactive atom releases a positron that collides with an electron in the immediate surroundings, the two particles annihilate each other and emit two gamma photons traveling in opposite directions. These gamma photons then hit blocks made of crystals, the scintillators, that surround the subject's head in the scanner. As the photons impinge on scintillators, a brief flash of light occurs and it is detected by high-performance optical cameras arranged directly outside the crystals.. From detections of thousands of such hits, the sources of emission from the brain can then be reconstructed. The image constructed by the PET scanner displays the density distribution of the radioactive tracers in the brain (Figure 5). When a brain region is active and blood flow in that region increases, more radioactive water enters the brain tissue, and the PET cameras detect the radioactivity to create a brain image. Temporal resolution for PET is quite low, since it requires at least 40 s to collect enough information to construct one single image. Spatial resolution is about 5 mm. A PET scanner is also expensive because it is necessary to have a cyclotron in the immediate vicinity. The expense of the cycloctron and the need for injection of radioactively labeled compounds are significant disadvantages of this method.

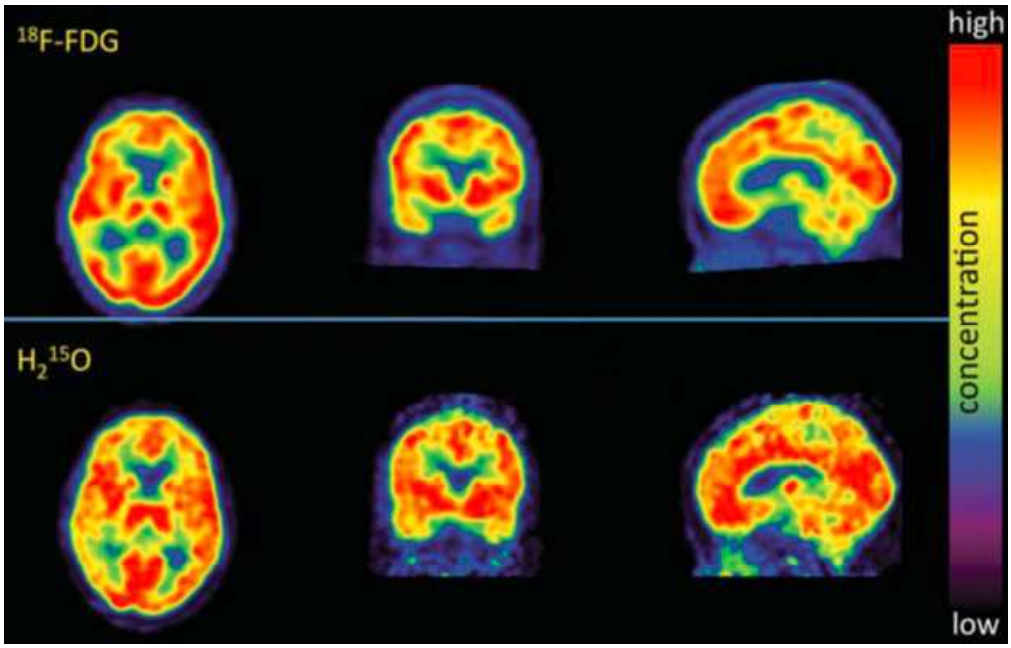

Figure 5: Example of a PET image using two different radioactive isotopes.(from [17])

1.2.3 FUNCTIONAL NEAR-INFRARED SPECTROSCOPY

Functional near-infrared spectroscopy (fNIRS) is a non invasive brain imaging technique which measures brain activity through the measurements of blood flow for only the top few mm of cortex and is based on the change in the blood's color when oxygen is delivered to brain tissue [18,19]. fNIRS is a BOLD-response technology that measures the changes in the relative levels of oxyhemoglobine (oxy-Hb) and deoxyhemoglobine (deoxy-Hb) during brain activity. When a subject performs a particular task, brain activity increases in those brain areas relevant to the task, and the amounts of oxy- and deoxy-Hb change in the immediate vicinity of those areas. fNIRS takes advantage of the fact that the relative amounts of oxy-Hb and deoxy-Hb in the area change, and this change is proportional to the level of neuronal activity. The changes in the oxy/deoxy ratio can be detected because the absorbance spectra at nearinfrared wavelengths differ for oxy-Hb and deoxy-Hb [19]. Deoxy-Hb is dark red; oxy-Hb is light red (Figure 6).
fNIRS is noninvasive, is relatively easy to use, and is portable and inexpensive compared to the other blood-flow measurement technologies. Its temporal resolution is relatively good (on the order of several seconds), but its spatial resolution is relatively low (on the order of cm).

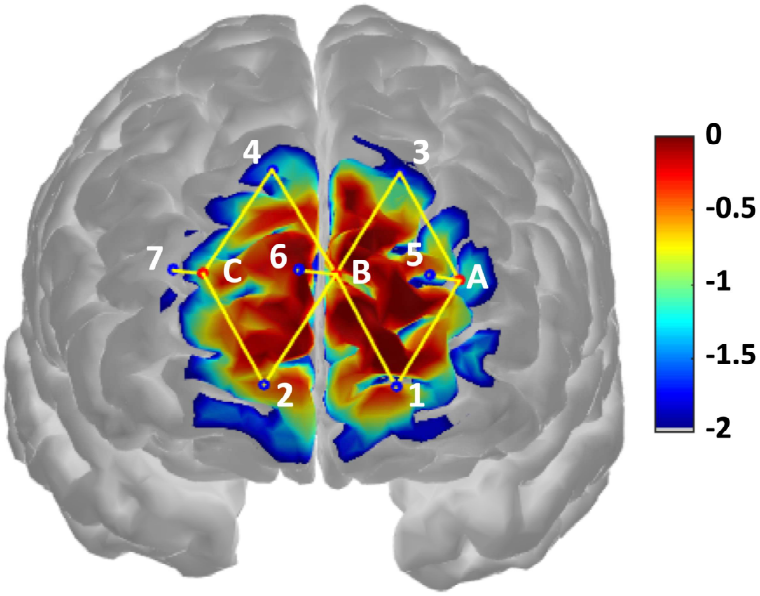

Figure 6: fNIRS example. Frontal view of the brain cortex showing the sources (A, B, C), the detectors (1-7) and result in 8 channels, shown as yellow lines (from [20])

1.2.3 ELECTROENCEPHALOGRAM

In 1929, Hans Berger in his paper "Über das Elektrenkephalogramm des Menschen" [21], demonstrated that the brain electrical activity can be recorded through electrodes on the surface of the scalp through a technique called ElectroEncephaloGram (EEG). EEG is a brain imaging method that detect brain electrical activity using different types of metal electrodes that are placed on the scalp. These electrodes measure small electrical potentials that reflect the activity of neurons within the brain. These potential, whose amplitude is tiny, are then amplified, digitized and then transmitted to a personal computer for the processing and the storage. EEG measures the potential difference (i.e., the voltage) between two electrodes. The second of these two electrodes could be the same and in this case measurements are "unipolar", or different, depending on the first electrode, and in this case measurements are "bipolar." In unipolar recording, measurements from all electrodes are referred to one common electrode, which is usually called "reference". To improve signal quality, EEG amplifiers require the connection of a "ground" electrode. EEG electrodes are small metal plates that are attached to the scalp using a conducting electrode gel. They can be made from various

materials. Most frequently, tin electrodes are used, but there are gold, platinum, and silver/silver-chloride (Ag/AgCl) electrodes as well.

For the positioning of the electrodes on the scalp to record EEG, there is a worldwide accepted standard, called the 10–20 international system [22]. It is based on an iterative subdivision of arcs on the scalp starting from particular reference points on the skull: Nasion (Ns), Inion (In), and Left and Right Pre-Auricular points (PAL and PAR, respectively). The intersection of the longitudinal (Ns–In) and lateral (PAL–PAR) diagonals is named the Vertex. The 10–20 system originally included only 19 electrodes (Figure 7). This standard was subsequently extended to more than 70 electrodes [23] (Figure 8). Usually an electrode placed on the ear lobe or mastoid is used as reference electrode. EEG has high temporal resolution, but low spatial resolution. Furthermore, due to the presence of the scalp, the cerebrospinal fluid and the dura which act as filters for high frequencies.

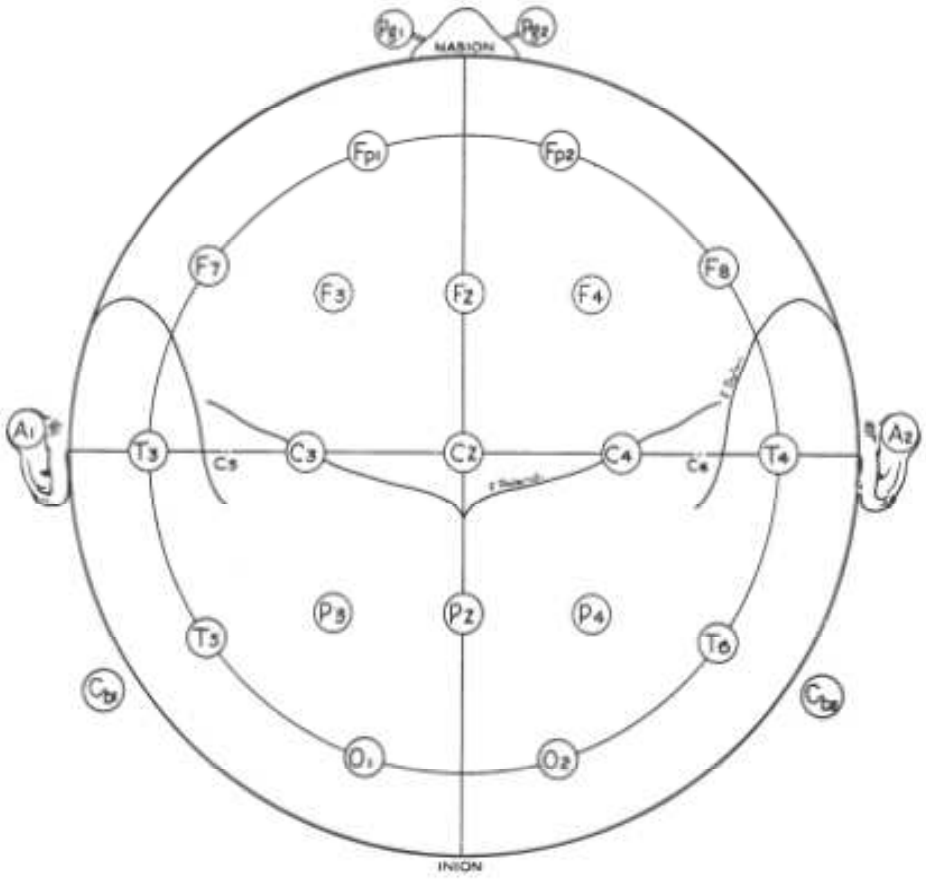

Figure 7: The 10-20 International System (from [24])

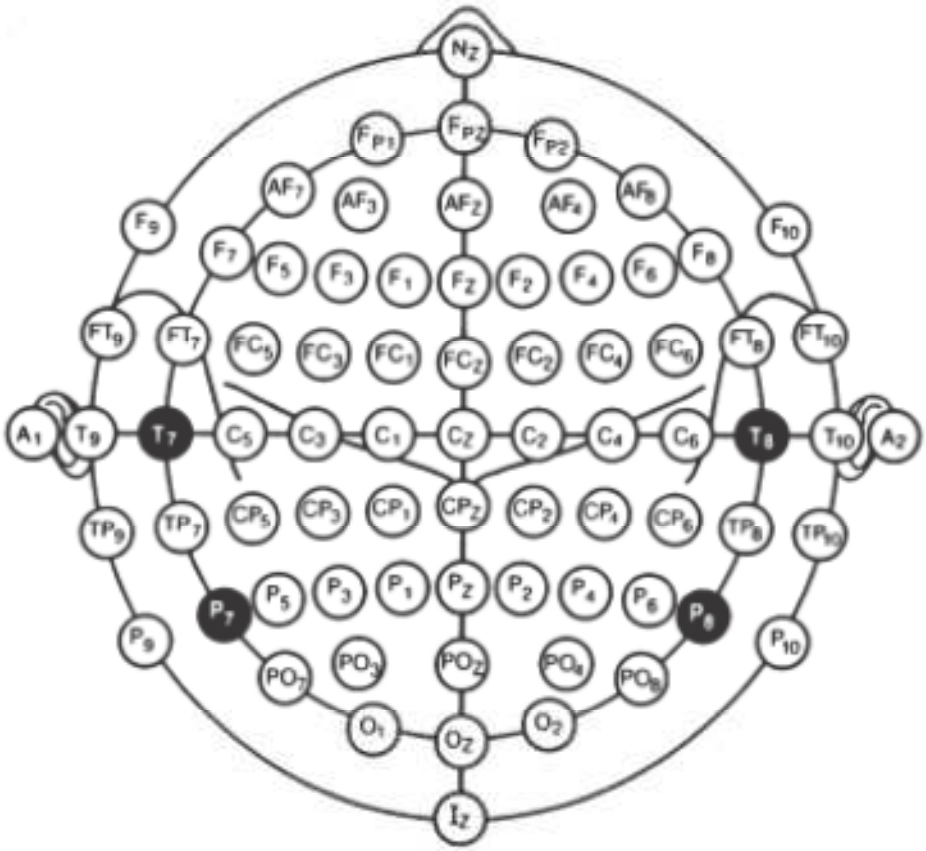

Figure 8: The extended 10 20 international system (from [24])

1.2.4 ELECTROCORTICOGRAM

Electrocorticogram (ECoG), also sometimes called intracranial EEG or iEEG, refers to the signal recorded from locations underneath the skull, but not within the brain itself. ECoG represents a midway point between scalp EEG and intracortical recordings, in fact, although surgery is needed to implant the ECoG electrodes, the electrodes do not penetrate into the brain. ECoG can be recorded from the surface of the dura mater (epidurally) using electrodes placed on the dura or using screws that penetrate the skull and serve as electrodes. Alternatively, ECoG can be recorded just below the dura (subdurally) using electrodes placed directly on the surface of the brain. ECoG signals, similar to the EEG, are the result of field potentials from population activity rather than action potentials from individual neurons. ECoG is superior to EEG in amplitude, topographical resolution, frequency range, and resistance to artifacts, and may be superior to intracortical signals in long-term stability. ECoG was first recorded from

animals and humans in the late 19th century [25]. Because placement of ECoG electrodes requires surgery, human studies are currently limited to people who are implanted with ECoG electrodes preparatory to brain surgery (usually to remove an epileptic focus or a tumor). The electrodes are typically 4 mm (2.3 mm exposed) platinum electrodes and are configured in either a grid (e.g., 8 × 8 electrodes) or strip (e.g., four or six electrodes) configuration with an interelectrode distance of usually 10 mm (Figure 9). They are typically implanted for periods of only several days to 1–2 weeks. When compared to EEG, ECoG has several major advantages:

- higher spatial resolution (1.25 mm for subdural recordings [26] and 1.4 mm for epidural recordings [27] vs. several centimeters for EEG)
- higher signal amplitude (50–100 μ V maximum vs. 10–20 μV maximum for EEG)
- far less vulnerability to artifacts such as electromyographic (EMG) [28] for electroocular (EOG) activity [29]
- broader bandwidth (i.e., 0–500 Hz [30] vs. 0–40 Hz for EEG)

With respect to ECoG's larger bandwidth, it is important to note that this advantage may in part be directly related to the larger amplitude of ECoG. Although ECoG generally displays a 1/frequency drop-off in signal power [31], task-related brain signals may still remain larger than the noise floor of the amplifier/digitizer, and thus they are detectable at higher frequencies than with EEG. In addition to these advantages
of signal quality, ECoG electrodes (which do not penetrate cortex) may provide greater long-term functional stability [32-36] than intracortical electrodes (which induce complex local responses that may degrade or prevent neuronal recordings (see chapter 5 in this volume). Furthermore, the signal-to-noise ratio of ECoG signals, and the cortical representations of motor functions that can be identified with ECoG, are stable over several months [37, 38]. Thus, there is strong theoretical and empirical evidence that ECoG could enable BCIs that have high functional specificity and that are less susceptible to the problems of reliability and long-term stability that often affect other electrophysiological signal-acquisition methodologies.

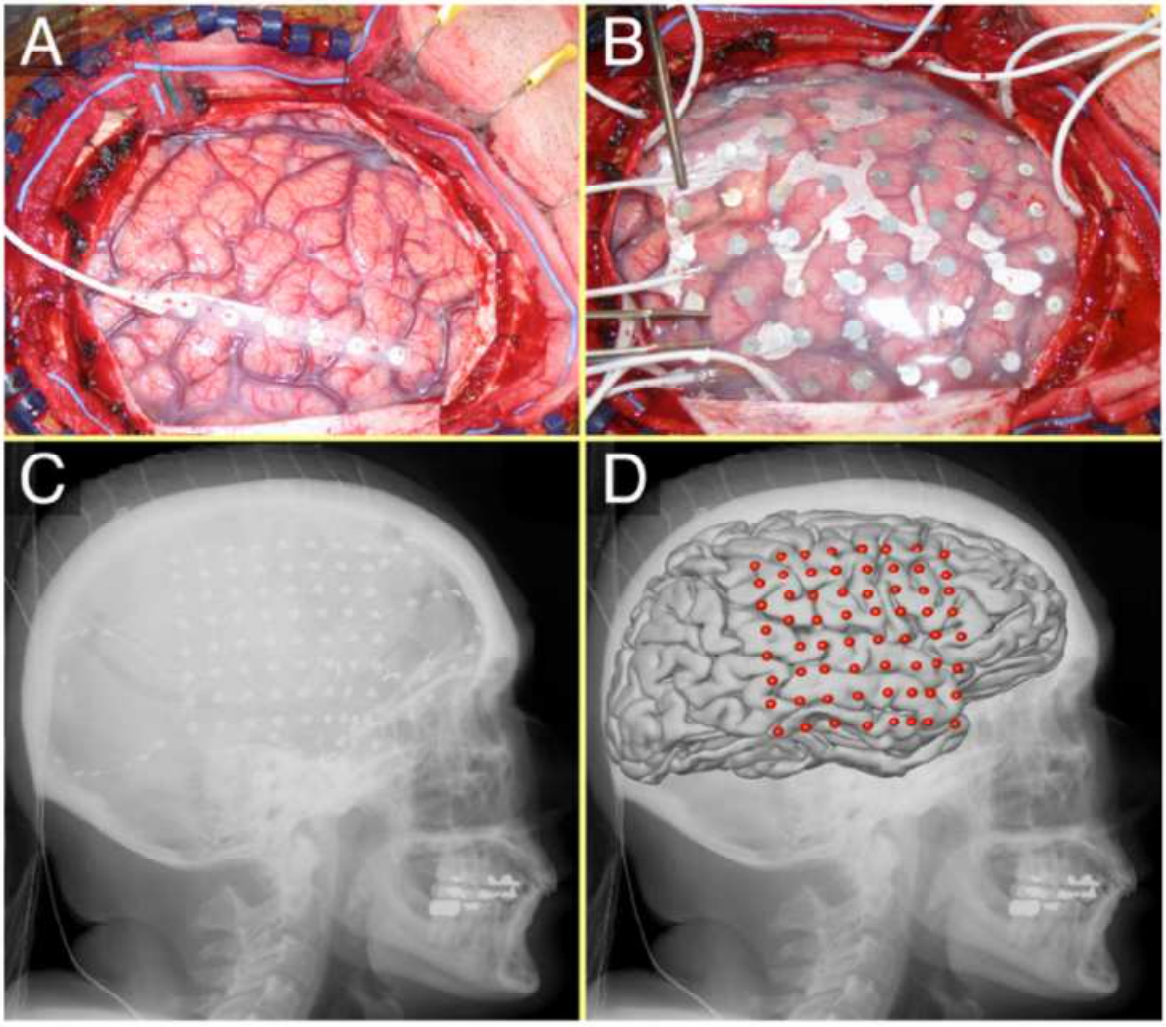

Figure 9: Example of ECoG electrodes array implantation. A: Brain after craniotomy. B: 8×8 subdural electrode grid. C: X-ray image of implanted grid. D: Electrodes localization on the brain surface.(from [39])

1.2.5 ACTION POTENTIALS (APS)

Neuronal spiking is of great interest, especially for BCI applications because it is a rich source of information. Spiking is generally assumed to be the major information output for long-distance, high-content communication for all neurons capable of spiking and to be a predominant form of coding in the nervous system [40]. Spike rate (number of spikes in a specific interval or a related mathematical function) is generally considered to represent neural output information, although additional information may be available in the higher-order statistics of spike trains. The amount of movement information available from the spiking activity of even a single neuron is impressive: it

includes information about future movements and movement parameters and also higher-order information about future movement sequences and goals. Spike recording makes special demands on the sensors, which must be very small, they must remain intact and functional in a warm and ionic environment for long periods, they must not induce infections, they must stay close to the neurons generating spikes, and they must not kill the neurons or induce gliosis that degrades or prevents spike recording.

1.2.6 MULTIUNIT ACTIVITY (MUA)

The neuronal spikes recorded extracellularly from different neurons usually differ from one another in shape and amplitude. The moveable microelectrodes used mainly in short-term laboratory settings can be adjusted to focus on a particular neuron and can thus maximize the signal-to-noise ratio and increase the certainty that the properties of that individual neuron are being evaluated. However, multiunit recordings use microelectrodes that are in relatively fixed positions, the spikes they record are often small and as a result, separating the spikes, the so called *spike sorting,* from different neurons is often difficult. Thus, sophisticated software is applied to extract specific features of the spike waveforms and use them to separate the spikes of different neurons. Alternatively, neuronal spiking can be treated as *multiunit activity* (MUA), without being sorted into individual neurons (Figure 10).

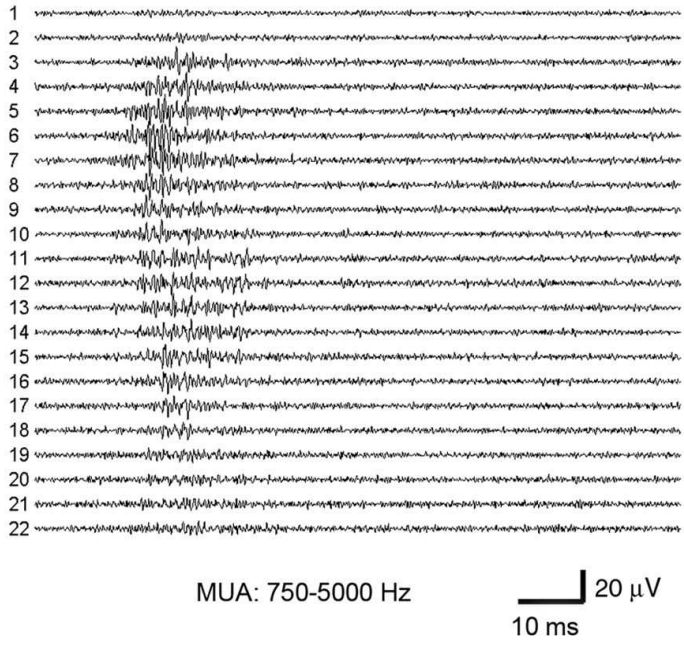

Figure 10: Example of MUA (fro [41]

1.2.7 LOCAL FIELD POTENTIALS (LFPS)

Field potentials (FPs) are signals that may reflect local or broadly distributed changes in electrical potential. Although the actual sources of FPs are complex, it is often convenient to think of them as a reflection of input to neurons. The FPs recorded by small sensors within brain tissue, such as the microelectrodes, are local field potentials (LFPs). Although LFP signals are complex mixtures of activity from many sources [42], they capture local electrical-fi eld changes originating close to the microelectrodes (Figure 11). In general, one expects electrodes with smaller recording surfaces to be relatively more sensitive to nearby activity than are electrodes with larger recording surfaces. FPs contain both rhythmic activity (sensorimotor rhythms) and potentials related to particular central or peripheral events (event-related potentials) [43]. All LFP bands have generated interest as possible signals for BCIs [44,45]. BCI sensors thus have a rich source of control signals that can be treated as information channels, including several LFP bands in addition to spikes. Whereas FPs have traditionally been assumed to contain only low frequencies (i.e., from low direct-current frequencies to those up to about 100 Hz), ECoG can record signals at higher frequencies (e.g., 500 Hz) [46].

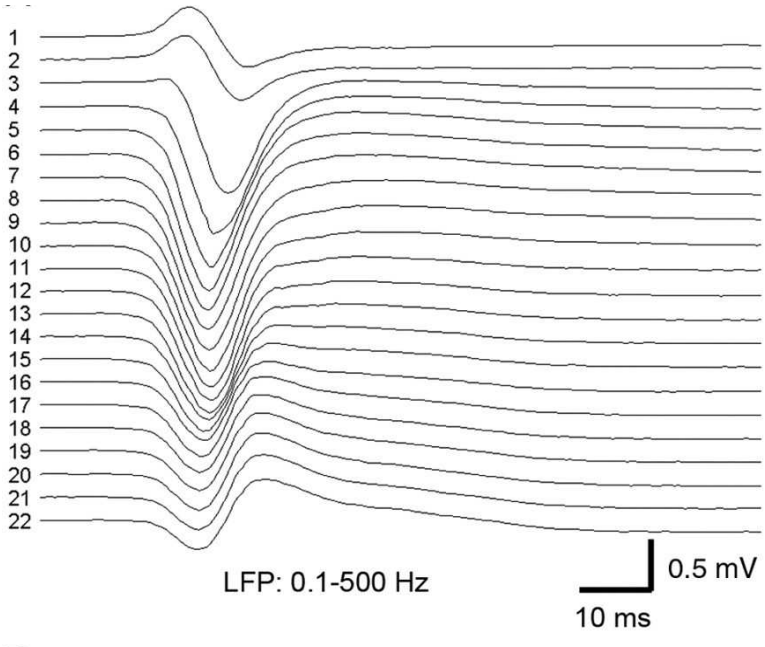

Figure 11: Example of LFP (from [41])

1.3 BRAIN COMPUTER INTERFACE (BCI)

1.31 OVERVIEW

In many patients affected by various neurological or neurodegenerative diseases, the normal pathway from the brain to the spinal cord and to the peripheral nervous system is disrupted. For this reasons, these patients are unable to perform basic functions or to communicate with the external environment., so that they lose all their communication abilities and become completely locked-in to their bodies and not able to control their muscles. One forefront opportunity, although still not completely developed into a commercial and clinical setting, to restore their lost functions is to provide them with a virtual and non muscular channel from the brain to the spinal cord or to the peripheral nervous system, the so-called Brain Computer Interface (BCI). A Brain Computer Interface (BCI) is a non muscular communication system that allows to directly communicate a user's intent from the brain to the external environment [47]. Such systems create a new communication channel between the brain and an external device (generally a computer), which translates the information coming from the brain in device commands. Any BCI system consists of four main components:

- Signal acquisition, which acquire brain signals;
- Signal processing, which extracts specific signal features from the acquired signals and translates those into device commands;
- Output device, which execute these commands and produces the user's intent;
- An operating protocol, that control the operations

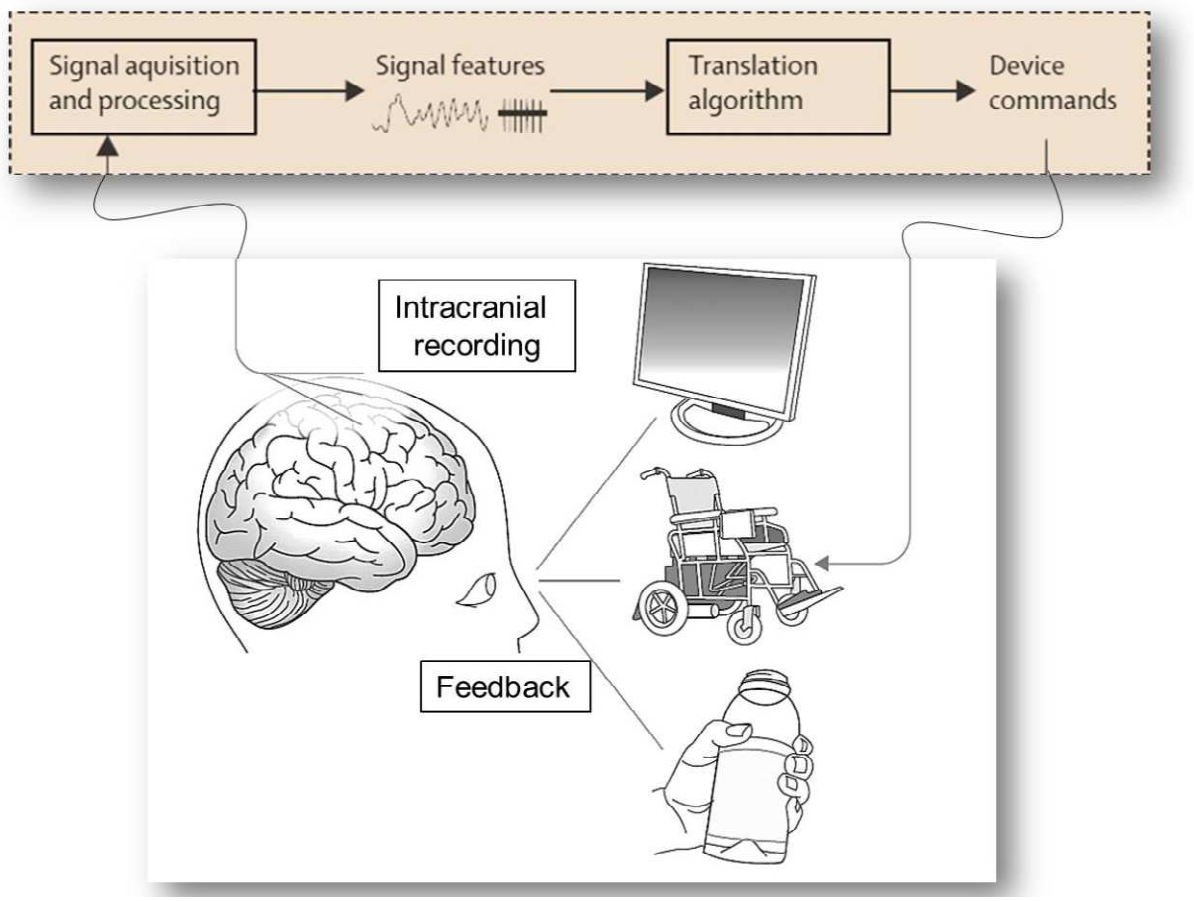

Figure 12: Schematic representation of a BCI system (from [47])

1.3.2 SENSORS FOR BCI SYSTEMS

A key component in the design of BCI system is the signal acquisition module, in particular the sensors and the brain signals to used to accurately translate the user's intent. There is a variety of sensors for monitoring brain activity and acquire brain signals which could provide the basis for the development of a BCI system.

All the exiting techniques for acquiring brain signals for BCI applications, can be divided into two main categories:

- *Non-invasive BCIs*, which do not require surgery to implant the sensors, so do not expose the patient to the risk of brain surgery;
- *Invasive BCIs,* performed through surgery by implanting the sensors essentially intracranially. These allow to acquire finest signals, but are invasive for the patient.

There are many non invasive recording technique that can be potentially used for a BCI system. Most of these techniques, including functional magnetic resonance imaging (fMRI), magnetoencephalography (MEG), positron emission tomography (PET) and functional Near InfraRed (fNIR) are still technically demanding and expensive, as well as practically wearable, and this impedes widespread and daily use. Furthermore, most of them, depends on metabolic processes, have low temporal resolution and seems to be not appropriate for a rapid communication. Despite these limitations, in the past years several studies have been conducted to evaluate the value of these modalities for BCI [48-52]. At the moment, the only non invasive technique which uses relative simple and not expensive equipment and which has high temporal resolution is the electroencephalogram (EEG) recorded from the scalp [53-56]. For all these reasons, EEG can offer the opportunity of a practical BCI system, providing higher performance than previously assumed, including, for example, two- or three- dimensional cursor movement [57,58]. However, EEG has low spatial resolution and this limits the quantity of information that can be extracted and it is also much susceptible to artifacts. Furthermore, EEG-based BCI requires an extensive training to achieve high levels of controls by the user. Another simple and inexpensive technology, although invasive, which can be used for a pratical BCI system is the electrocorticogram (ECoG), which is recorded directly from the cortical surface [59-61]. ECoG has higher spatial resolution than EEG, broader bandwidth, higher amplitude and is less vulnerable to artifacts or ambient noise. Although this method is invasive because requires surgery for the implantation of electrodes, the use of electrodes that do not penetrate the cortex may combine excellent signal fidelity with good long-term stability [62-64]. The third and most invasive alternative uses microelectrodes to measure action or field potential from multiple neurons in the brain [65,66]. While this technique provide signals with higher fidelity and might require less training than EEG-based systems, its clinical implementation are impeded by the difficulties in maintaining stable long-term recordings [67-69].

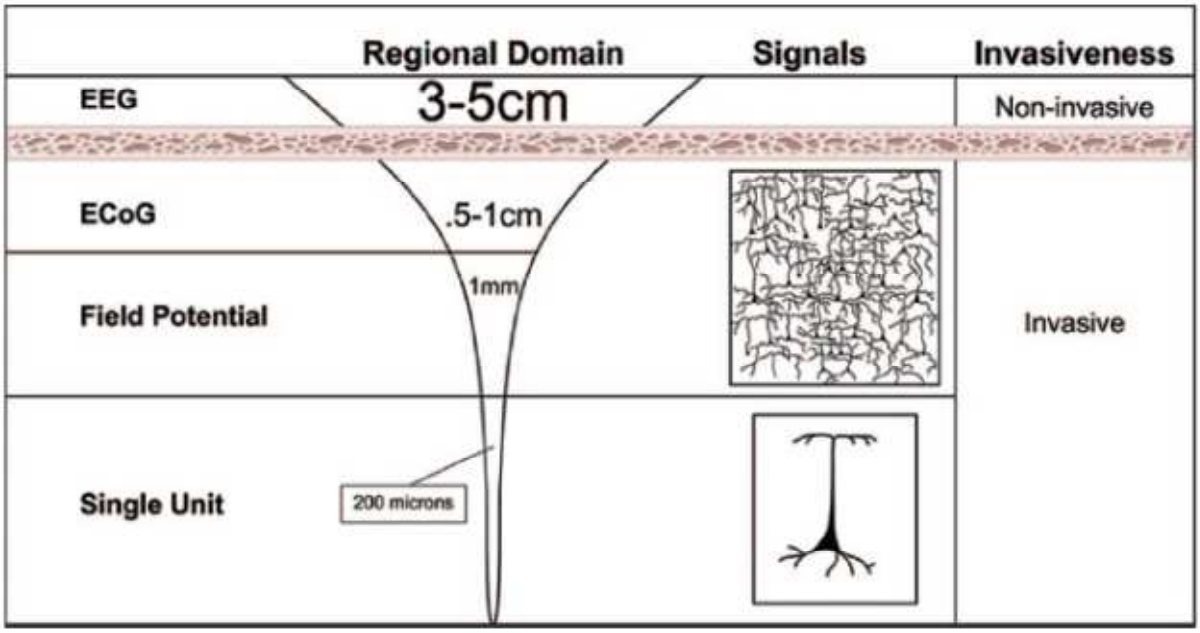

Figure 13: The relationship between the various signals used in BCI operation. They are distinguished in regard to the area of the cortex distinguishable, neuronal population, and level of invasiveness (from [70])

1.4 RECORDING SIGNALS FROM ELECTRODES IMPLANTED IN THE BRAIN

With the invasive techniques it is possible to detect single action potential in the brain. These potential can be differentiated basically in extracellular and intracellular. Extracellular recordings cannot be observed above noise farther than approximately 100 μm from a recording site and that the neuron cell body contributes to the majority of the recorded signal. Thus, the distance required between an electrode site and a neuron cell body to catch reliable signals is of the order of cell dimensions [71]. The intracellular recordings can be in tens of millivolts but the electrical signals recorded from neurons in the brain range in tens of microvolts in the case of single spike activity (in the range of kHz) or local field potentials (from zero to hundreds of Hz).

1.4.1 INTRACELLULAR RECORDINGS

Intracellular recordings allow the study of the physiology of single cells, catching information about post synaptic potentials or other small potential changes. It measures voltage or current across the membrane of a cell. It usually comprises an electrode inserted inside the cell and a reference electrode placed outside the cell. The classical

type of microelectrode used for this application is a glass micropipette filled with an electrolyte and a contact wire which act as interface with the pipette to the recording instrumentation. There are two different methods to perform intracellular recordings: current clamp and voltage clamp. In the former, the electrode is connected to an amplifier to measure the membrane potential, in response to a current injected through the electrode (Figure 14), in the latter, the current passing through the electrode when the membrane potential is held at a fixed value (Figure 15). The method is based on the penetration of the micropipette into the cell membrane, allowing the creation of an electrical connection with low resistance. It is characterized by very good electrical coupling with the cell and provide accurate readout of the entire dynamic range of voltages generated by cells without distorting the readout over time.

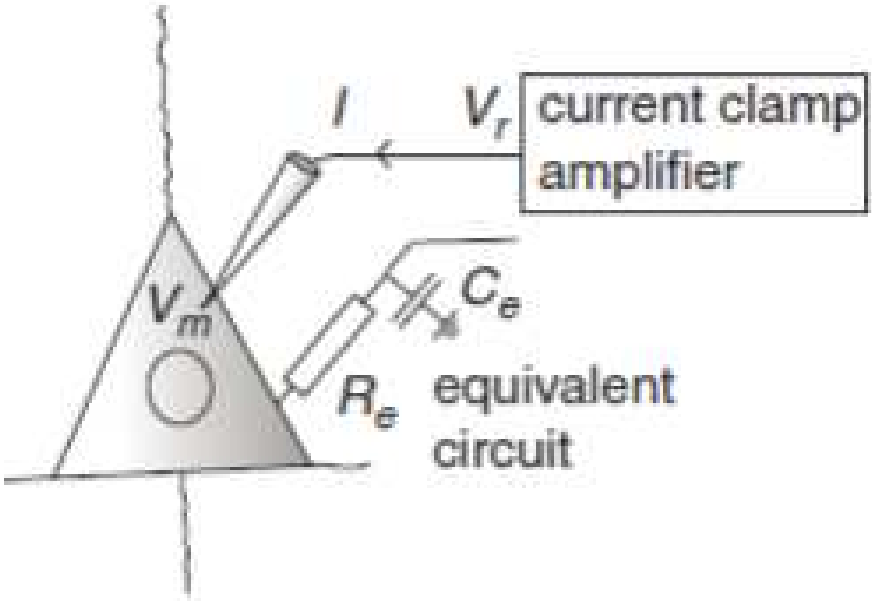

Figure 14: Current clamp recording. Experimental setup: a current clamp amplifier records the electrode potential (Vr) while injecting a current I through the electrode. Ideally, the recorded potential equals the membrane potential Vm but the electrode resistance (Re) and capacitance (Ce) introduce artifacts (from [72])

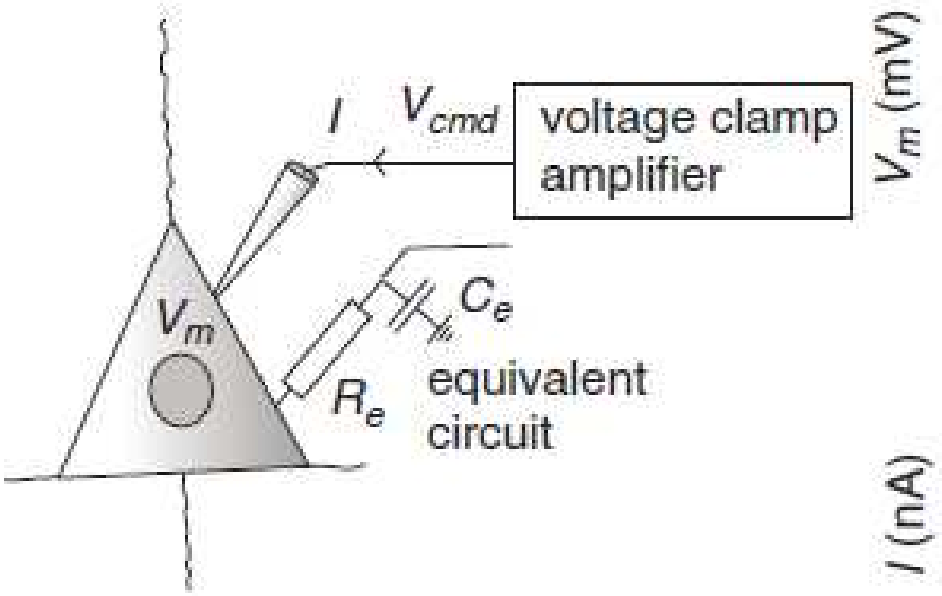

Figure 15: Voltage clamp recording. (from [72])

The most used method for the intracellular recording is the patch-clamp method (Figure 16), allowed for the first time to record currents of single ion channels [73]. This method, however, has several drawbacks: it is invasive, the contact between the electrode and cell is strong enough to be functional for more than several hours[74] and the electrolyte in the pipette tip will spread into the tissue after a certain time. Furthermore, it is very difficult to integrate these electrodes with microelectronics for recording, for example, from freely moving animals.

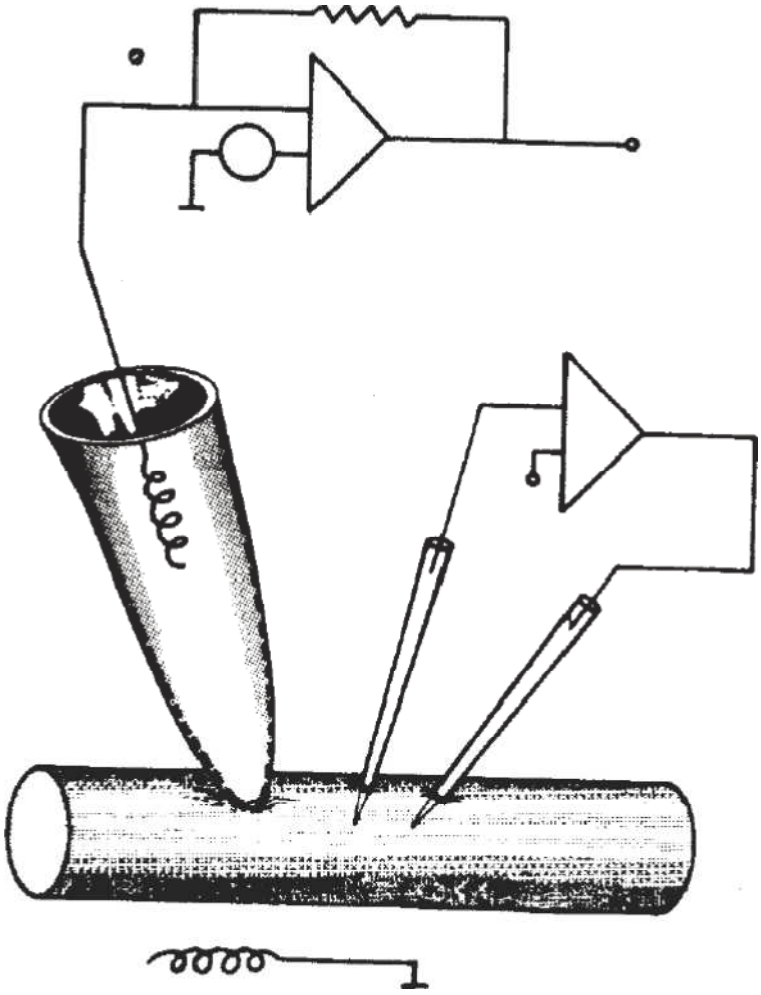

Figure 16: The patch clamp technique. The transmembrane current is recorded with the large patch electrode while the membrane potential is held fixed with two conventional microelectrodes

1.4.2 EXTRACELLULAR RECORDINGS

Extracellular recordings overcome the main problems existing with the intracellular recordings, as with such recordings there is no need to penetrate the cell membrane and, moreover, they allow recording from individual cells or complete networks [75, 76]. This methods have also drawbacks, for example they have low signal-to-noise ratio and poor electrical communication at the electrode/cell interfacial contact [77]. The most used electrodes for such recordings are extracellular MEAs used for in vitro recordings and polytrodes for in vivo recordings (Figure 17). Althouogh they largely attenuate and temporally filter the electrical signals, nonetheless, they enable simultaneous recording and stimulation of large populations of excitable cells for few

days (for in vitro) or months (for in vivo), without inflicting mechanical damage to the neuron plasma membrane.

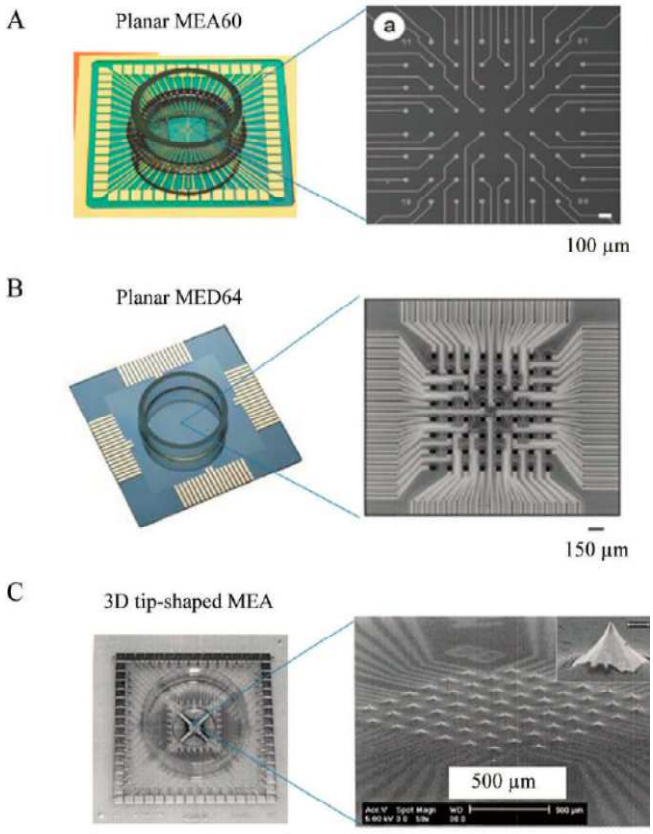

Figure 17: Example of standard multi-microelectrode arrays (MEAs). (from [78])

1.4.3 ELECTROCORTICOGRAPHY AND MICRO - ELECTROCORTICOGRAPHY

Multichannel neural interfaces are very important tools in neuroscience research and for the diagnosis and the treatment of many neurological disorders, like epilepsy and stroke. ElectroCorticoGraphy (ECoG) measure local field potentials directly from the contact surface. Conventional arrays of ECoG electrodes normally have an electrode site size of approximately 1 cm in diameter, which limits the spatial resolution of neural recording and stimulation [79]. ECoG showed its advantages over EEG, providing greater spatial and temporal resolution than EEG, especially for detecting high gamma modulations (70–105 Hz) as the skull attenuates higher-frequency signals [80–81]. ECoG is currently used as a standard of care for clinical mapping of eloquent cortex prior to therapeutic resection of brain tissue and in epilepsy monitoring and treatment. ECoG

electrodes are placed on the surface of the cortex and, for this reasons, are less invasive than traditional intracortical microelectrodes by eliciting less of an immune response, and providing better signal longevity [82–84]. ECoG has shown as a valuable tool for decoding of continuous three-dimensional (3D) hand trajectories in non-human primates over several months [85], in decoding pediatric brain signals for hand movement [86], in controlling prosthetic devices through BCI approaches [87-90]. Chronic BCI testing using ECoGs to control devices is limited, as most subjects are epilepsy patients performing short-term ECoG recordings [91,92]. High-density ECoG was also used to decode motor imagery of sign language gestures as an alternative mode of communication [93]. Chronic ECoG implantation in humans was also investigated as a treatment/warning system for epilepsy [94].

Micro-ECoG (μECoG) electrode arrays utilize microelectrodes with contact site diameters many orders of magnitude smaller than traditional ECoG electrode and minimized inter-electrode spacing, allowing greater spatial resolution of the measured signals (Figure 18).

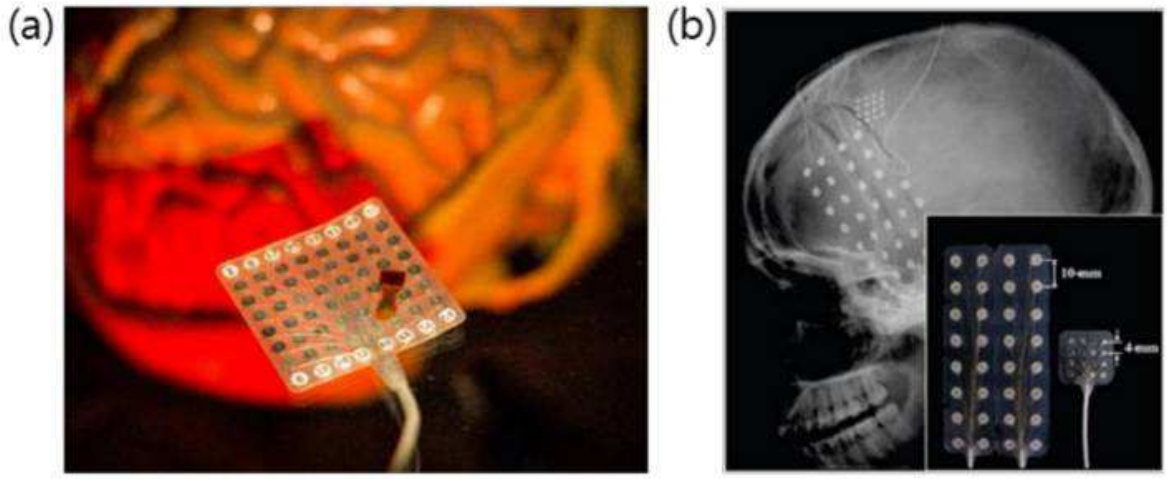

*Figure 18: A clinical electrocorticographic (ECoG) grid underneath a micro-ECoG (μECoG) array. (a) Comparison of the regular ECoG (white square) and μECoG arrays (yellow). (**b**) X-ray image regular ECoG and μECoG (modified from [95])*

Moreover, μECoG devices have ultrathin structure, and this results in less invasive implantations [97]. μECoG provides a promising balance of information acquisition and spatial resolution with an acceptable degree of invasiveness (Figure 19).

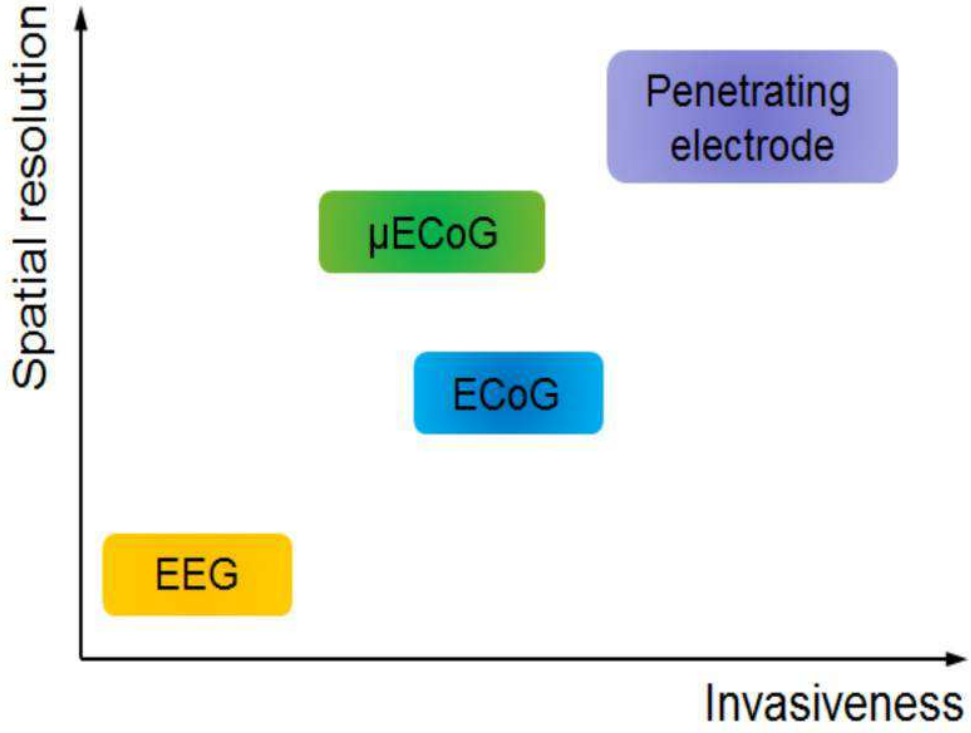

Figure 19. Spatial resolution versus invasiveness for various types of neural electrodes. (from [95])

Micro-ECoG has been demonstrated to provide higher temporal and spatial resolution than typical ECoG [96,97], often comparable to intracortical microelectrodes [98,99]. The main advantage is the smaller size of the electrodes, which provides more precise and accurate recordings and less invasiveness than normal ECoG, due to the reduced size of the craniotomy required for the implantation, as well as the quantity of bulk material implanted. Like ECoG, μECoG demonstrated applications for restoring communication and controlling prosthesis. Due to its balance between invasiveness, spatial resolution, μECoG is a promising technology to provide stable, reliable neural in both the research and clinical domains.

1.5 ELECTRODES

In the last years an intense research has been conducted in order to improve the technology behind the electrodes used for neural interfaces. There are many types of implantable electrodes, which differ between each other for many characteristics, including the layout, the dimensions, the type of signal which they are able to record and so on. Different categories of electrodes exist, many of them are listed below.

Insulated microwires and tetrode: These electrodes represent the first generation of implantable microelectrodes, they are made by well-known electrically conductive materials, insulated except for the tip, stiff enough to be inserted through the pia or the dura mater and access deep brain regions (Figure 20). These insulated microwires allowed neurophysiologists to study the activity of individual neurons in awake, behaving animals and they could be fabricated easily with available technology [100]. This technique is still widely used for both acute and chronic extracellular recordings.

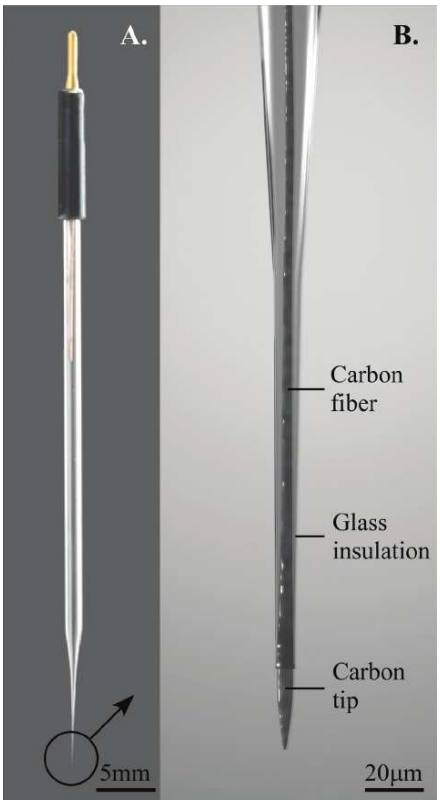

Figure 20: A carbon fiber microelectrode (from [101])

Another commonly used implantable device is the microwire tetrode (Figure 21), which allowed estimating the position of individual recorded neurons by triangulation. Such devices are characterized by high impedance and small site sizes and thus in order to be effective they must be accurately positioned near their target neurons using precision micromanipulation. These electrodes allow neuronal recordings from several minutes to several hours, afterward they should be repositioned. Furthermore, they cause marked insertion damage, and the exact site placements is often uncertain, because they are

prone to expand into the tissue. For all these reasons, they are not suitable for long-term chronic implant.

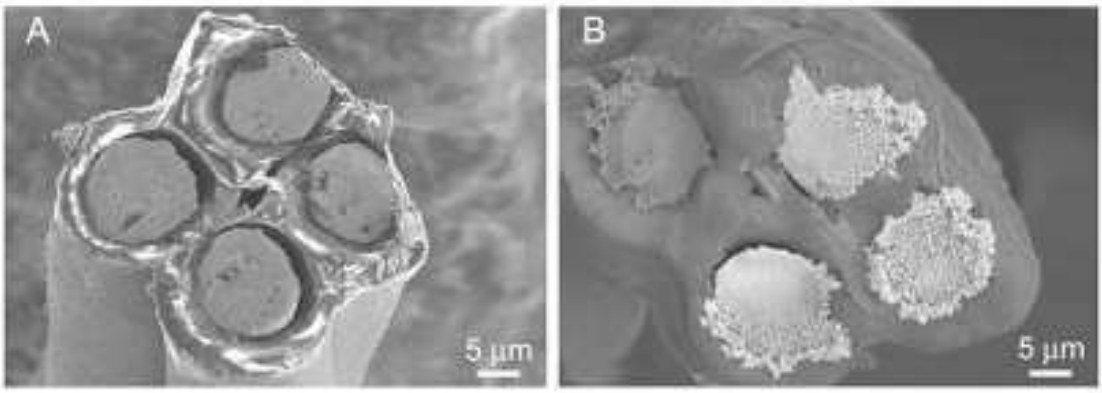

Figure 21: A 4-microwire electrodes tetrode (from [102])

Microelectrode arrays: These category of implanted devices was developed in order to perform multi-neuronal simultaneous recording at the level of neuronal populations as well as the single-neuron level, allowing the extraction of more information from the brain[104,105]. The microfabrication of such devices was possible after the introduction and the development of photolithographic techniques and silicon etching technology, which permitted the microfabrication of array of electrodes with high precision, allowing to fix and define the spatial resolution between the electrodes and the position of each electrode. This technology was developed as part of the more general development of microelectromechanical systems (MEMS) [105]. The most known examples of such technology are the Michigan array (Figure 22) and the Utah array (Figure 23). In the former several microelectrode are patterned on each shank of the structure, providing higher density of sensors while reducing the displaced tissue. The latter, consists in 100 conductive sharpened silicon needles, electrically isolated between each other, with the tip is coated with platinum and the shanks are insulated with polyimide. Electrical contact is made from the back side of the structure using insulated gold wire [106, 107]. Strong research efforts are made in order to develop multiple single microelectrodes aligned into arrays to try to increase the number of electrode sites included in one device. These devices can preserve their functionality for few months, can remain into the brain for prolonged time periods, but recording quality decrease with time.

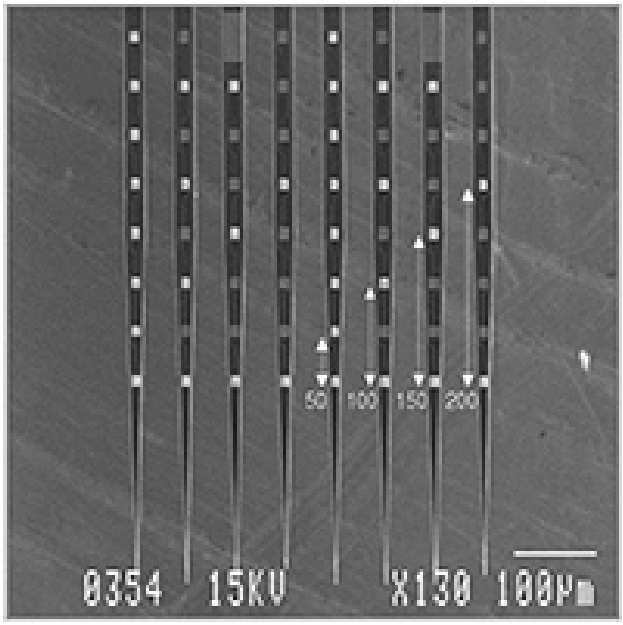

Figure 22: The Michigan microelectrode array

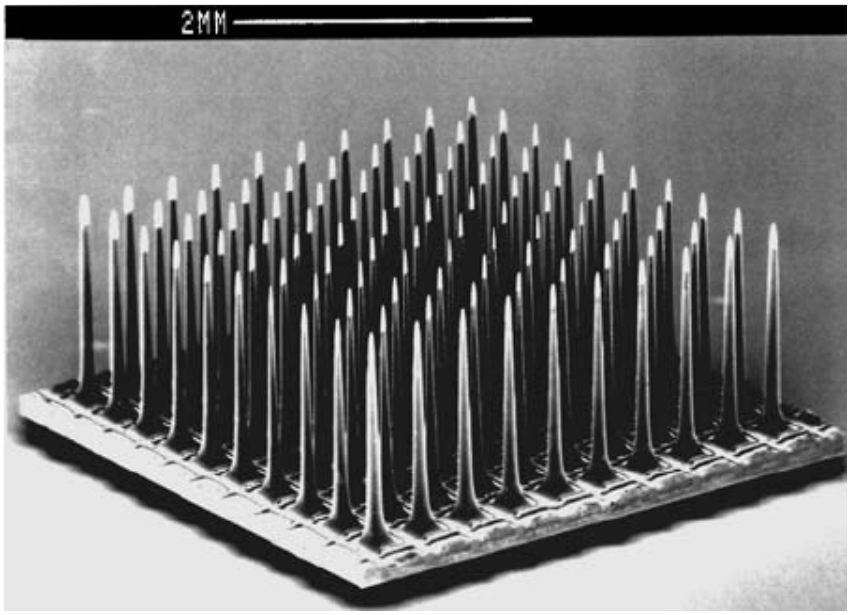

Figure 23: The Utah microelectrode array

Implantable electrodes on soft substrate: A huge research effort has been done in order to develop implantable devices flexible enough to be compliant with the brain tissue and to reduce the mechanical damage without inducing any tissue reaction. In the last 20 years, polymer-based implants have been microfabricated for both acute and chronic recordings [108]. The fabrication of these devices typically involves metal electrodes

embedded in a thin polymer film using standard photolithographic techniques (Figure 24).

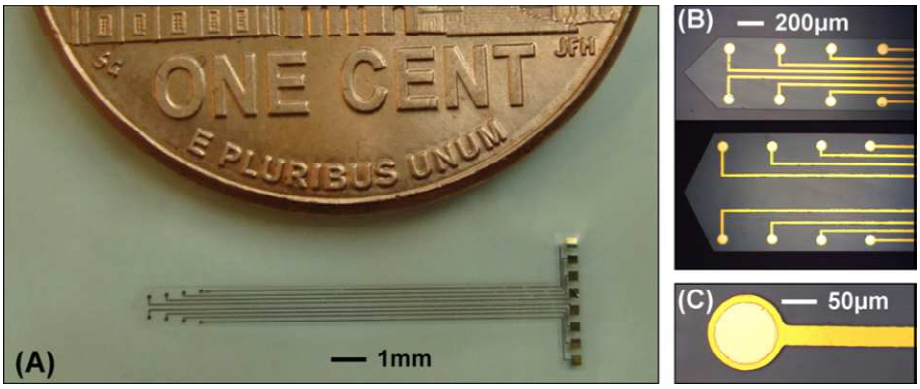

Figure 24: Example of implantable electrodes on soft substrate. (A) Dimensions of the electrodes array in comparison with a US penny. (B) Photomicrograph of two arrays with different transverse spacing values between the recording electrodes. (C) Photomicrograph of a single recording electrode showing the exposed gold pad (light yellow) and the parylene-insulated region (dark yellow). (from [109])

Implantable electrodes with bioactive coatings: To this category belong intracortical electrodes with "bioactive" components. This kind of electrodes make use of classical electrically conductive materials in combination with biologically active materials, with the aim of improving the performance and functionality of the neural interface. The incorporation of bioactive materials could be achieved by the use of hydrogels [110] or biodegradable polymer embedding the whole electrode (Figure 25).

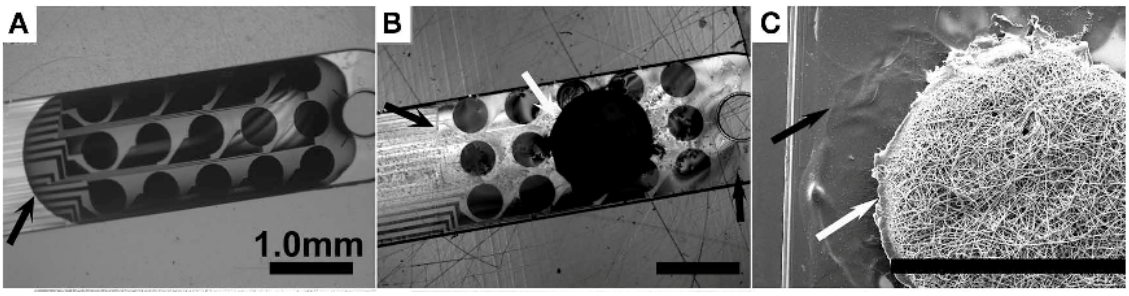

Figure 25: Implantable electrodes with different bioactive coatings. A) Optical micrographs of the tip of a microeletrode array coated with PEGPCL hydrogel and B) coated with PEGPCL hydrogel-EFM composite. C) Scanning electron microscope (SEM) micrograph of the tip of an MEA coated with PEGPCL hydrogel-PCL EFM composite (from [111])

µECoG electrodes: A wide variety of materials have been used to fabricate µECoG electrodes, ranging from traditional metals such as platinum, to advanced two-dimensional materials. The most used materials for the fabrication of µECoG devices are listed below:

- Platinum-based electrodes: Platinum is one of the most common metal used in various applications of neural recording and stimulation due to its resistance to corrosion and to its biocompatibility with the brain tissue. Platinum ensure long-term reliability of electrodes to be used in chronic settings [112]. Also, it is characterized by an easy fabrication process, and is able to electrically stimulate the brain limiting damage to the cortex.

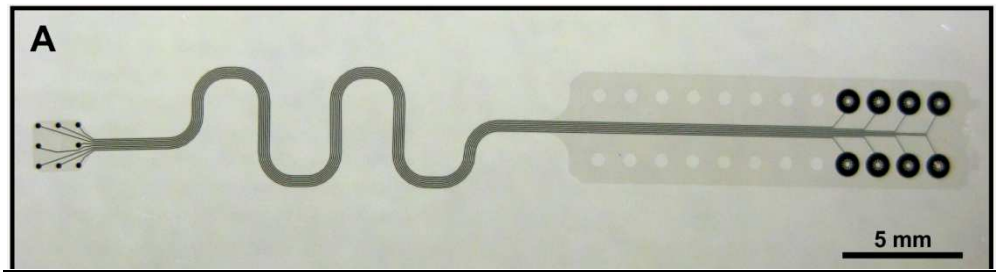

Figure 26: Example of a Pt microelectrode array

- Graphene-based electrodes: In recent years, optical imaging of the cortical areas of the brain while recording the electrical activity through surface electrodes became possible [113, 114]. This is due to the availability of conductive, optically transparent materials, unlike conventional metal-based conductive materials. Graphene's optically transparent nature and electrically conductive properties make it a good material for cortical electrode implementation. In addition, graphene's mechanical compliance may help improve the long-term biocompatibility of the electrode. It is reported that graphene electrodes remain viable for chronic recording for extended time periods [113]. Graphene's high transmittance and low electrical impedance make it a promising candidate for optically clear electrodes.

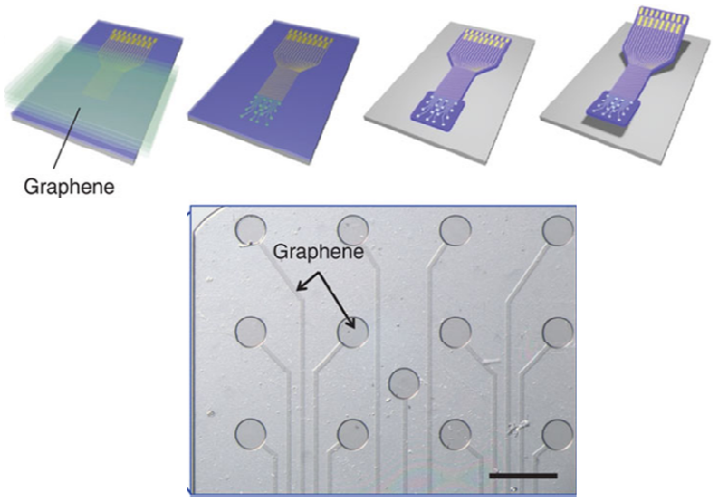

Figure 27: Example of grapheme-based microelectrode array (modified from [113])

- Indium tin oxide-based electrodes: Indium tin is used for commercial transparent electrodes in displays such as liquid crystal displays (LCDs) or active-matrix organic light-emitting diodes (AMOLEDs) and recently was used also for the fabrication and characterization of a 49-channel ITO-based µECoG array [115]. Due to the transparency of Indium tin oxide (ITO), ITO-based µECoG arrays were used also to perform cortical electrical stimulation (CES) through to investigate activation profiles of the cortex using a voltage-sensitive dye [116]. The implementation of CES through µECoG provides a useful tool in determining many of the effects that electrical stimulation has on the brain.

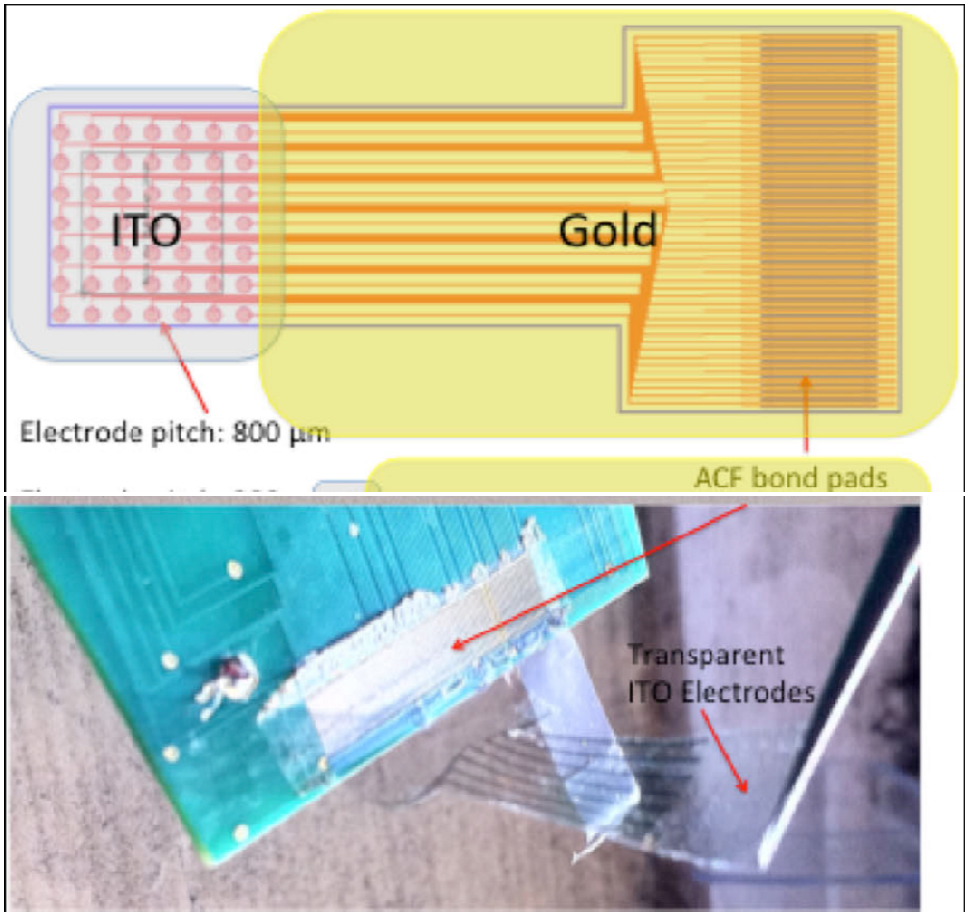

Figure 28: Example of ITO-based microelectrode array (modified from [117])

- Sputtered Iridium Oxide film (SIROF)-based electrodes: Iridium-oxide films are emerging as a technology in neural stimulation electrodes as a means to increase the electrode's ability to inject charge. These electrodes are able to inject charge via reversible reduction and oxidation between Ir3+/Ir4+ valence states within the oxide film. By changing the thickness of the iridium-oxide layer, the electrical characteristics of the electrode can be tuned. This leads to a large variety of properties that can be obtained for the electrode [118]. One downside to iridium oxide is that it is more brittle compared to platinum, which prevents it from being used in flexible electrodes. This can prevent good contact with the cortical surface electrodes, as well as reduce the biocompatibility of the electrode due to the difference in the mechanical compliance of the electrode versus that of the brain tissue [119].

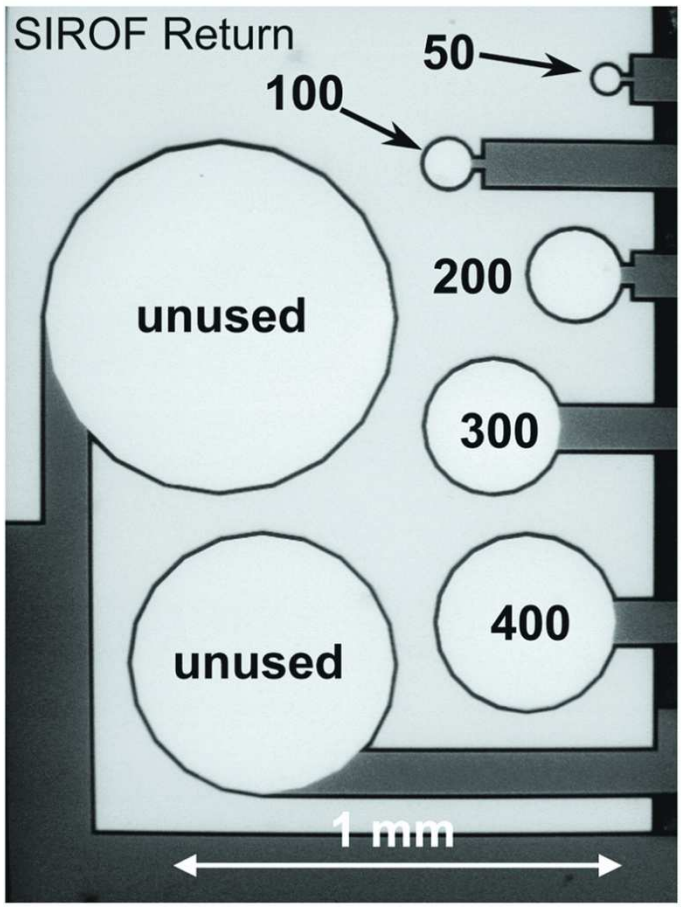

Figure 29: SEM image of Sputtered Iridium Oxide-based microelectrode array. The light areas in the image are SIROF (from [118])

- Bioresorbable Silicon: In clinical neurological monitoring involving μECoG with the abovementioned materials, a second surgical procedure for removal of the device is typically performed after the recording is over. Whether the implant is extensive or not, such a second procedure often adds cost and risk. In most cases, one to three weeks of recording is required. Ideally, a temporary monitoring system that can dissolve or disappear after the suggested period of implant time would eliminate such a second surgical procedure. Recent advances in silicon devices demonstrated bioresorbable forms of silicon sensors and electronics, where ultrathin silicon nanomembranes disappear after a certain period of time in fluids. It was also demonstrated that the constituent materials comprising such bioresorbable sensors and electronics are biocompatible, which is suitable for biomedical applications [120]. Precise recordings of brain signals from the cerebral cortex were achieved utilizing bioresorbable silicon electronics [121].

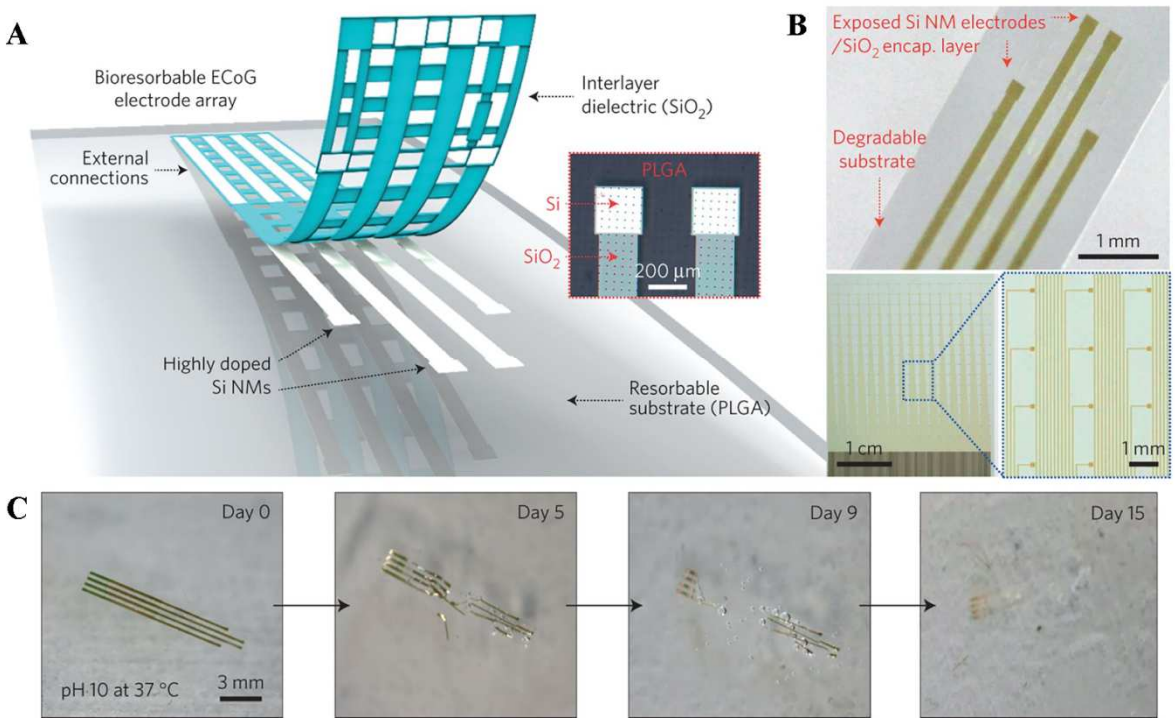

Figure 30: Example of bioresorbable silicon-based microelectrode array (modified from [121])

1.6 BIOCOMPATIBILITY

Of particular interest in the field of the fabrication of microelectrodes is the chronic foreign body response (FBR), because one of the most unaddressed issue regarding the fabrication of microelectrodes for chronic applications is that they often induce an FBR, which can both affect the performance of implanted electrodes and the health of the surrounding brain tissue [122,123]. In fact, very often, the foreign body (the electrode) induces chronic inflammation at the biotic–abiotic interface [124] At the biotic–abiotic interface, microglia, that is the resident immune cells of the central nervous system (CNS), become activated, undergo gliosis, and eventually encapsulate the implanted device [126]. The primary cause of this reaction could be due to a mismatch between implanted materials and tissue compliance that strongly mediates the activation of microglia [126,127]. Increasing evidence demonstrates the importance of material properties on cell fate, including neural stem and progenitor cells, which holds implications for neural regeneration around the electrode site [128]. The most invasive

electrodes, such as penetrating electrode arrays, cause the most trauma at the time of implant, and also elicit the greatest FBR response as a result of increased surface area between the implanted foreign body and the native tissue [122,123]. In contrast, μECoG has been demonstrated to be less invasive, since it elicit less of a response and this was confirmed by greater electrode longevity [129-131]. Typically, the implanted neural electrodes show a large increase in the impedance of the electrode after implantation for the first 7–10 days [113-133]. This is speculated to primarily be due to the host response to the implantation surgery rather than electrode degradation. The foreign body response is dynamic, and considered an evolutionary survival mechanism to either remove or compartmentalize foreign objects (not self), preventing their interaction with surrounding tissues (self) as a means of self-preservation. The glial scar, astrocytes and microglia responding to a foreign body, can isolate the electrode from the desired neurons and insulate it from the rest of the cortex. This can lead to an increase in impedance, and make it harder for the electrode to record the electrical activity of the underlying tissue [71,122,123,133]. Astrocytes can be identified, for example, by increased expression of glial fibrillary acidic protein (GFAP) [134,135]. Microglia are often identified by immunostaining for ionized calcium-binding adaptor molecule 1 (Iba1). The host response can significantly affect the performance of the electrode, in fact the increase in inflammatory cell density and extracellular matrix deposition both lead to increased impedance and decreased recording capability [123,133]. Electrode design factors such as geometry, materials, and level of invasiveness all play important roles in the longevity of electrodes by reducing glial scar formation and biofouling. Reducing invasiveness (μECoG vs. penetrating arrays) may also reduce scaring through reducing trauma, both to the parenchyma and the blood–brain barrier [130,136].

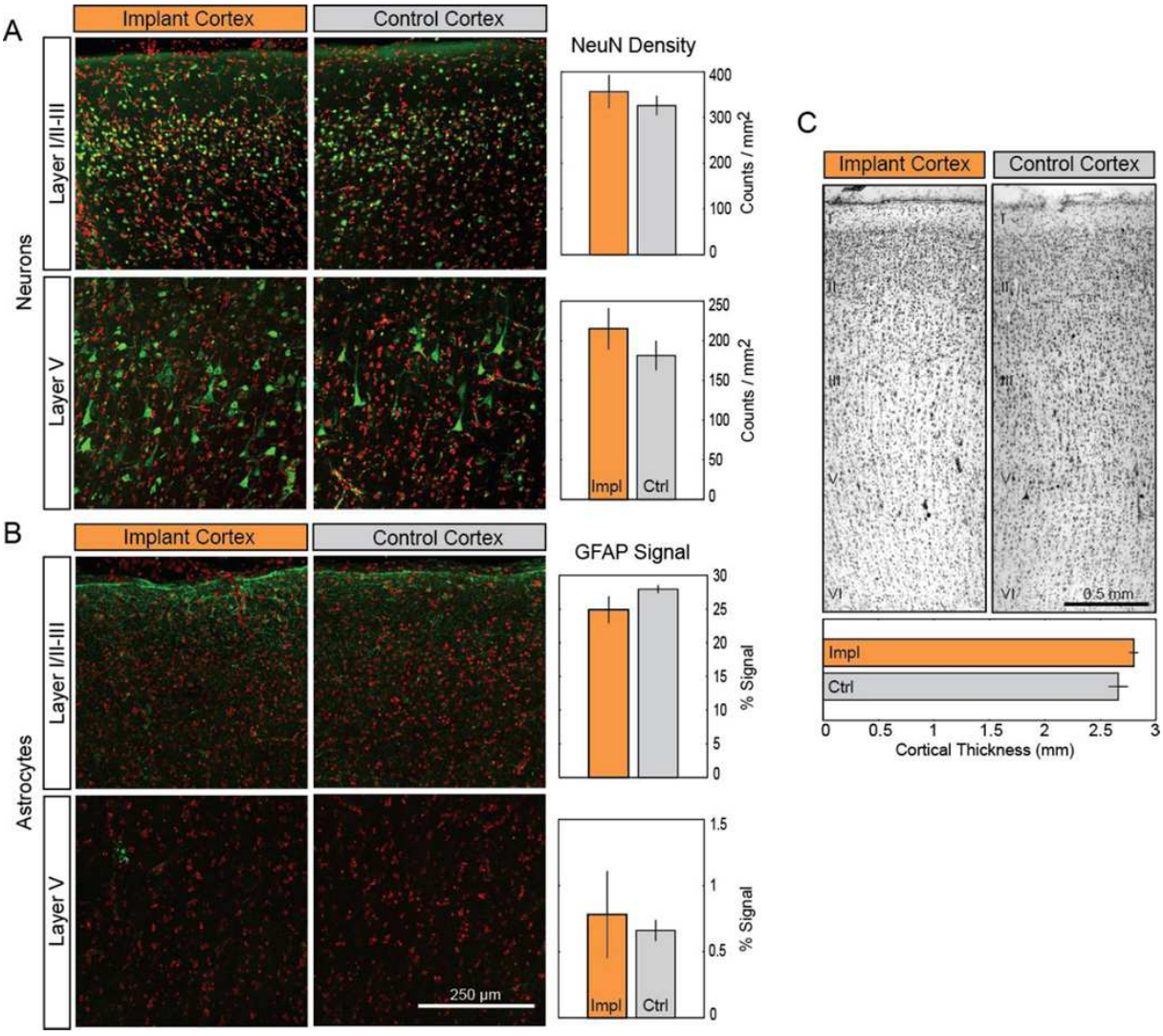

Figure 31: Example of biocompatibility analysis of brain tissue with the relative inflammation/neurodegeneration markers (from [137])

1.7 FLEXIBILITY

The mechanical properties of a neural interface are extremely important for in vivo applications and for the translation of these application in the clinical environment. In order to allow minimal implantation damage and to fit the curved surface of the neuronal tissues, device thickness, flexibility and bio-compatibility are the criteria to design functional ECoG electrodes that allow in vivo recording. Although conventional stiff and rigid neural interfaces can provide easy and reliable implants, however, they have some limitations in the long-term stability and biocompatibility of the implant. In fact, mainly due to micromotions, stiff implants are often able to operate for a limited

period of time before the degradation of the sensor substrate, delamination of the interfacial layer of the sensor [118], or formation of gaps between neurons and sensors [138]. Moreover, micromotions between the neural tissue and the implant can cause an inflammatory response of the surrounding tissues, thus leading to the device failure and the rejection of the implant itself [139]. On the other hand, soft and flexible materials allow to fabricate conformable interfaces able to adapt to irregular surfaces [140,141], providing a better match between implants and neural tissues with consequent reduction of inflammations and rejections. For this reason. soft, lightweight, flexible and organic materials are getting great interesting for the developing of neural interfaces. Given the softness of these materials, organic neural interfaces usually consist in non-penetrating implant and are typically oriented towards the subdural or epidural ECoG implants. Moreover, unlike penetrating electrodes, the position of soft and flexible ECoG arrays can be easily adjusted during surgery without damaging the brain tissues, thus ensuring that the implant perfectly adheres to the curved surface of the brain and make possible the recording in sites which are difficult to reach with the classical rigid implants. Another important advantage of flexible ECoG electrodes is that the implants fabricated onto organic substrates can be easily fabricated in a lot of different forms and shapes.

1.8 AIM OF THE PROJECT

The aim of this PhD project was to find new solutions to improve the existing neural interfaces in order to provide a permanent interface with the brain to people who are affected by several neurodegenerative diseases or neurological conditions, which do not allow them to interact with the external environment. These neural interfaces, if could provide high fidelity recorded signals, long-term stability and high biocompatibility with the brain tissue, can be a valuable tool to develop useful and reliable BCI applications. Neural electrodes have been successfully used and their clinical relevance has been demonstrated in many medical applications, but, despite the increasing research in this field and the recent improvements in the fabrication of these interfaces, there are still many issues that preclude the use of such electrodes in clinically accepted BCI applications. In particular, we have tried to address the main problems related to the use of existing neural interfaces, in particular:

- the biocompatibility with the brain tissue of the materials of which such neural interfaces are made;
- the long term electrical stability and reliability of the signal recorded by means of such interfaces;
- the flexibility of these neural interfaces, which often is limited and does not allow the recording in particular brain structures.

In order to do this, we decided to develop a device using Single Walled Carbon Nanotube (SWCNT) as conductive material for the electrodes and Medium Density Polyethylene (MD-PE) as substrate into which embed these electrodes. We chose to implant such device subdurally in laboratory rats in order to record subdural ECoG signals in a period of two months. In our experiments, we evaluated the flexibility of the fabricated devices, implanting these devices both on the dorsal (parietal association cortex) and the lateral cortex (primary somatosensory cortex) of laboratory rats and then we compared the electrical characteristics between the ECoG signals record on the dorsal cortex and those recorder in the lateral cortex. Furthermore, the flexibility of such devices was demonstrated also by the ability of such electrodes to record reliable Spike and Wave Discharges (SWDs) in a WAG/Rji rats and also by means of mechanical characterization of the whole device. Then, we characterize electrically the recorded ECoG signals and we evaluated their stability over time, comparing the signals recorded in the first week with those recorded in the last week of experiments. The biocompatibility profile of such devices was investigated by means of immunohistochemical and histological analysis of the brain tissue underneath the devices and comparing these data with those observed in the controlateral tissue, which served as control. Furthermore, as a demonstration that SWCNT electrodes are comparable with those available in the clinical setting, we realized a similar device with electrodes made in Platinum, which is the most used metal for the commercially available electrodes. Although the comparison is affected by the different fabrication process, we demonstrated that our SWCNTs electrodes are able to record ECoG signals, at least comparable with those recorded by means of electrodes made in Platinum. Finally, a special SWCNT/Polyamide composite electrode was also created, in order to demonstrate that SWCNTs can be used also to record reliable extracellular synaptic responses in ex-vivo experiments on rat's brain slices. In this work, our aim was to develop a highly flexible neural probe fully biocompatible for

subdural ECoG recordings. In this way, we would like to provide an answer to the major critical requirements for long-term ECoG implantations. Of course, additional experiments are needed and other aspects should be evaluated, for example the compatibility of such devices with imaging scanner, in particular with the Magnetic Resonance Imaging (MRI), so these findings should be considered as a first work toward the realization of a biocompatible, flexible and stable ECoG electrode array.

CHAPTER 2

DESIGN CHOICES

2.1 ECoG

We chose to record subdural ECoG since it is a method for recording of neuronal electrical activity directly from the cortical surface that provides optimal Signal-to-Noise Ratio (SNR) and finer spatial and temporal fidelity in comparison with noninvasive standard EEG. Furthermore, in the last years, subdural ECoG recordings have been proposed as part of BCI technology for neural motor prostheses that can enable people paralyzed by disorders such as amyotrophic lateral sclerosis, spinal cord injury or ischemic stroke to achieve successful closed-loop control of movements. ECoG has more advantages than other brain recording techniques, for example with respect to ElectroEncephaloGram (EEG) recorded directly from the scalp, because ECoG has much higher SNR, due to the presence of the scalp, the cerebrospinal fluid and the dura which act as filters for high frequencies, much higher spatial resolution. Morevoer, it is characterized by lower clinical risk, lower technical complexity and higher electrical stability with respect to single unit recording [70]. Taking into account advantages and disadvantages of all the techniques commonly used to record brain electrical activity, ECoG represents the right technological trade-off and can be considered a mesoscopic measure of neural activity [142].

Furthermore, it has been demonstrated that ECoG could offer the basis for developing BCI applications to help people with motor disabilities, providing results much better than those provided using EEG or intracerebral electrodes [61].

Nevertheless, commercial subdural ECoG electrodes have been already used for BCI applications in humans [143,144], but they can induce complications, such as infections

or hemorrhages, and this limit their usage to a restricted period of time. The development of biocompatible electrodes for subdural ECoG recordings can reduce considerably these kind of complications. For all these reasons, for this project, we decided to implant the fabricated ECoG micro electrodes subdurally on the cortex of laboratory rats, in order to demonstrate that the fabricated ECoG micro electrode array are able to record reliable ECoG signals in chronic conditions, without inducing complications to the rats, demonstrating that these arrays can be used for prolonged ECoG recording and thus for BCI applications.

2.2 MATERIALS

Before designing the device for the present project, we performed a preliminary study in order to choose the right materials to use for the fabrication of the micro electrode array, according to the aim of the project. Generally, the design and fabrication of micro electrode arrays for epidural or subdural ECoG recording, as a chronically implantable part of BCIs, should meet specific requirements [145,146]. In particular, the electrodes of these grids should have stable electrical properties, including low electrode/tissue impedance, good signal-to-noise ratio (SNR), appropriate mechanical properties, and biocompatibility, especially for long-term use. Normally, electrodes for invasive subdural ECoG recordings in humans are tailored in grids consisting of disks, usually made of metals embedded in a plastic film (generally silicon) and are usually made of metals. However, metal electrodes are not suitable for prolonged chronic applications, because they are heavy and, more importantly, undergo oxidation and degradation of characteristics over time [147]. So, the availability of stretchable, flexible, mechanically strong, and highly conducting electrodes with micro-sized diameters could offer ideal alternatives to replace the existing rigid and expensive noble metal electrodes in the ECoG grids. Knowing this, the aims of the preliminary study were essentially:

1. To choose which conductive material to use for the fabrication of micro electrodes;
2. To choose which substrate to use in order to embed the electrodes into.

2.2.1 CARBON NANOTUBES (CNT)

Since the discovery of carbon nanotubes (CNT) and of their interesting mechanical and electrical properties [148], large efforts have been devoted to obtaining composite materials based on CNT, both in their single-wall (SWCNT) and multi-wall form (MWCNT) [149]. As is widely recognized, due to their inert graphitic structure, carbon nanotubes are non-reactive and hardly soluble both in water and in organic solvents, which limits the possibilities of producing composites and, in spite of effort, no general recipe has been found [150–151]. The process of grafting of CNT onto polymer film surfaces is of particular importance for obtaining flexible and stretchable planar devices [152,153]. Indeed, such surface composites would find wide applications for sensors, electronic devices, artificial muscles, implantable prosthetic aids [154,155,156,157], extensible displays and even smart luminous clothing.

Being biocompatible and flexible, the CNTs have attracted great interest as a material for neurobiological applications [153,154], as these properties are very important for neuronal activity recording and stimulation [154,155,156]. CNTs have been used, for example, as capacitive electrode materials to overcome the limitations of Faradaic metallic electrodes, such as inflammation, tissue damage and low flexibility [155]. The availability of stretchable, flexible, mechanically strong, and highly conducting electrodes with micro -sized diameters could offer ideal alternatives to replace the existing rigid and expensive noble metal electrodes in the ECoG grids.

The use of this type of flat, stretchable CNT based probe, is justified by previous findings [153,158], showing that neurons easily colonize CNT bundles and meet the requirements of biocompatible, flexible and elasto-plastic neuroprosthetic devices for Brain computer interface (BCI) applications.

2.2.2 SINGLE – WALLED (SWCNT) VS MULTI WALLED (MWCNT) CARBON NANOTUBES

Purified SWCNT produced by the HiPCo method [159] were purchased from Carbon Nanotechnologies Inc.. Impurities declared by the manufacturer are less than 5%, mainly consisting of excess metal clusters catalizing CNT initial growth. As is widely known, this material appears as a black fluffy powder made of intertwined clusters of

dimensions ranging from fractions of a millimeter to few μm. Their average density is very low, so that these clusters easily float in air, while they tend to stick to surfaces where they deposit, making a precise measurement of the overall mass rather difficult. On Scanning Electron Microscopy (SEM) analysis, the material shows the complex coiling of single nanotubes, as well as of their bundles. The diameter of the individual SWCNT in this material is 0.7nm as declared by the manufacturer, which is approximately 40 times smaller than that of multi-walled carbon nanotubes (MWCNT, Aldrich), having an external diameter of the order of 20–40 nm. Both types of CNT samples have mixed chirality. In order to compare this two material, we performed a characterization by using Field Emission Gun Scanning Electron Microscopy (FEGSEM). Representative images of SWCNT and MWCNT we used, and of their very different arrangements in clusters, are given in the Figure 32.

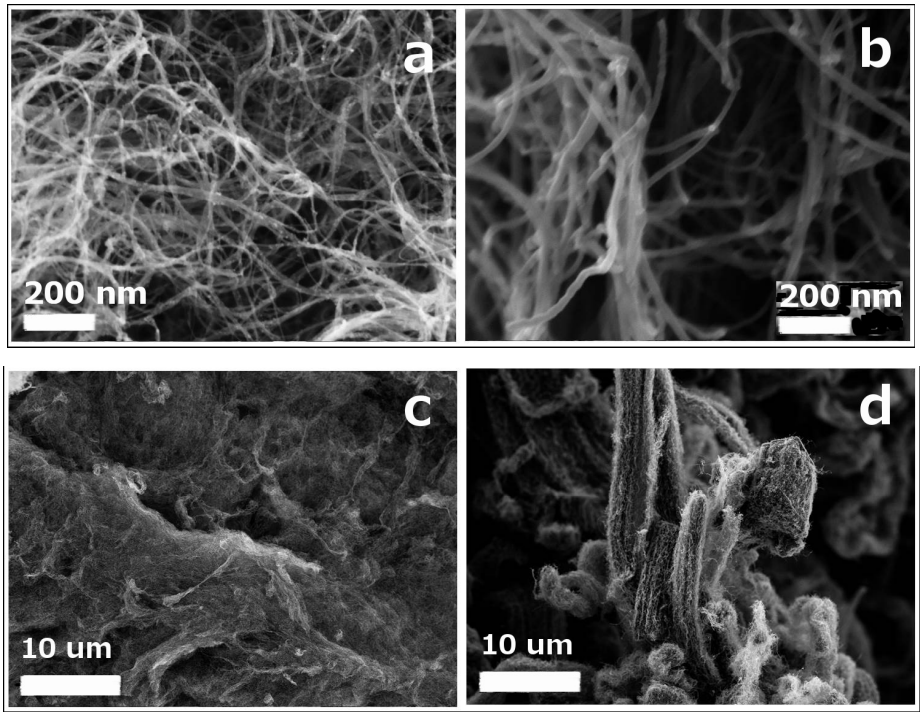

Figure 32: FEGSEM characterization of the Carbon Nanotubes used. a) SWCNTs as observed at high magnification (250000x) show a minimum dimension below 1 nm, together with bundles of several single CNTs of sizes around 5-10 nm; b) MWCNTs observed at 250000x show a distribution of sizes between 10 and 30 nm approximately. At lower magnification we can observe the different arrangements, more uniform for SWCNTs (c) and more organized in shaped clusters for the more rigid MWCNTs (d)

FEGSEM showed clearly that the buckling together in larger clusters is very different for the two types of nanotubes; in fact, while SWCNTs are interwined in a fairly uniform fashion (Figure 32 c), MWCNTs assemble to form well defined structures of typical sizes of 2-50 μm (Figure 32 d), tipically in columnar shapes or stacks of columns giving rise to sheets. Such uneven organization of MWCNTs may decrease the contact surface with a flat polymeric film. Furthermore, compared to SWCNTs, MWCNTs normally need some type of chemical or physical functionalization in order to bind polymers. For all these reasons, we choose to use SWCNT as conductive material for the fabrication of the electrodes.

2.2.3 POLYMERIC SUBSTRATES

As said before, electrodes for invasive subdural ECoG recordings in humans are embedded in a plastic film (generally silicon).

CNT-polymers composite materials may have a central role in flexible electronic applications [152,160] and the process of grafting of CNT onto polymer film surfaces is of particular importance to obtain flexible and stretchable planar devices [161,162].

We investigated the reliability of self-grafting of SWCNT bundles on several polymer films. In order to do this, various thin films of a number of polymers having different elastic and plastic properties have been investigated:

1) medium-density poly-ethylene (MD-PE);
2) high-density poly-ethylene (HD-PE);
3) acrylonitrile/butadiene (nitrile), a very elastic polymer;
4) poly-vinyl chloride (PVC);
5) Poly-isoprene chains, the main component of the natural rubber latex.

These polymers were chosen because of their biocompatibility and their viscoelastic characteristics; in particular we focused on two of them with opposite mechanical behaviors: highly elastic over a large extension range for rubber latex and elastic over a short extension range while highly plastic over a wider range for MD-PE.

2.2.4 FABRICATION OF COMPOSITE SWCNT-POLYMERIC DEVICE

The polymeric film substrate was pulled around a bulk aluminum cylindrical drum (4 cm diameter), which had an electric heater at the center and a thermocouple just under

its surface to control the temperature of the film. A stencil was then made out of 7 parallel steel or nylon 6 wires (0.5 - 0.3 mm diameter) which were slightly pulled around the drum to guarantee a perfect adherence of the wires to the film substrate, slightly squeezing the film against the aluminium drum surface. During the deposition of SWCNTs on the film surface, performed by slow drop casting, the temperature was kept at approximately 80°C; the ethanol/water solvent evaporated quickly at that temperature, leaving a brown/black deposit on the polymer surface. The operation was repeated until the space between the steel wires was completely filled and appeared uniformly black. To stabilize the adhesion to the film, we then raised the temperature of the dry deposit to approximately 110°C (few degrees below the melting temperature of the MD-PE film), and then let the film cool down naturally at room temperature.

2.2.5 CHARACTERIZATION OF THE FABRICATED SWCNT-POLYMERIC DEVICES

After the deposition, we carried out the first electrical characterization of the composite CNT/polymer composite wires by measuring the conductance as a function of their extension, the applied voltage and the temperature. To this purpose, the film carrying the conductive tracks was fixed onto a micrometric slide, with one side gripped onto the static part and the other-to the cursor part by means of copper jaws electrically connected to a multimeter. Particular care was taken to avoid slipping of the film out of the copper gripping plates as a consequence of film stretching and thinning. This was obtained by inserting a thin strip of a sanding tissue on one side of the gripping jaws, making sure that the CNT tracks were in firm contact with the other copper jaw. The slide was placed under the objective of a stereomicroscope to observe visually the process of stretching of the CNT tracks. Resistance values of CNT tracks were acquired by an Agilent 3458A digital multimeter. To avoid polymeric film charging, SEM characterization was performed, after sputter-coating the composite film surface with gold, at an incident beam energy of 15-20 keV, mostly at low incidence angle. Some of the carbon nanotube coated films were cut by sharp scissors and the exposed section was carefully explored by SEM looking for those regions where the SWCNT grafted film does not cover and obscure the polymer.

The SEM images in Figure 1 show how the self-grafted SWCNTs ropes hold a large layer onto a polymeric film surface by deep physisorption mechanisms. We brushed the

specimens vigorously before observation in order to remove any loosely attached nanotube bundles. Figure 1 shows a notably different behavior of the SWCNT grafting mechanism onto MD-PE and natural rubber latex (predominantly made of poly-isoprene chains) substrates: the first layer of bundles of SWCNTs grafted and anchored to poly-ethylene film in (Figure 33 a) covers its surface almost completely, while several "ropes" of SWCNTs hold an upper layer, or flake, of conductive material strictly bound onto the first one; Figure 33 b shows the corresponding resistance vs. strain behaviour for a 15 mm long, 800 μm wide SWCNT conductor grafted on a 25 μm thick PE film. A fairly large hysteresis can be observed on releasing the composite conductor strain, due to the low elasticity of MD-PE. On the contrary, Figure 33 c shows that after our brushing procedure, only a much thinner SWCNT layer is left at the rubber latex surface, almost completely embedded in the polymer; the SWCNTs hardly appear above the surface, and yet endow the polymer with non-negligible electrical conductivity. As shown in Figure 33 d, due to the very elastic nature of the poly-isoprene rubber chains, such low conductivity of the much thinner residual conductive layer (compared to the PE grafted CNT layer) shows negligible hysteresis. Also, this high resistance conductor has a reliable strain dependence on different strain-release cycles (Figure 33 e). Thus, in these two extreme cases (highest plasticity and highest elasticity among all the polymers used in the present study), we observed different structuring of the grafted layer: the PE chains appear to wet more deeply the CNT bundles on heating the composite material to about 110°C (just below the melting point of MD-PE) allowing for better adhesion of the upper SWCNT layers on PE with a consequent higher conduction with respect to rubber latex where the upper layer easily delaminates; but the strained MD-PE/SWCNT composite does not easily return to the original conductance after releasing of the conductor. Therefore, these two composites are suitable for different applications: in particular, the plastic PE based composite is suitable for uses where the conducting wires need to be shaped on a 3-D surface.

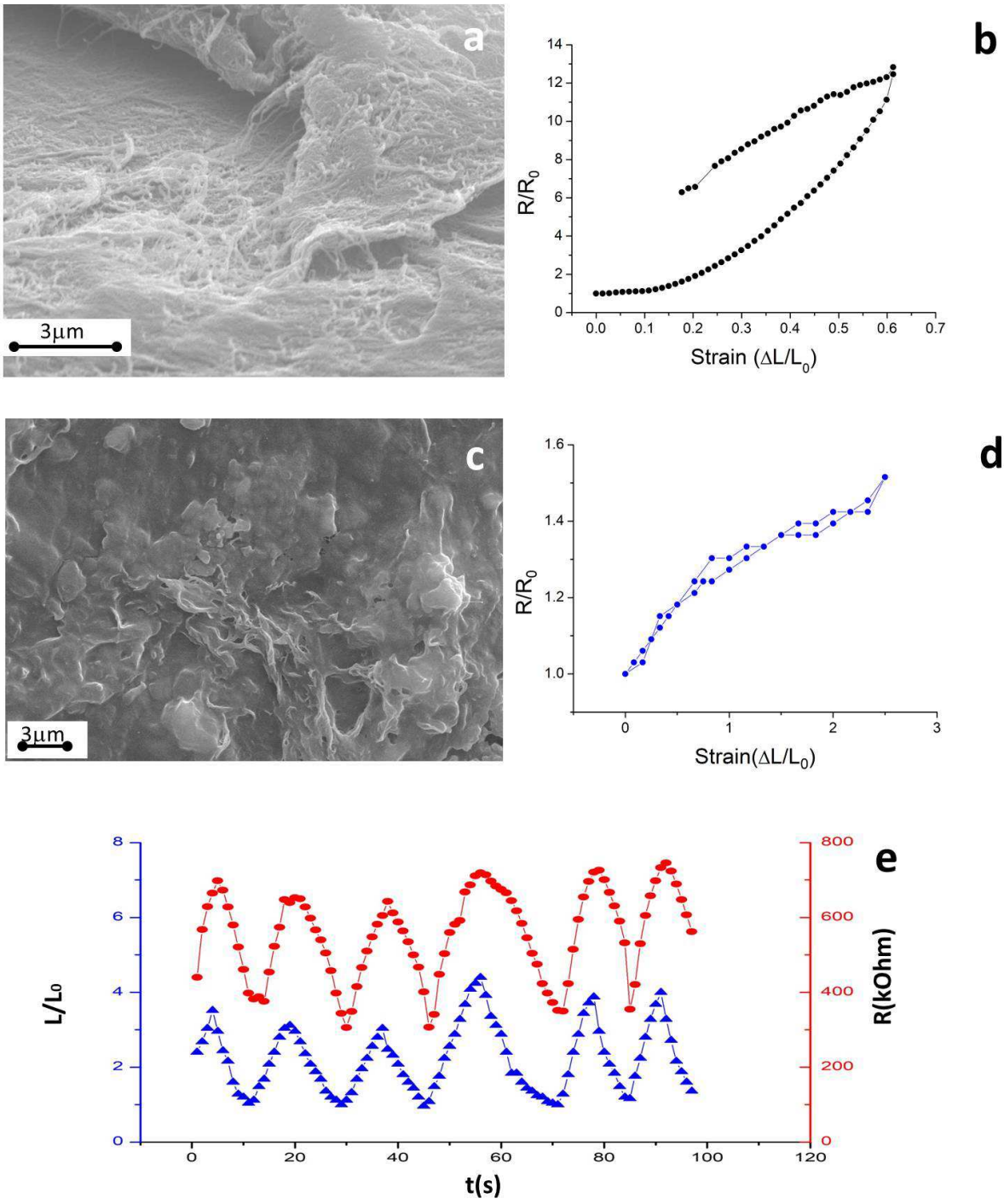

Figure 33: Characterization of the fabricated SWCNT-polymeric devices. (a) SEM image of self-grafted SWCNTs onto poly-ethylene film; (b) resistance vs. strain behavior for a 15 mm long, 800 µm wide SWCNT conductor grafted on a 25 µm thick PE film; (c) SEM image of self-grafted SWCNTs onto rubber latex surface; (d) resistance vs. strain behavior of 800 µm wide SWCNT conductor grafted on the rubber latex surface; (e) strain dependence on different strain-release cycles

Figure 34 shows the same type of resistance-strain plots also for poly-vinyl chloride, poly-acryl-nitrile and HD-PE composites, together with the MD-PE composite for comparison. Depending on the polymer, the electrical conductivity varies more or less, allowing for a wide choice of ranges of strain sensing in different application fields. Analysis was also made with the purpose of testing potential electronic applications with applying an increasing voltage to the SWCNT wires.

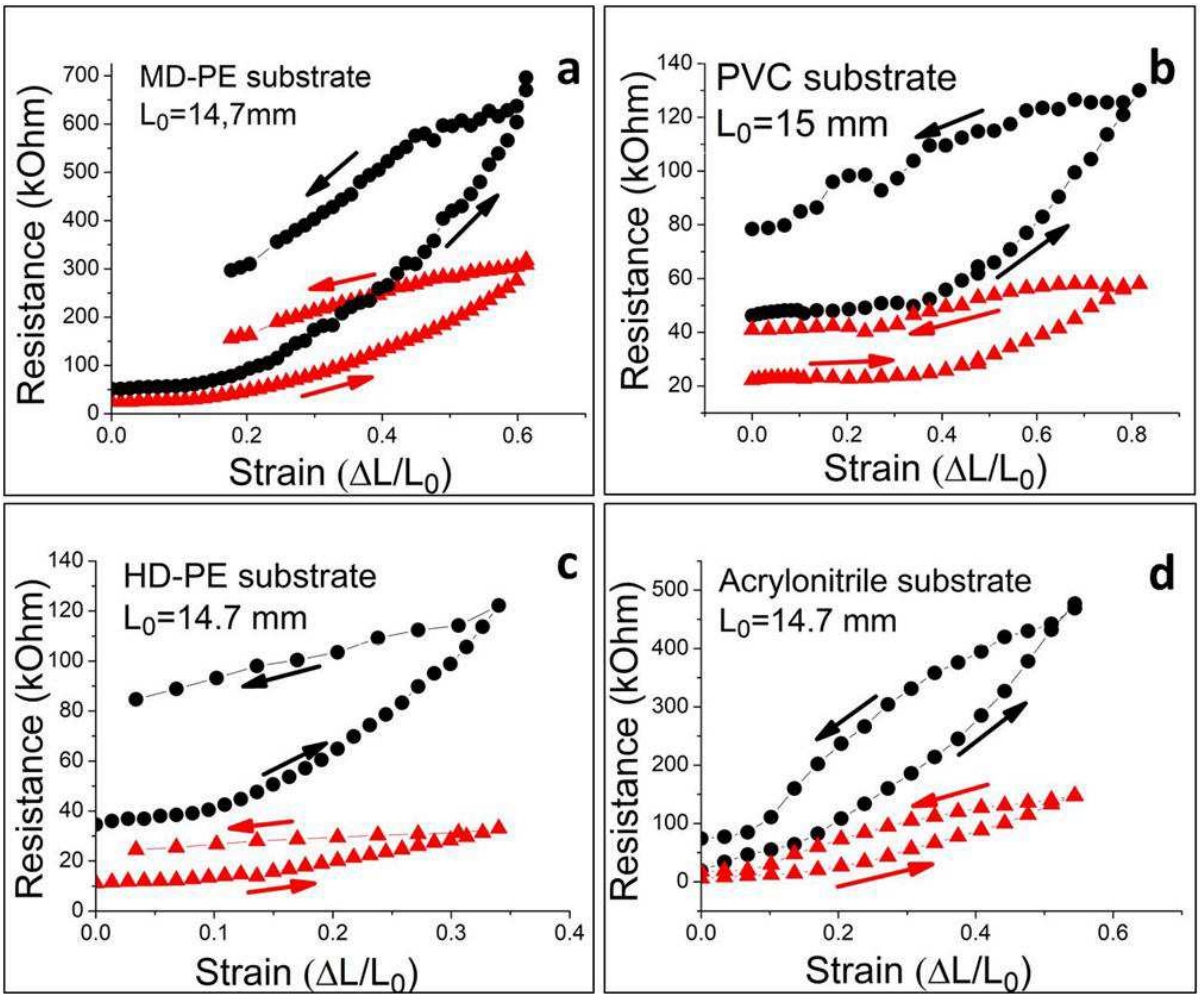

Figure 34: Comparison of resistance-strain plots of the different polymers. MD-PE composite (a), poly-vinyl chloride (b), HD-PE (c) and poly-acryl-nitrile (d)

Figure 35 reports the trend of temperature versus current flowing through a 3 mm wide, 10 μm at controlled applied voltage. The quasi-ohmic behavior of wires is shown in the inset, while the figure reports the wire temperature evolution as a function of current in a cyclical variation from 0 to 28 mA and back. The hysteresis is not due to the electrical

properties but only to the thermal capacity of the composite material. To understand the limits of CNT wires for application, we studied the current and temperature behavior on increasing the voltage up to the breakdown threshold.

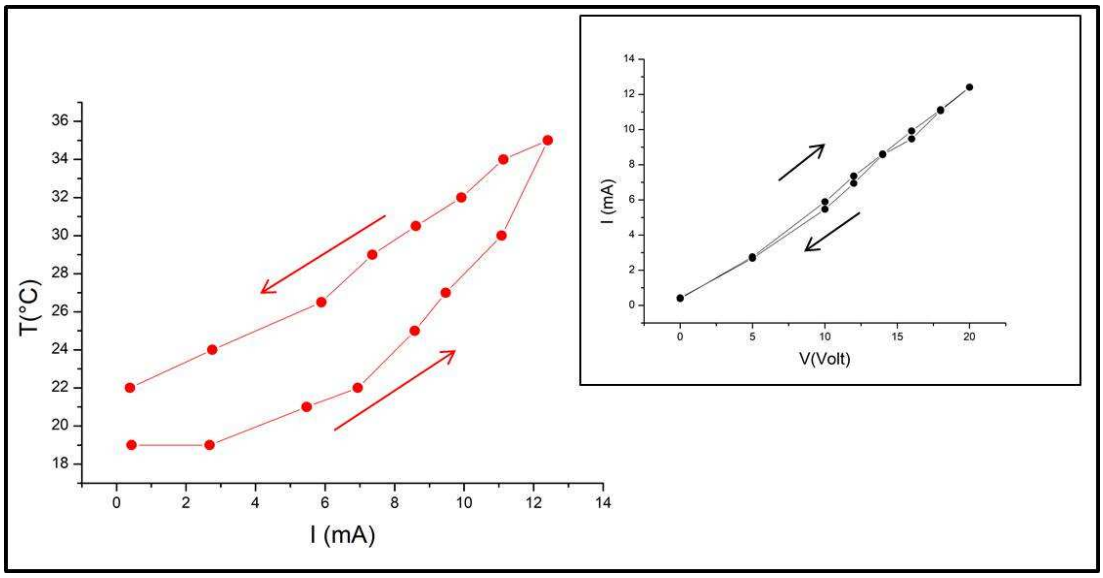

Figure 35: Temperature versus current flowing through a 3 mm wide, 10 µm at controlled applied voltage

Figure 36 shows the temperature dependence (red dots and red scale on the right) and the current dependence on the applied voltage (green triangles and green scale on the left).

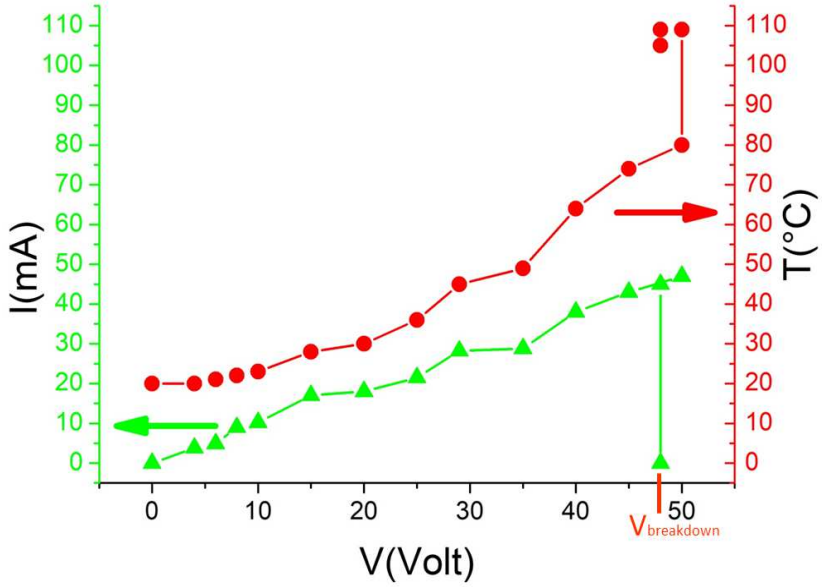

Figure 36: Temperature (red) and the current (green) dependence on the applied voltage

Figure 37 shows part of the active area of the device, where the 50 μm apertures, laser drilled in the polymer MD-PE film, and then covered by the SWCNT conducting tracks on the membrane side (facing the dura mater), serve as electrodes.

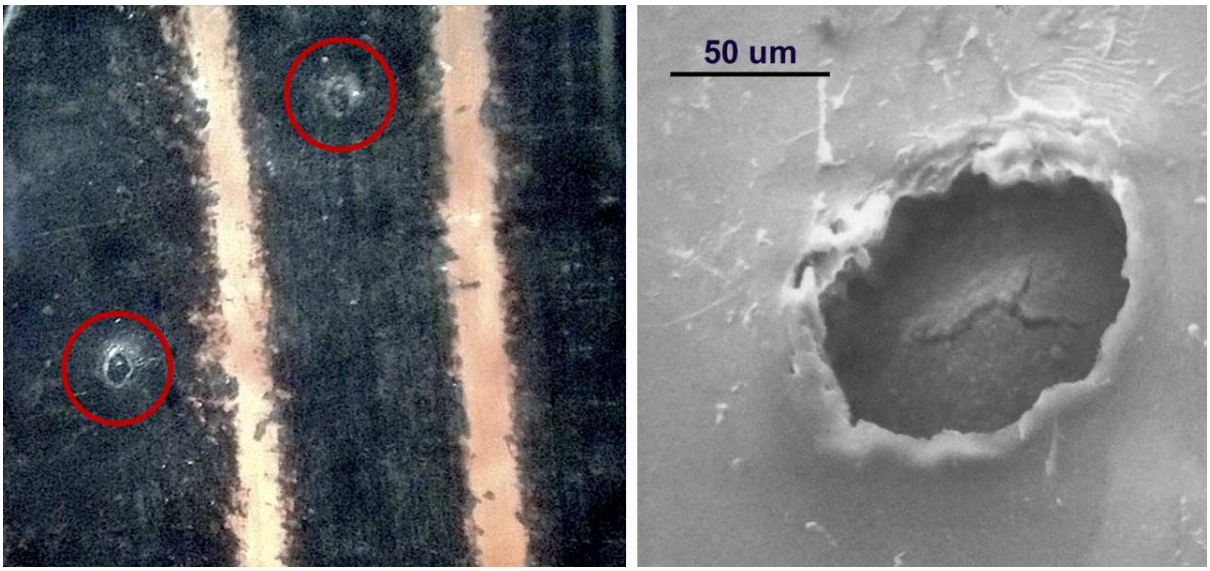

Figure 37: A picture of the active area of the device. The 50 μm apertures, laser drilled in the polymer MD-PE film, served as electrodes (red dots)

We carried out the first electrical characterization of the conducting CNT/polymer film wires by measuring their conductance as a function of track length. This was performed by platinum wire microprobes micrometrically shifted by a micrometric slide (Carl Suss) along a 0.8 mm wide track on a MD-PE film glued on a rigid substrate. Further characterization was made by measuring the current through the conducting CNT tracks versus applied voltage and versus film stretching. To this purpose the film was immobilized on a micrometric slide, with one side gripped onto the static part and the other gripped to the cursor part. Particular care was taken to avoid sliding of the film out of the copper gripping plates as a consequence of film stretching and thinning. This was obtained by inserting thin strips of sanding tissue on both sides of the gripping plates (see Figure 38) making sure that the CNT tracks were in firm contact with the copper. We placed the slide under the objective of a stereomicroscope and observed the process of stretching of the CNT tracks deposited on the polymer. Simultaneously, resistance values of CNT tracks were acquired by an Agilent 3458A digital multimeter.

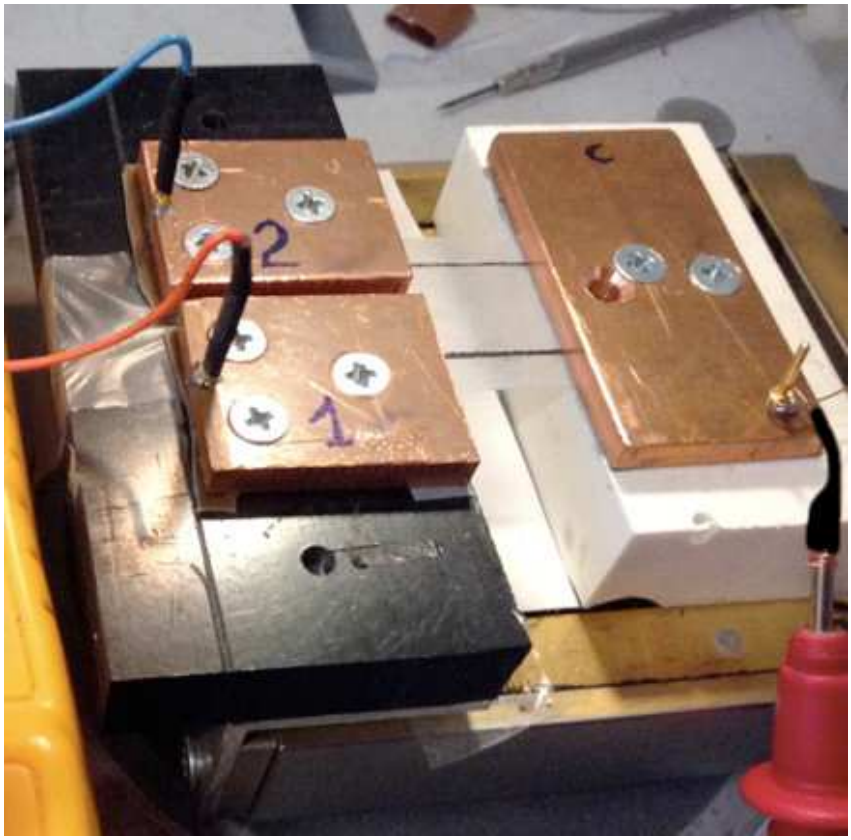

Figure 38: The resistance vs. strain measuring system. Copper clamping plates press the polymer film against a stripe of sanding tissue to increase friction and avoid slipping of the film out of the clamping electrodes. This configuration allows for simultaneous recordings of resistance vs. strain curves for two wires of different sections and resistances

Figure 39 demonstrates the almost linear behaviour of the current (I)-voltage (V) plots of four SWCNT wires, together with the resistance measured vs. distance between two microprobes sliding along a 500 μm wide SWCNT wire, grafted onto an unstrained MD-PE film. Although the latter curve is noisy at a few points where the microprobes met with some inhomogeneity of the bundled layer, it shows on average an almost linear ohmic behaviour. The I-V curves in Figure 39 a show significant spread in the slopes, i.e. in the resistances, of apparently similar wires. This may be due to the fluctuations in the SWCNT wire thickness because of the non-uniform manual casting.

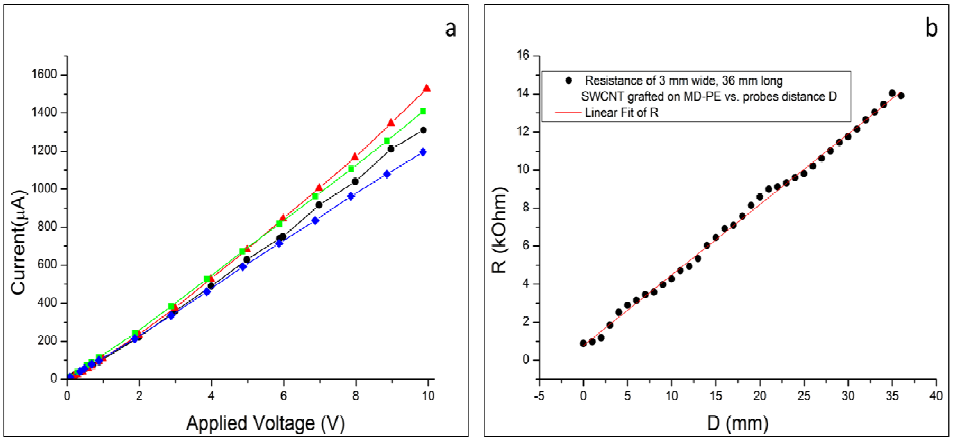

Figure 39: current (I)-voltage (V) plots of SWCNT wires. (a) I-V curves of four wires of the same width and length; (b) plot of resistance vs length measured by shifting a needle probe along a 3 mm wide, 36 mm long SWCNT/MD-PE track. The red line is a linear fit

2.3 ANIMAL MODELS

Male 6–7 months Wistar (mean body weight ca. 250 gr) and one WAG/Rij rats (weight ca. 350 gr, 6 months age) served as experimental subjects. The rats were born and raised in the animal facility of IRCCS Neuromed. Rats were kept in cages on a 12:12 light cycle (lights off phase between 6:30 and 18:30), at a constant ambient temperature of 21 °C with food and water ad libitum. All efforts were made to restrict the number of rats and to limit discomfort. The experiments were conducted in accordance with the legislations and regulations for animal care and were approved by the Ethical Committee of IRCCS Neuromed and approved from the Italian Ministry of Health. Distress and suffering of animals was kept to a minimum. For our experiments, we used 5 healthy Wistar rats and 1 WAG/Rji rat. The Wistar rat is an outbred stock, used in all fields of medical and biological research. Wistar rats encompass a number of rat substrains that have been derived from a common lineage over the past 50+ years. We used these rats in order to record non pathological ECoGs. The WAG/Rij rats are descendants of an inbred strain, that was originally created by A.L. Bacharach in 1924 from outbred Wistar rats, maintained by Glaxo laboratories in UK, then kept at the Radiobiological REPGO institute of TNO in Rijswijk, the Netherlands, by Harlan (from 1994) onwards, by the Department of Comparative and Physiological Psychology (now Donders Centre for Cognition) of the Radboud University Nijmegen from the mid

seventies, and also since the late sixties or early seventies of the previous century by Yale University, School of Medicine, New Haven, CT, USA. They were obtained from the colony of IRCCS Neuromed. Rats of the Wistar Albino Glaxo/Rijswijk (WAG/Rij) strain represent a genetic absence model, and they develop spontaneous absence seizures after 2-3 months of age [163,164]. WAG/Rij rats are currently at the forefront of basic research towards mechanisms involved in the pathogenesis of absence epilepsy. Absence seizures are non-convulsive seizures associated with bilateral symmetrical so-called "generalized" spike-and-wave discharges (SWDs) at the EEG, which are generated by pathological oscillations of a cortico-thalamo-cortical neuronal network formed by the somatosensory cortex, the ventrobasal thalamic nuclei, and the reticular thalamic nuclei [165]. We used a WAG/Rji rat in order to demonstrate that the fabricated electrodes are flexible enough to mantain a good contact with the lateral cortex, in particular in the primary somatosensory cortex (perioral region), were cortical source of SWDs are situated.

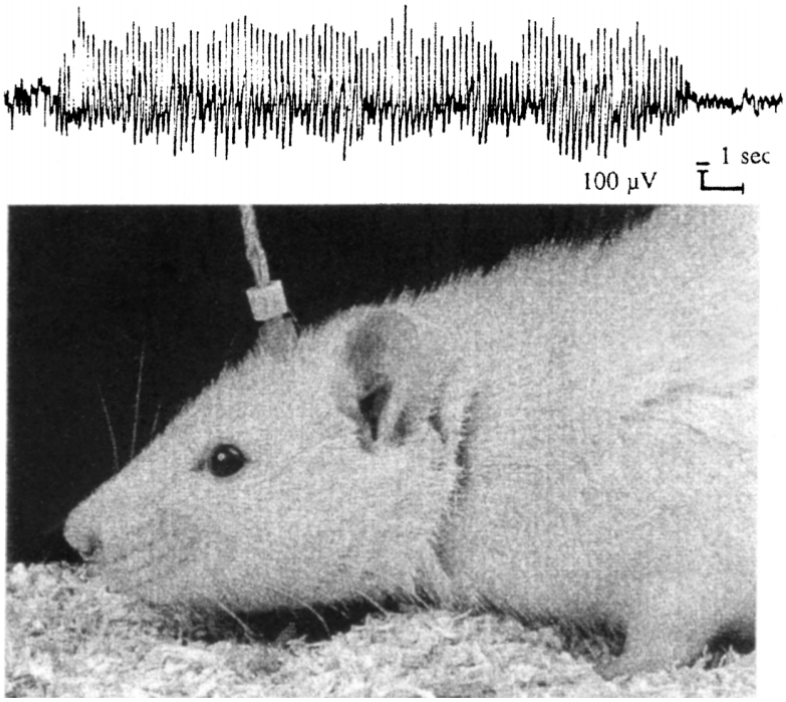

Figure 40: A WAG/Rij rat, with a typical spike-wave discharge (from [166])

2.4 VIDEO-EEG

Video-EEG monitoring is an important diagnostic tool that is generally used to confirm the diagnosis of epilepsy and classify epilepsy type. It consist in the simultaneous recording and displaying of EEG/ECoG patterns and the behavior of the monitored subject and may be used to confirm the diagnosis of epilepsy, to classify seizure type, assess seizure frequency, and for surgical localization of epilepsy focus [167-171]. Video-EEG allows to record and monitor additional physiologic parameters including electrocardiogram (ECG), electrooculogram (EOG), electromyogram (EMG), and other biological parameters [172]. In adult patients, video-EEG monitoring is used predominantly for diagnostic classification (i.e., epilepsy vs. nonepileptic spells), and to evaluate surgical candidacy in patients with medically refractory partial seizure disorders. Video-EEG monitoring is essential in determining the localization of the epileptogenic zone (i.e., the site of seizure onset and initial seizure propagation) in adult patients being considered for surgical ablative procedures [173].

In order to monitor animal's behavior during the recording, a video-EEG system was used for the ECoG recording. In this way, it was possible to check, together with ECoG signal, the animal's behavior and to visually identify the different sleep stages quiet (passive) waking (PW), slow wave (SWS-1 and SWS-2) and paradoxical REM sleep and correlate them to the ECoG signals. This allowed us also to identify artifacts in the ECoG signals, due, for example, to the shaking and/or hitting the recording cable by the animal. Each ECoG session was acquired using A Grass-Telefactor video-EEG acquisition system (Astro-Med, Inc., W. Warwick, RI, U.S.A.).

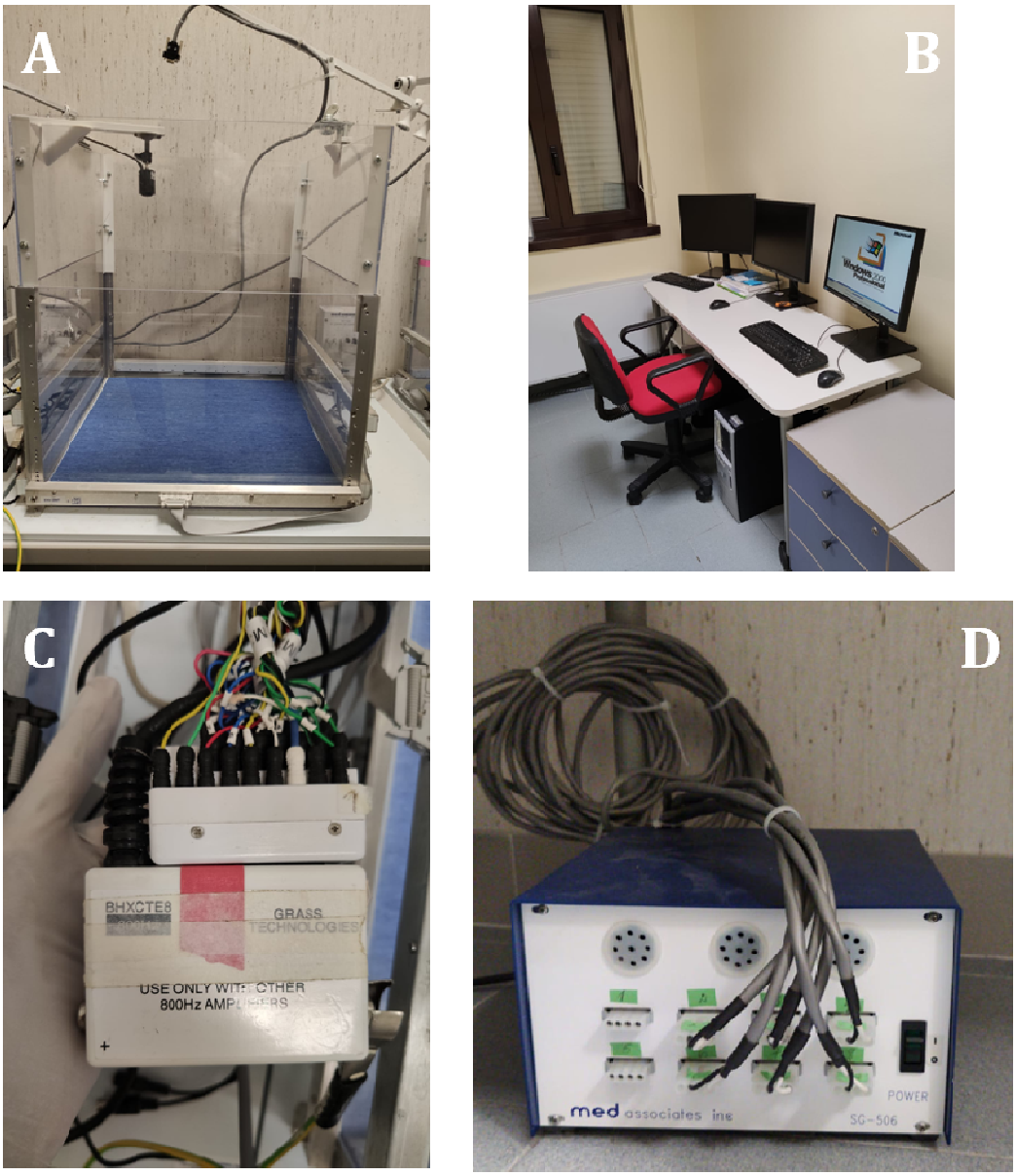

Figure 41: The Video-EEG system used for the experiments. A: the box where the animal was during each recording, with the integrated camera and tethering system; B: The computer running the software displaying the signal and the simultaneous video; C: the amplifier headbox; D: the video acquisition system

CHAPTER 3

METHODS

3.1 DESIGN AND CHARACTERIZATION OF THE ECOG ARRAYS

Each rat was implanted with one electrode array and each array was tailored to be compliant to the cortical regions of interest. Four SWCNT arrays, one mixed array with SWCNT and Pt electrodes and one array with only Pt electrodes have been used. A schematic layout of one of the devices is shown in Figure 42. The remaining panels in the figure show the fabrication procedure for electrodes and conductive tracks. The conductive tracks and electrodes in the arrays were deposited and embedded in a medium-density polyethylene (MD-PE) film substrate (weight, 0.94 g/cm3, thickness 25 μm, dimensions 4 mm × 22 mm). Apertures in the film were drilled by Pulsed Laser Ablation (PLA) in micrometrically determined positions. The apertures exposed micrometric areas (diameter ~ 50 μm) of the conductive single-walled carbon nanotube (SWCNT) tracks deposited on the opposite face of the film, which served as ECoG electrodes when positioned on the cortical surface. The polymer film substrate served as insulating membrane between the conductive tracks and the cortex (pia mater). The SWCNT conductive tracks (0.4-0.7 mm wide) were deposited by drop casting of a suitable suspension taking care that the sensing micro-apertures were completely obstructed by the SWCNT track. The center-to center track distance was 0.9±0.1 mm. Platinum (Pt) tracks (0.5 mm wide) were deposited by Pulsed Laser Deposition (PLD) through suitable stencils. The surface of the Pt target was locally vaporized in a plasma plume and deposited as a thin film on the sample, facing the target. The micro-drilled MD-PE film was completely protected by a metal mask except for the area to be covered by the conductive tracks. To obtain probing areas comparable to those of the SWCNT

electrodes, each Pt electrode was made of a pattern of 3x3 micro-apertures, partially obstructed by the Pt deposition (<10μm diameter) with a total surface of the same order as that of the larger single aperture in the SWCNT tracks.

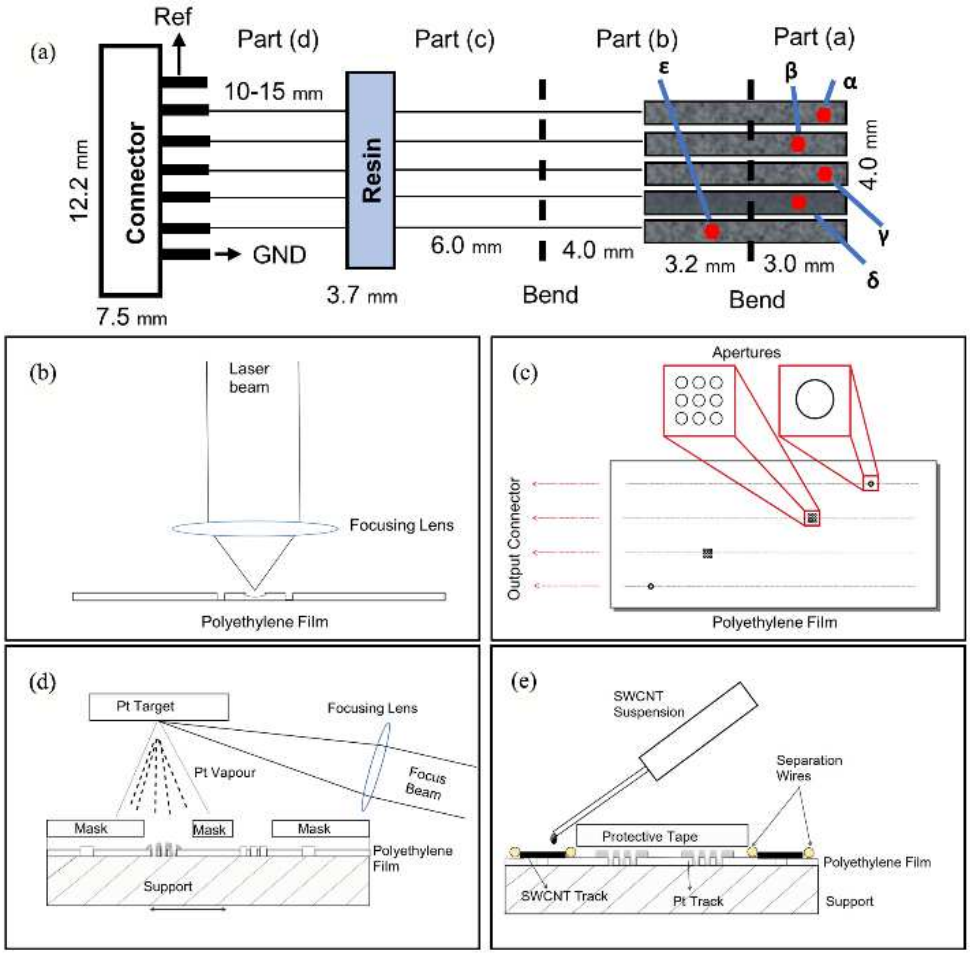

Figure 42: Scheme and fabrication methodology of the devices. (a) The flexible part contained three main sections: Part (a), which was positioned on lateral brain convexity (primary somatosensory cortex), Part (b) positioned on the dorsal convexity (parietal association cortex) and Part (c) with only tracks (without electrodes). The red dots are the electrodes. The hard part (Part d) contained stainless steel insulated wires, embedded in a silicone rubber and served as intermediate connections between the SWCNT (or Pt) tracks/electrodes and the pins of a connector. Two of the pins of the connector served to connect two screws fixed on the scalp as reference (Ref) and ground (GND) electrodes. (b) Pulse Laser Ablation (PLA) configuration; (c) micro-hole patterns on the MD-PE film:10 microns diameter, 3x3 apertures array for Pt electrodes, single 50 microns diameter aperture for SWCNT electrodes; (d) PLD technique of Pt tracks; and (e) drop casting deposition of the SWCNT tracks

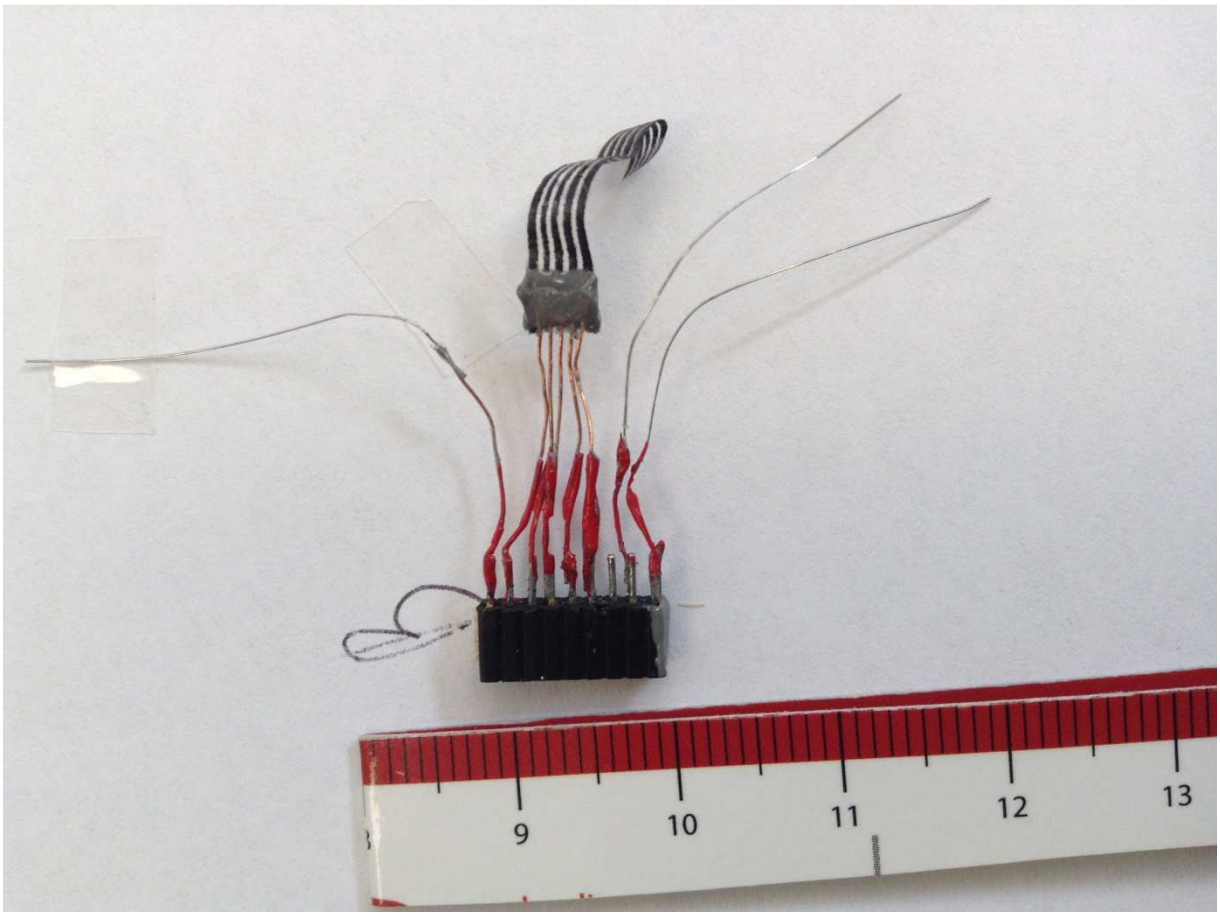

Figure 43. The layout of the device used for the in vivo experiments

3.2 DESIGN AND CHARACTERIZATION OF SWCNT- POLY-AMIDE PROBES FOR EX-VIVO RECORDING

In order to probe thin and extremely delicate brain slices with no damage and high spatial precision, a thin, soft and flexible specific electrode was fabricated. A 40 mm long poly-amide (PA) fishing line, 0.30 mm diameter (Caperlan Line Resist) was immersed in a SWCNT dispersion for 5 minutes and then heated at 110°C. The procedure was repeated 5 times to obtain a homogenous layer of SWCNT on the total surface of the polyamide (PA) wire. Then the conductive SWCNT/PA wire was inserted in the signal wire of a BNC coaxial cable insulated by a heat shrinkable sheath (Figure 44) and finally soldered to the connector's pin. The resistivity (measured after deposition of the SWCNT) varied in different devices, from 0.6 to 2 kOhm/cm.

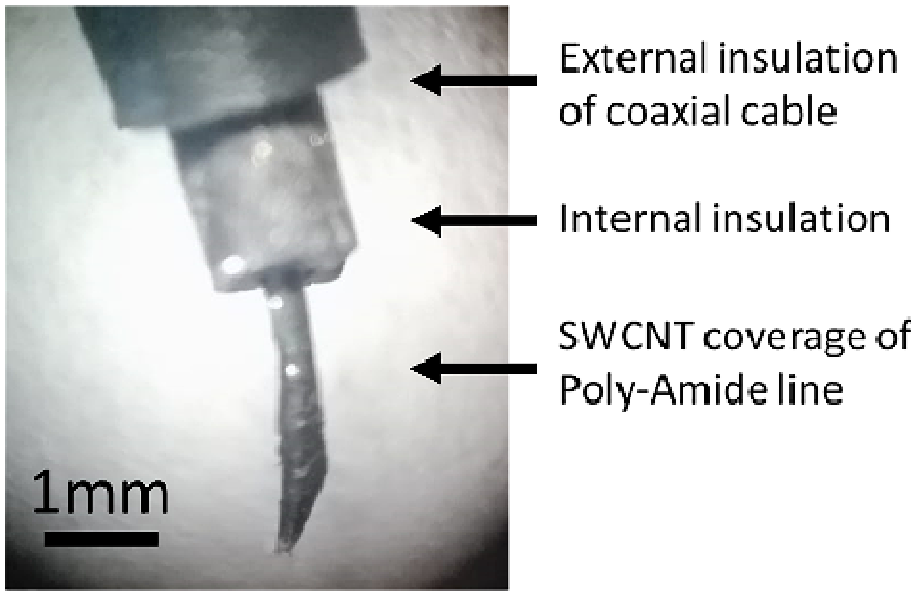

Figure 44. Optical image of CNT/PA composite wire for ex-vivo electrical activity recording

3.3 SURGICAL PROCEDURES FOR ELECTRODES IMPLANTATION FOR IN-VIVO ECOG RECORDINGS

The procedures used in this study were approved by the Ethics Committee of IRCCS Neuromed and by the Italian Ministry of Health. Before performing the surgery to implant the device in the rat's brain, we followed an internal protocol for its cleaning and sterilization, in order to eliminate as much bacterial contamination of the tissue as possible. For this purpose, one day before the surgery, we placed the device into a small container, which had been previously sterilized for 20 minutes in an autoclave (Systec V-series) at 120oC. Then, we placed the container in a solution of penicillin-streptomycin (Pen-Strep, 10000 U-10 mg/ml, Sigma-Aldrich) for approximately 2 hours. We performed these two steps of the protocol under fume hood (VBN Compact cabinet). Immediately before the surgery, we removed the device from the container and cleaned the connector and wires with Ethanol 100%. Then, we washed the entire device with phosphate buffer (PBS) solution to remove any residual Pen-Strep solution and dried it by means of a dryer, cleaned previously with Ethanol 100%. For surgery, the rat was anesthetized with a solution of mixture of Ketamine hydrochloride (60 mg/kg) and Xylazine (12 mg/kg) injected intramuscularly. We tested the death of anesthesia using

two tests: the reflex test by foot pinching and the test of muscle tone by pulling on a limb. If the rat went out of the anesthesia, we added approximately 20% additional volume of the mixture. When anesthetized, the skin over the dorsal surface of the cranium was soaked with 10% Polivinilpirrolidineiodine O.P. (Pharmatek PMC) and then shaved. When the rat was fully anesthetized, it was placed into a stereotaxic frame (World Precision Instruments, LLC, FL) with its head in horizontal position (bregma and lambda were at the same horizontal plane). We placed the rat on a heating blanket and the body's temperature was maintained at 370°C using a rectal probe and a feedback-controlled electronic device ATC1000 (World Precision Instr.). After local anaesthesia with 2% Lidocaine (Astra Pharma Inc.), we made a coronal section of the skin in order to expose the dorsal surface of the skull by retraction of the periosteum over both hemispheres and carefully cleaned the calvarium from any organic substances and bone chips. We made four holes in the skull with a fine drill bit (size 0.7 mm) for drilling screws in them. The drill press was not used for more than 15 seconds continuously and the skull was bathed with sterile saline every 10–15 seconds to avoid thermal damage to the cortex due to drilling. First, we fixed epidurally two stainless steel screws (TX0.2, 0x1/8 SL FLT TY A S/S) with thread diameter 1.4 mm and length 2.64 mm into the skull of the left hemisphere: one fixed anterior to bregma near the midline, served as reference (Ref) electrode, and the second fixed posterior to Lambda, served as ground (GND) electrode (Figure 45 a). We fixed another 4 screws (00-80 x 3.32, Plastics One Inc., VA) to serve for implant anchoring. The threads of the anchoring screws were wrapped around with a piece of insulated stainless-steel wire in order to increase the stability of the implant. The Ref and GND screws were connected with the gold-plated pins of a male socket by means of small pieces of PFA-coated stainless steel wires (A-M Systems, Inc., WA) with diameter of 127.0 μm (bare)/203.2 μm (coated). To have access to the lateral convexity of the brain, we cut the temporal muscles in lateral direction of approximately 6 mm length. The main steps of the surgery procedures are shown in Figure 45.

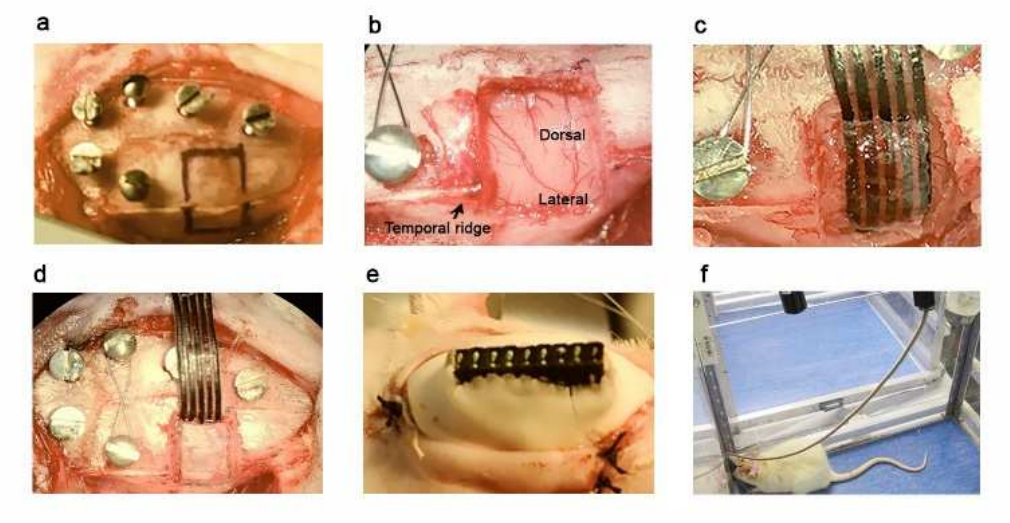

Figure 45: Surgery procedures. (a) - View from above the rat's head with 6 screws fixed on the skull, 4 for anchoring and 2 for Ref and GND. The position of the bone window is outlined with a black marker; (b) - cortical surface after removing the bone and dura mater in the window. Temporal ridge of the skull is marked with an arrow; (c) - the device is attached to a frame of a stereotaxic apparatus for precise positioning of the grid in the bone window; (d) - the grid covered with the dura and the bone flap. The remaining part of the device with interfacing wires and connector is placed on the unopen skull of the left hemisphere; (e) - the rat's head with the cement cup of the implant; (f) - the rat in the recording box one week after the surgery

We made a cranial rectangular window in the right hemisphere (Figure 45 a) oriented medio-laterally using the following coordinates: anterior-posterior (AP), from +1.5 to -5.0 mm and medio-lateral (ML), from 0.2 to -6.4, with bregma as a reference. The dimensions of the bone window were almost equal to those of the part of the grid containing the electrodes [Part (a) and Part (b) in Figure 45]. The craniotomy was made by thinning the skull using a high-speed dental drill. The skull was periodically bathed in saline to ensure that the underlying cortex did not experience thermal damage from drilling. After opening the bone window, possible bone chips were washed away with sterile saline until the dura surface was clean. Care was also taken to prevent vasculature damage during drilling and removal of the bone (Figure 45 b). We kept the bone flap aside in sterile solution. By using an optical microscope, we cut the dura very carefully with a 27-gauge injection needle, then we held the edges of the incised dura with fine biceps and made sharp dissections using microscissors. The cutting was made near to the most anterior and both lateral margins of the bone window, then the dura

was retracted over the posterior bone margin in such a way that the exposed pia surface remained clean and undamaged (Figure 45 b). In order to prevent drying, the exposed brain surface was treated regularly with warm sterile saline. The device was then secured to the stereotaxic holder (Figure 45 c) using sterile tape making sure that the electrodes were facing downward the cortical surface. Then, we advanced the stereotaxic arm over the open window and positioned carefully the grid in direct contact with the cortical surface. We sneezed a very small portion of the most lateral part of the grid under the temporal bone in order to fix a bit the grid. Then we repositioned the dura mater and the bone flap over the exposed cortical surface under microscope visualization (Figure 45 d) and carefully coated the bone flap with biocompatible ionomer glass cement (KetacTMCem radiopaque). After hardening of the cement, we connected the wires from the Ref and GND screws to a female 9-pin connector, to which the wires from the grid electrodes have been previously soldered. Then, we placed both the soft part of the device with interfacing wires as close as possible to the skull of the left hemisphere, and covered with cement the anchoring, Ref and GND screws, together with their connected wires, thus creating a well fixed to the skull headcup of cement (Figure 45 e). Finally, we sutured the temporal muscles over the lateral part of the bone and the skin flaps around the headcup with a 4/0 chirurgical absorbable file. After the surgery, a powder of antibiotic Bimixin was applied copiously around the wound. Animals were then removed from the stereotaxic apparatus and allowed to recover on a heated pad placed under their body and a bit later in a Termo Scientific incubator (Termo Fisher). Then we placed the rat in a plastic cage of a volume of 800 cm2 with sufficient height (18 cm) in such that the animal to not touch the cage's ceiling with the implant. During the first 1-2 days after the surgery, the food (standard pellets) was placed on the floor of the cage in order to facilitate the access. The animals were treated daily for 7 days after the surgery with antibiotic Baytril 2.5%, 0.1 ml/kg subcutaneously (diluted with Saline 200 μl/rat) and anti-inflammatory drug Voren, 0.1 ml/kg i.m. During all in-vivo experiments, light and temperature were kept constant (light:dark 12:12, 22±10C); food and water were available ad libitum. The experiments started only after the weight and the behavioral activity of the animals were fully recovered (Figure 45 f).

3.4 ELECTRODE – BRAIN TISSUE IMPEDANCE MEASUREMENTS DURING IN-VIVO EXPERIMENTS

In order to evaluate the performance of the electrodes in the grids, in-vivo impedance measurements were performed between each electrode in the ECoG grids and a common remote reference electrode (screw fixed on the rat's skull over the frontal sinus), immediately after the end of surgery and before each of the eight ECoG recording sessions (once a week for two months). For this purpose, an impedance meter (model EZM 4, Astro-Med, Inc. GRASS, W. Warwick RI, U.S.A) was used, which delivered 1mA alternating current with frequency of 30 Hz to the electrodes.

3.5 IN – VIVO ECOG RECORDINGS AND ANALYSIS

After the surgery, a recovery period of 7 days was given to the animals before starting the ECoG recordings. Each animal was placed into a transparent box situated in an acoustically and electrically shielded room for at least 2 hours before each ECoG recording for habituation to the box. The ECoG recordings were acquired using Grass-Telefactor acquisition system (Astro-Med, Inc., W. Warwick, RI, U.S.A.) with a sampling frequency of 400 Hz and 12 bit digital resolution. The grid was connected to the recording system using a cable attached to a rotating system and a weighted counterbalance arm allowing unrestricted mobility of the animal (Figure 46). Animals' behavior was acquired and stored with a video recorder simultaneously with the ECoG across 8 weeks post-implantation of the grids (once per week).

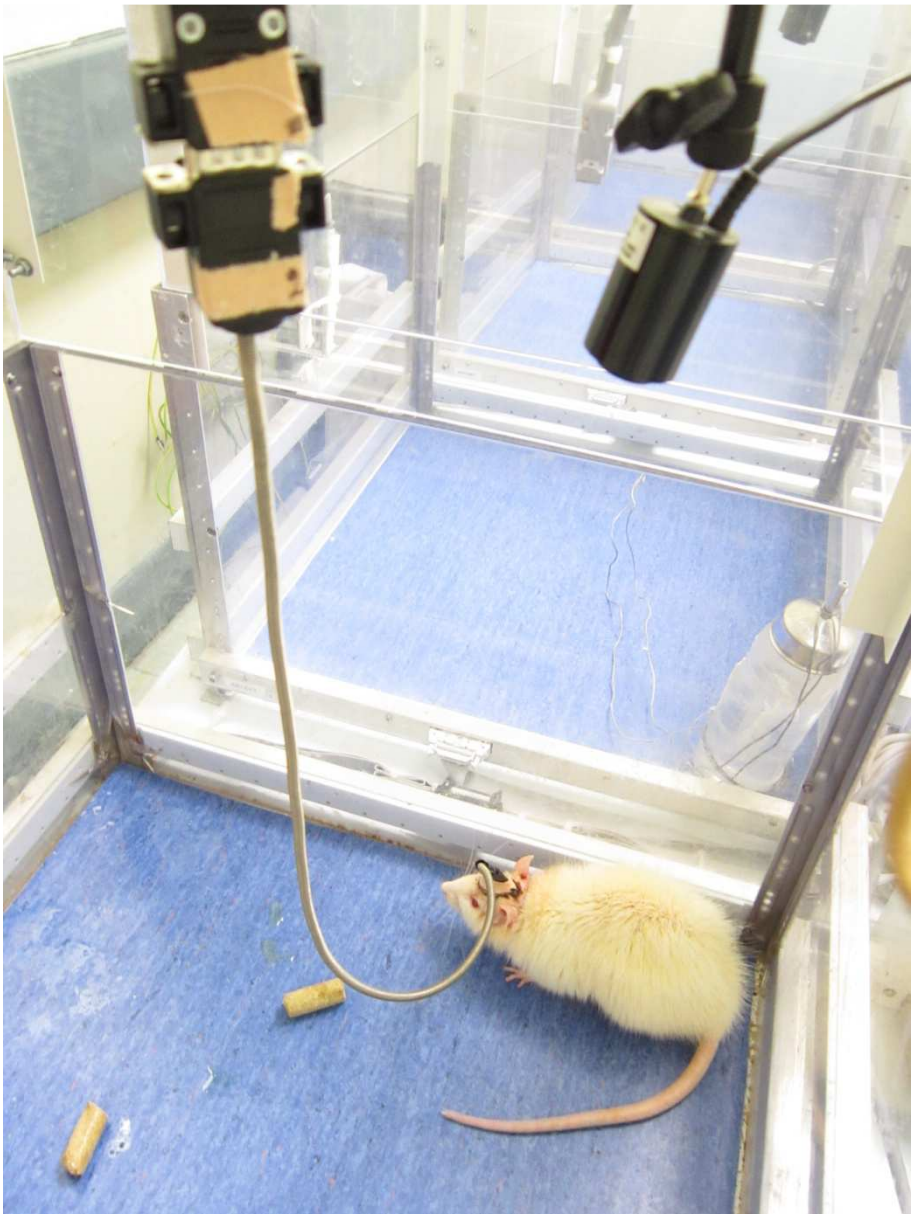

Figure 46: The ECoG recording system

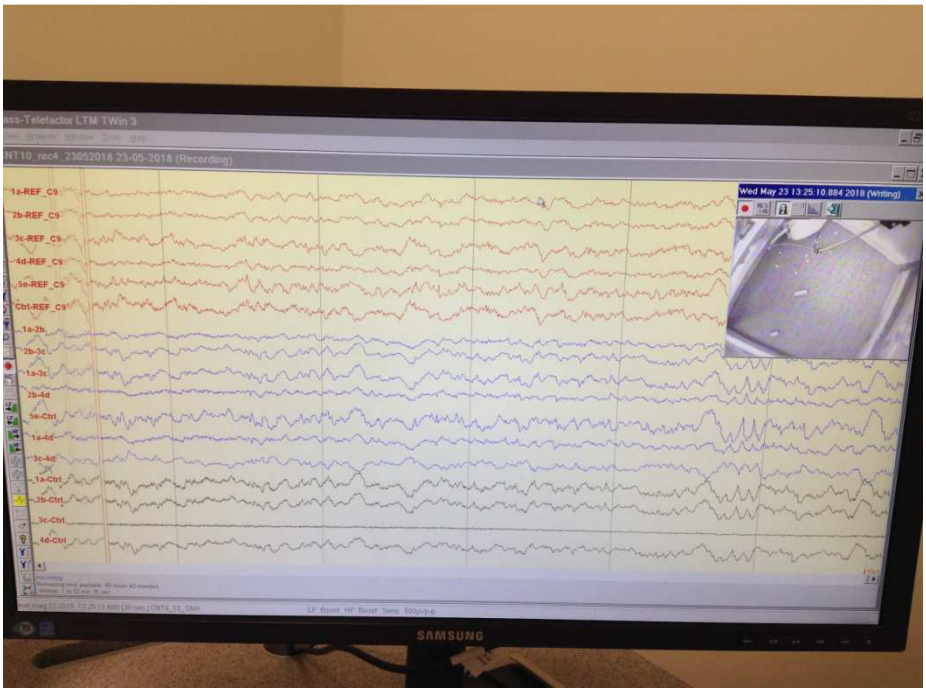

Figure 47: The acquired ECoG signals and the simultaneous video recording

The assessment of the quality of ECoG and long-term feasibility of the SWCNT grids was made by calculating the power spectra of ECoG using Fast Fourier Transformation (FFT) and Continuous Wavelet Transform (CWT, analytic Morse wavelet), Power Spectral Density (PSD), signal-to-noise ratio (SNR), mean spectral power, median frequency (F50) and spectral edge (F95). For power spectral analysis, ECoG records were visually inspected off-line and 4-seconds ECoG epochs were manually selected during passive (quiet) waking (PW) state, when the rat was in a sitting or lying down position without performing any activity. Epochs with artifacts due to the grooming were discarded by inspection of the simultaneous video recording of rats's behavior. PSD was computed by Welsh approximation algorithm, after removing slow drifts (detrending) and the mean of the signal (baseline correction). A Hamming-windowed FFT analysis in the range of 0-200 Hz was used. Then, to obtain the mean power spectrum for the ECoG from each electrode, the PSD values of 30 consecutive 4-seconds ECoG epochs were averaged. Furthermore, the values of the spectral power values for each of the 30 epochs were integrated for the following six frequency bands: delta (0.4-4 Hz), theta (4-8 Hz), alpha (8-13 Hz), beta (13-30 Hz), gamma-1 (30-80 Hz), and gamma-2 (80-200 Hz). The power of these spectral bands was calculated and expressed as percentage of the total power. Signal-to-noise (SNR) was computed as ratio of the summed squared magnitude of the

signal to that of noise. CWT and SNR were computed by means of a custom homemade script in MATLAB environment. The SNR was determined as a ratio of spectral power of the signal to that of the noise for each of randomly chosen 30 ECoG epochs of 4-s duration. Thirty epochs of noise were chosen from records with disconnected recording system from the animal's implant.

3.6 HISTOLOGICAL AND IMMUNOHISTOCHEMICAL ANALYSIS

In order to check if the implanted microelectrode arrays created any damage to the underlying cortex of rats, we performed a biocompatibility analysis of the implanted devices with the brain tissue. The biocompatibility analyses included: i) histological analysis; ii) immunohistochemistry for neuronal marker NeuN and glial marker GFAP (glial fibrillary acidic protein) e iba1. For histological analyses, after the ECoG recordings, all animals were sacrificed, the grid removed, the dissected brains were fixed in the Carnoy's solution (60% ethanol, 30% chloroform and 10% glacial acetic acid) and embebbed in paraffin. Coronal sections of 10 μm thickness were sampled every 300 μm along the entire rostro-caudal extension of the brain involved by the grid implantation. To assess presence of cellular damage or cortical cytoarchitecture alterations, a Nissl staining was performed on images of deparaffinized sections acquired at 5X magnification in the dorsal and lateral part of the cortex below the grid implantation. Moreover, the cortical thickness was measured on images acquired at 2.5X magnification in three different points under the grid by using NIH image 1.61. For immunohistochemical analyses, deparaffinized 10 μm sections were incubated overnight at +4°C with the following primary antibodies: mouse monoclonal anti-NeuN (1:100, Millipore, Billerica, MA,USA, code: MAB377) or anti-mouse monoclonal anti-GFAP (1:300, Sigma-Aldrich, Milan, Italy, code: G3893). Then, the sections were incubated for 1 hour at room temperature with a secondary biotinylated anti-mouse IgG (Vector Laboratories, Burlingame, CA, USA, code: BA2000). The 3,3-Diaminobenzidine tetrachloride (Sigma-Aldrich) was used as chromogen substrate.

3.7 ANALYSIS OF RATS BEHAVIOUR

The biocompatibility of any device implanted in the brain includes the preservation of normal behavioral status of the animal. In order to assess whether the animals

experienced unilateral sensorimotor deficits (contralateral to the implanted hemisphere), which might happen if there is a great mechanical pressure on the cortical surface by the implanted grid, a 4-score grading neurological test was applied to the rats [174] (Table 1A). In addition, each animal was observed for general behavioral status (Table 1B). Finally, the behavior of each animal was characterized by a sum of total neurological score and total general behavioral score. Measurement of the body weight of the rats was also performed. The behavioral scoring and measurement of weight were made preoperatively and once a week starting from the first week after the surgery until the end of the experiments (week 8).

Table 1A. Examination of neurological deficit

Scores of neurological assessment:	
3 – normal behavior (absence of I, II, III, and IV) *2 – slight neurological deficit (presence of I or II)*	*1 – moderate neurological deficit (presence of I and II)* *0 – severe neurological deficit (presence of I+II+III+IV)*

Item	Side	Grade
Rat suspended by tail:		
Flexion of forepaw and/or hindlimb	Ipsilateral	0
	Contralateral	I
Shoulder adduction	Ipsilateral	0
	Contralateral	I
Full twisting of the body	Ipsilateral	0
	Contralateral	I
Rat placed on the table		
Asymmetry in resistance (reduced resistance toward the contralateral side)	Ipsilateral resistance < than controlateral	II
Spasmodic turning of the body	Ipsilateral	0
	Contralateral	III
Consistent circling	Ipsilateral	0
	Contralateral	IV

Table 1B. Examination of general behavior		
Item	Behavior	Score (1 if present, 0 otherwise)
Passive behavior	Sleeping	1
	Standing Still	1
	Sitting still	1
Active behavior	Running	1
	Walking	1
Explorative behavior	Digging	1
	Sniffing	1
	Rearing	1
Automatic behavior	Eating	1
	Drinking	1
	Licking	1

Table 1: Behavioral examination grading scale for rats implanted with ECoG grids. Total score for the general normal behavior = 11; Total score = neurological score (Table 1A) + general behavioral score (Table 1B)

3.8 EX- VIVO RECORDING

Local Field Potentials (LFPs) were recorded from transverse hippocampal and neocortex slices (400 μm thick) from P40–P50 Wistar rats, prepared as described elsewhere [175]. The procedure was in accordance with the regulations of the Italian Animal Welfare Act approved by the local authority veterinary service. Briefly, animals were decapitated after being anesthetized with 2-Bromo-2-Chloro-1,1,1-trifluoro-ethane. The brain was quickly removed from the skull and placed in ice-cold artificial glycerol-based cerebrospinal fluid containing (in mM) Glycerol 130, KCl 3.5, NaH2PO4 1.2, NaHCO3 25, MgCl2 1.3, CaCl2 2, glucose 10, saturated with 95% O2-5% CO2 (pH 7.3–7.4). After 1 hour, an individual slice was transferred to the recording chamber

where it was continuously superfused with oxygenated ACSF at a rate of 2–3 ml/min at 25°C. All drugs were purchased from Sigma or Tocris Bioscience (Bristol, UK) and freshly prepared before the experiments. LFPs were evoked by minimal stimulation of the Schaffer collateral when recorded at CA1 stratum radiatum in hippocampus and by minimal stimulation of L4 when recorded at L5 region of neocortex. The stimulus (100-μs long in duration and with a range of 4–10 V in amplitude) was applied with bipolar twisted tungsten stereotrodes (2 MOhm impedance, WPI) every 30 seconds. In hippocampus, the following High Frequency Stimulation (HFS) protocol was applied: after 15 min of baseline (one stimulus every 30 seconds) recorded at CA1 stratum radiatum, 1 s burst of equally spaced pulses at 100 Hz was applied to Shaffer Collateral. LFP amplitude were followed for 1 hour after the HFS.

3.9 STATISTICAL ANALYSIS

We used in this study two types of devices: 6 devices for in-vivo experiments and one device for ex-vivo experiments. Each rat was implanted with only one device, so six rats were used for the in-vivo experiments. Four of the arrays had 5 SWCNT electrodes, one 3 Pt electrodes, and one 2 SWCNT and 2 Pt electrodes. The in-vivo recording of impedance and ECoG was made once per week up to 2 months, thus we had 195 measurements with 20 SWCNT electrodes and 41 measurements with 5 Pt electrodes. The statistical analysis was performed with statistical package “Statistica 7.0” (Statsoft, Inc., Tulsa, OK, USA). The bars in the figures are presented as mean ± standard deviation (s.d.). The differences were considered significant with minimum value of significance level $P < 0.05$.

CHAPTER 4

RESULTS

In order to fully characterize SWCNT grids and demontrate that such grids are at least comparable with similar grids with Pt electrodes, the following analyses were performed: (i) Physico-chemical characterization of grids with Pt electrodes; (ii) Measurement of electrode/cortical tissue impedance in-vivo; (iii) Analysis of ECoG; (iv) Comparison of electrical performance of SWCNT and Pt electrode arrays; (v) Analysis of grid biostability; (vi) Biocompatibility analysis; (vii) Ex-vivo recordings of evoked local field potentials.

4.1 PHYSICO – CHEMICAL CHARACTERIZATION OF ECOG ARRAYS

We compared the performance of the SWCNT and Pt electrodes in twoarrays: that with only Pt electrodes and the mixed one, with both SWCNT and Pt electrodes. The Pulsed Laser Deposition (PLD) fabrication of platinum conductive tracks implies that the metal vapour cannot completely obstruct the sensing apertures drilled in the polymer insulating foil, particularly if apertures are as wide as 50 μm as we used for the SWCNT recording sites. Therefore, we opted for a different geometry of the Pt sites, drilling 9 smaller apertures instead of a single larger one (Figure 48 (a)). Since the cylindrical side wall of the 10 μm apertures are fully Pt coated (Figure 48 (b)), the total sensing surface for the Pt recording sites is comparable to that of the SWCNT ones.

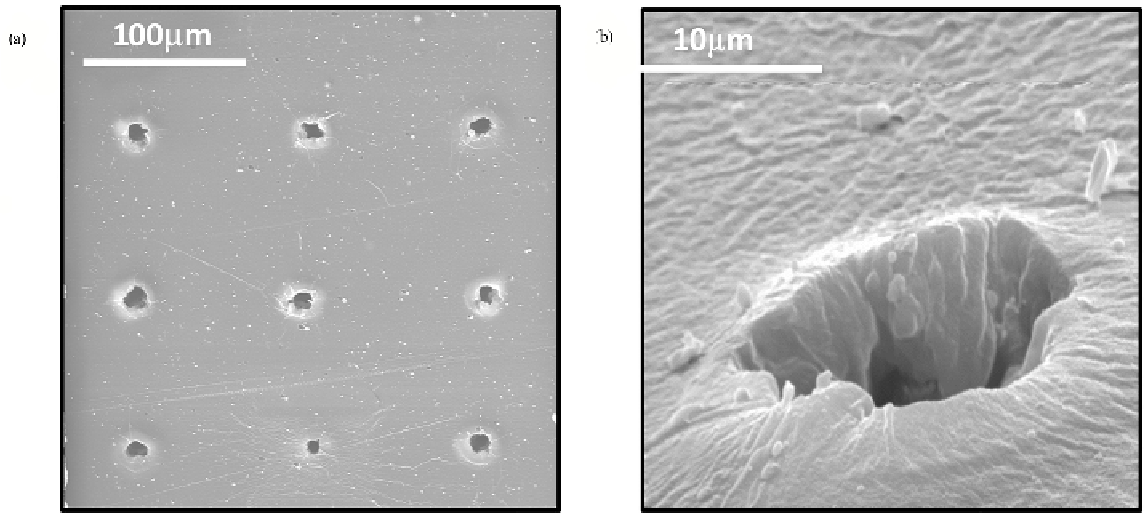

Figure 48: Scanning Electron Microscope (SEM) images of Pt-coated microapertures in the conductive Pt track. (a) Electrodes are only partially obstructed by the Pt vapour, but the internal walls of the apertures are fully Pt-coated; (b) the total sensing surface of the Pt electrodes is comparable to that of the SWCNT electrodes

The examination of the resistance versus strain for both types of materials, SWCNT and Pt, on the same polymer substrate (Figure 49 a)) showed that the conductance of the SWCNT decreased regularly on stretching the conductor, although with a double slope, suggesting different regimes of conductance for strains up to 70% and more; while the Pt wire broke at very small strains (2.5%). Figure 49 (b) shows an optical image of SWCNT and Pt parallel tracks under a small strain; minor stretch marks are seen as a result of strain in the SWCNT track, while the less elastic Pt track, although appearing more uniform, lost its electrical conductance with a small strain.

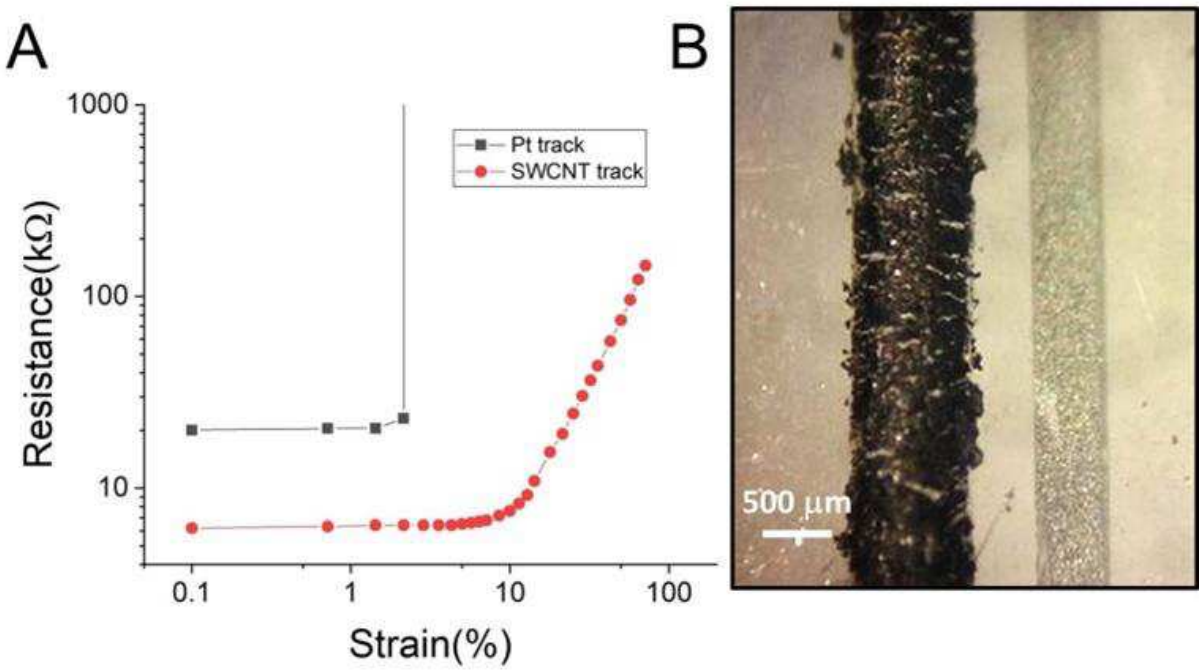

Figure 49: Characterization of resistance of SWCNT and Pt tracks to different strains. (a) Double log-plot of resistance vs strain for Pt and SWCNT tracks deposited on the MD-PE film; (b) Optical microscopic photo of parallel SWCNT and Pt tracks after 5% stretching of the ECoG array

4.2 IN VIVO IMPEDANCE MEASUREMENTS

The average electrode/cortical tissue impedance of all SWCNT electrodes in the implanted grids across the 2-month-duration of the in-vivo experiments was approximately 10 kOhm. The individual values were stable from week 1 (w1) to week 8 (w8). Figure 50 (a) shows that the values of the SWCNT-tissue impedance increased slightly and then stabilized from week 1 (w1) to week 8 (w8). However, the impedance of the Pt electrodes increased strongly at w1 and subsequently was not stable. The mean impedance of the Pt electrodes across all weeks was greater than that of the SWCNT electrodes (66±40 kOhm and 10±6 kOhm, mean±s.d., respectively) with $P < 0.05$ (Student T-test). Two-way repeated measures ANOVA on the electrode/cortical tissue impedance values showed very high significant effects ($P < 0.001$) of factors "Type of electrodes" (SWCNT and Pt), "Weeks" (w0, w1, w2, w3, w4, w5, w6, w7, and w8), and of their interaction. The average impedance value of SWCNT and Pt electrodes measured on the day of the surgery (immediately after the grid implantation at w0) were almost

comparable and, more important, the values of the SWCNT impedance stabilized from w1 to w8(Figure 50 b)).

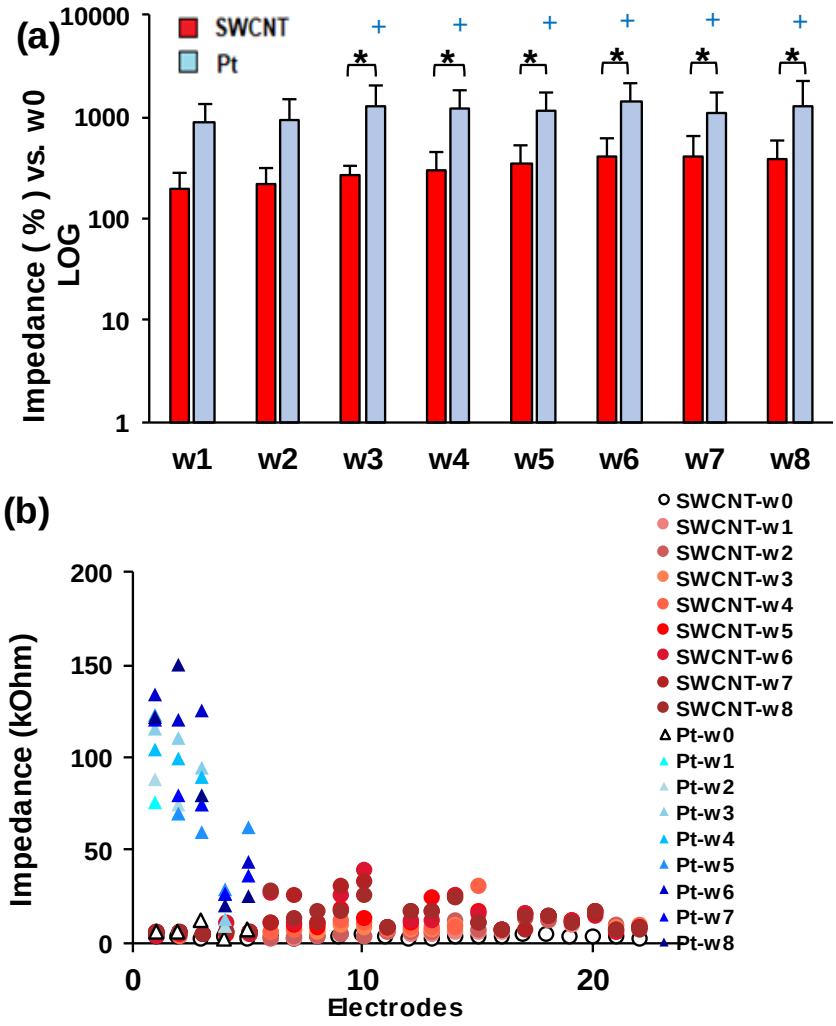

*Figure 50: Analysis of the in-vivo electrode/cortical tissue impedance of the SWCNT and Pt electrodes in the implanted arrays. (a) Mean impedances of all SWCNT (n=22, 5 grids, 195 measurements) and Pt electrodes (n=5, 2 grids, 41 measurements) for each week from w0 (just following the grid implantation) to w8 (eight weeks thereafter). * - Comparison between SWCNT (red bars) and Pt (blue bars); # - Comparison vs. w0; + - Comparison vs. w1, Tukey post-hoc test (P < 0.05 was accepted as statistical significance); (b) Distribution of impedance values (y-axis) measured at each week (from w0 to w8) for all SWCNT (n=22) and Pt (n=5) electrodes (x-axis). Legend on the right: white circles (SWCNT) and triangles (Pt) are for measurements at w0, then the increasing intensity of color shades are for measurements from w1 to w8 as follows: for the SWCNT electrodes - from light coral to brown and for the Pt electrodes - from light blue to dark blue*

4.3 ANALYSIS OF ECOG RECORDED WITH SWCNT ARRAYS

The results obtained on the reliability and stability of ECoG recorded by SWCNT grids implanted on the dorsal cortical surface (parietal cortex) in rats (Figure 51 (a), (b)) were coherent with those obtained in our previous study [176]. The spectral parameters of ECoG were stable and reliable (Figure 51 (c), (d), (e), (f), (g) dorsal). Repeated measures 2-way ANOVA did not show statistical effects of the factor "Week" on any of the characteristics of the ECoG recorded from the dorsal parietal cortex, which means that the ECoG was stable starting already from the first week after the implantation of the grid until the end of the experiments. The median frequency showed that 50% of the power of the dorsal ECoG was below 7.6 Hz, and 50% at higher frequencies of the spectrum. The calculated spectral edge revealed that 67.4 Hz was the frequency at which the power was separated into 95 and 5%. The SNR ratio (mean 5±2 dB) did not change over time. To ascertain that the grid positioned on the dorsolateral curvilinear cortical surface made good conformal contacts of the electrodes with the cortex, comparison of the electrode/cortical impedance and ECoG spectral characteristics for the lateral somatosensory cortex was made with those of the dorsal parietal cortex. The averaged impedance of the SWCNT electrodes positioned on the lateral surface (13.5 kOhm, n=17 electrodes, 3 rats) did not differ from that of the SWCNT electrodes placed on the dorsal surface (14.0 kOhm, n=5 electrodes, 3 rats), both measured at week 8. The comparative 2-way repeated measures ANOVA on the spectral ECoG parameters (Figure 51) did not show statistically significant effect of the factor "dorsal/lateral".

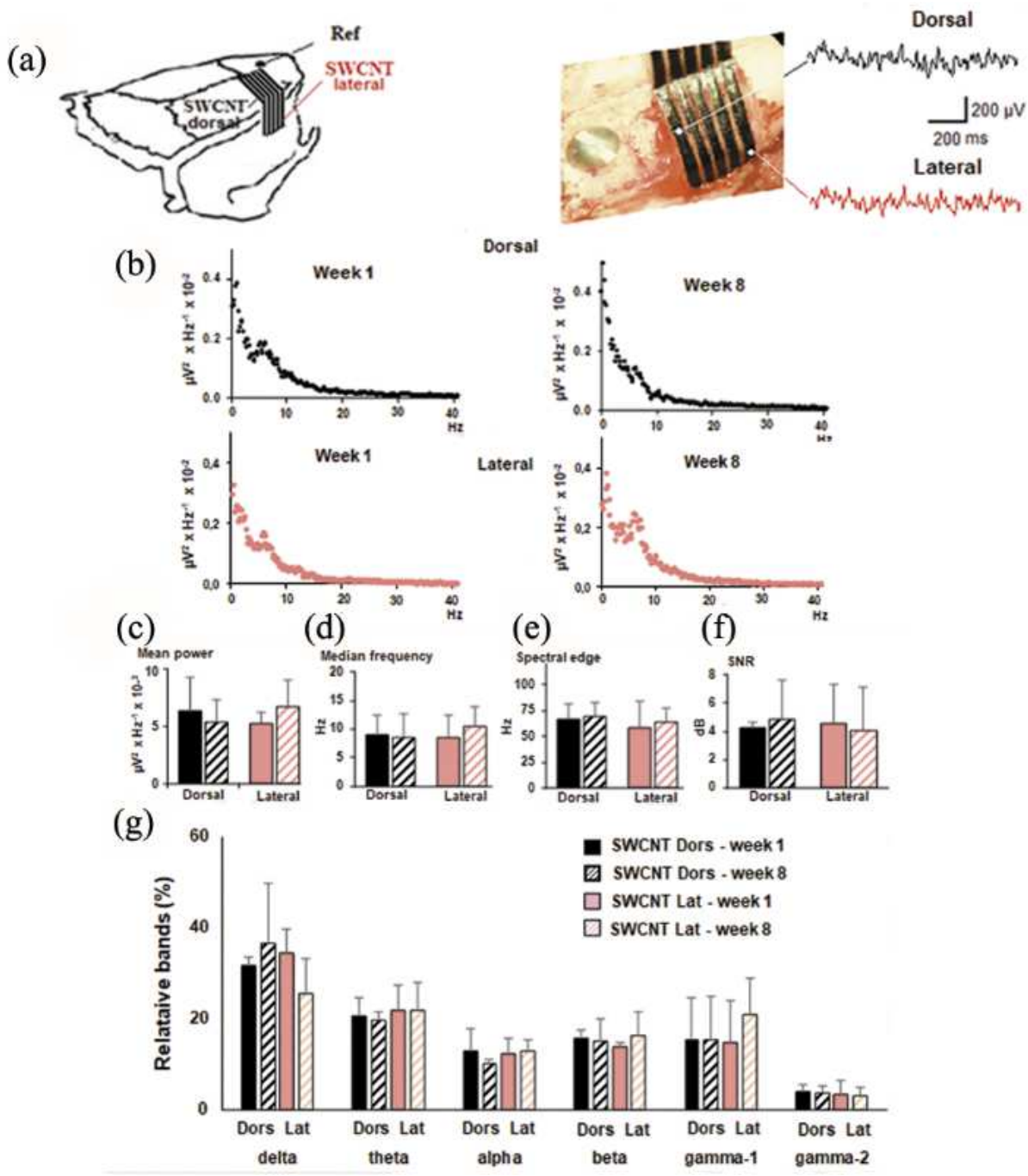

Figure 51: Comparison of dorsal and lateral ECoG characteristics. (a) - On the left, a scheme of the SWCNT/MD-PE grid positioned on the dorso-lateral cortical surface of rats; on the right, a real photo of the grid and cortex in the open bone window with the corresponding 1-s ECoG fragments from the dorsal and lateral cortical regions; (b) - Averaged PSD values (n=3 rats, 30 4-s ECoG epochs in each rat) at w1 and w8; (c), (d), (e), (f), and (g)- Averaged values (mean±SD, 30 4-s ECoG epochs) of Mean power, Median Frequency, Spectral edge, Signal-to-noise ratio, and Relative power (% of total power) in delta, theta, alpha, beta, gamma-1, and gamma-2 frequency bands, respectively

To further characterize the quality of the ECoG signal recorded by means of the electrodes in the SWCNT grids, a recording of the ECoG during quiet (passive) waking (PW), slow wave (SWS-1 and SWS-2) and paradoxical REM sleep was made (Figure 52 (a)). We used validated criteria for the sleep stages identification [177]. During PW, there was a mix of low-voltage fast and slow ECoG. During SWS, the rats usually were lying down on the abdomen and the cortical ECoG progressively became slower and increased in amplitude (0.4-10 Hz and 200-300 μV). Slow waves and typical sleep spindles were recorded during SWS-1, while the ECoG waves were slower and higher in amplitude during SWS-2 compared with SWS-1. During REM sleep, the ECoG waves were of low-amplitude (50-80 μV) and high-frequency (20-40 Hz). The simultaneous video-stream recording was used to check the behavior of rats as additional criteria for the waking-sleep stages identification. To further determine whether the contacts of the SWCNT electrodes with the cortical surface of the lateral convexity were suitable to record reliable ECoG, one device was implanted in a rat from the colony of adult WAG/Rij rats, which were validated as a model of absence epilepsy [178]. Well-characterized absence epilepsy-like spike-wave discharges (SWD) were recorded from the perioral cortical surface in the lateral convexity (Figure 52 (b)). The plot of continuous wavelet performed on a 8-s ECoG epoch shows pre-SWD increase in the low frequency bands (delta, theta) and an increase in the wavelet energy at approximately 10 Hz during the SWD (Figure 52 (c)).

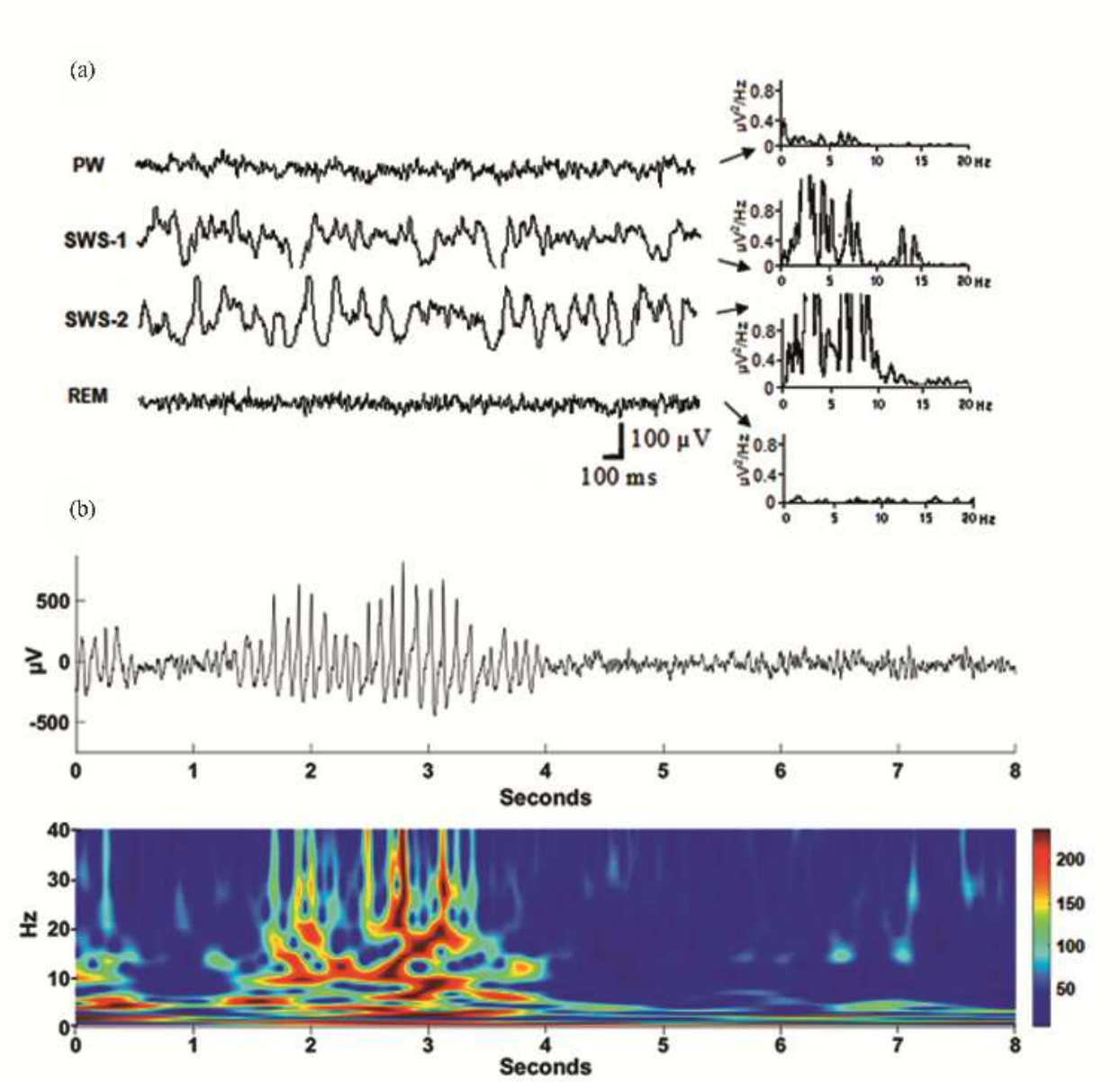

Figure 52: Examples of ECoG recorded by SWCNT grid. A- Representative ECoG recorded with one representative electrode during different vigilance states: PW, SWS-1, SWS-2, and REM. On the right, PSDs of single 4-s ECoG epochs during each vigilance state are shown. The values of PSDs during SWS were much greater than those during PW and REM; B- ECoG recorded from the perioral primary somatosensory cortex of a WAG/Rij rat containing SWD (upper panel) and the corresponding continuous wavelet transform (lower panel)

4.4 BIOSTABILITY ANALYSIS

After termination of the ECoG recordings, the electrode arrays were explanted in order to examine their biostability over two months of implantation. Optical microscopic

investigation of the explanted arrays showed that there was no damage to the material of the SWCNT tracks in any of the four SWCNT arrays (Figure 53 (a)). There was a noticeable delamination of the Pt foil from the MD-PE film in the array with four Pt conductive tracks (Figure 53 (b)), while we observed a less pronounced delamination in the array with two SWCNT and two Pt tracks (Figure 53 (c)).

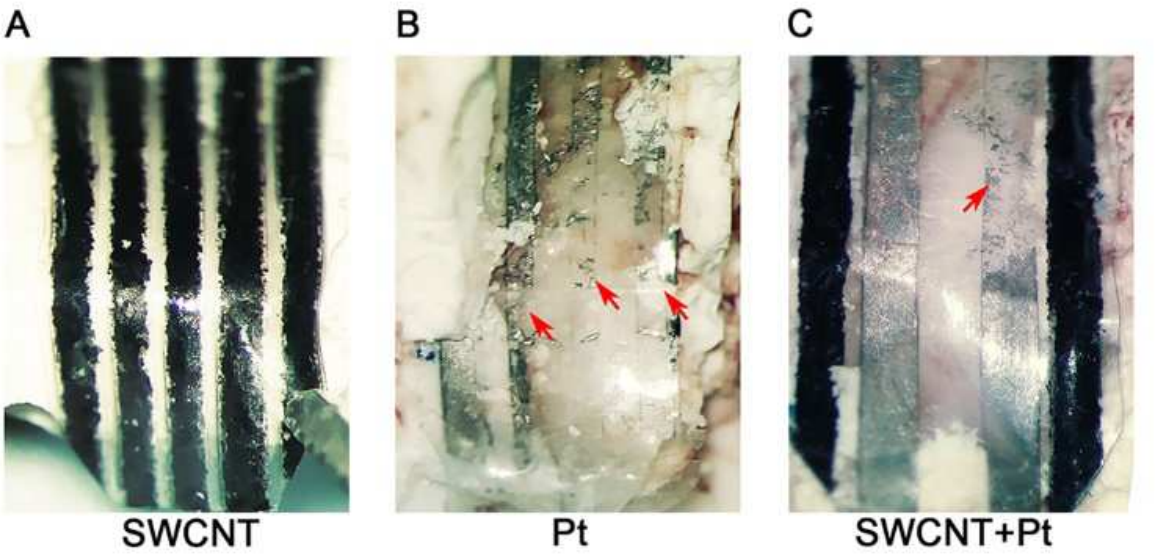

Figure 53: Optical microscopy photos of the explanted grids. (a) array with five SWCNT traces (black); (b) array with four Pt traces (light gray); (c) array with two SWCNT traces (black) and two Pt traces (light grey). Regions in the Pt traces with delamination of the platinum foil from the MD-PE film are shown with small red arrows

4.5 HISTOLOGICAL AND IMMUNOHISTOCHEMICAL ANALYSIS

This analysis comprises histological and immunohistochemical evaluation of brain tissue after explantation of the devices and the analysis of the behaviour of rats during the whole period of experiments. The cytoarchitecture analysis of the cortical tissue showed no or very small indentation of the tissue underneath the SWCNT grids. The comparison of the cortical thickness in three different portions of the cortex (dorsal, medio-lateral and ventro-lateral) revealed that the implanted SWCNT grid had negligible impact on the thickness of the underlying cortex (Figure 54 (a), right panel). Nissl stained sections (Figure 54 (b)) showed an intact neuropil with no evident loss of neurons underneath the grid. The immunohistochemical analysis of the dorsal and lateral portions of the cortex above which the SWCNT grid was implanted showed no

differences in NeuN positive cell between the ipsilateral and contralateral side, which served as a control (Figure 54 (b)). Only a mild reactive gliosis, expressed as a small increase in the signal intensity of GFAP labelling in astrocytes was observed in the cortical tissue underneath the SWCNT-based grid compared to the contralateral non-implanted cortex. The comparative analysis of cortical tissue integrity below the grids showed a bit lower Nissl positive and NeuN positive cell density associated with higher reactive gliosis in the cortical tissue of rats implanted with Pt-based grid as compared to rats implanted with SWCNT-based grid (Figure 54).

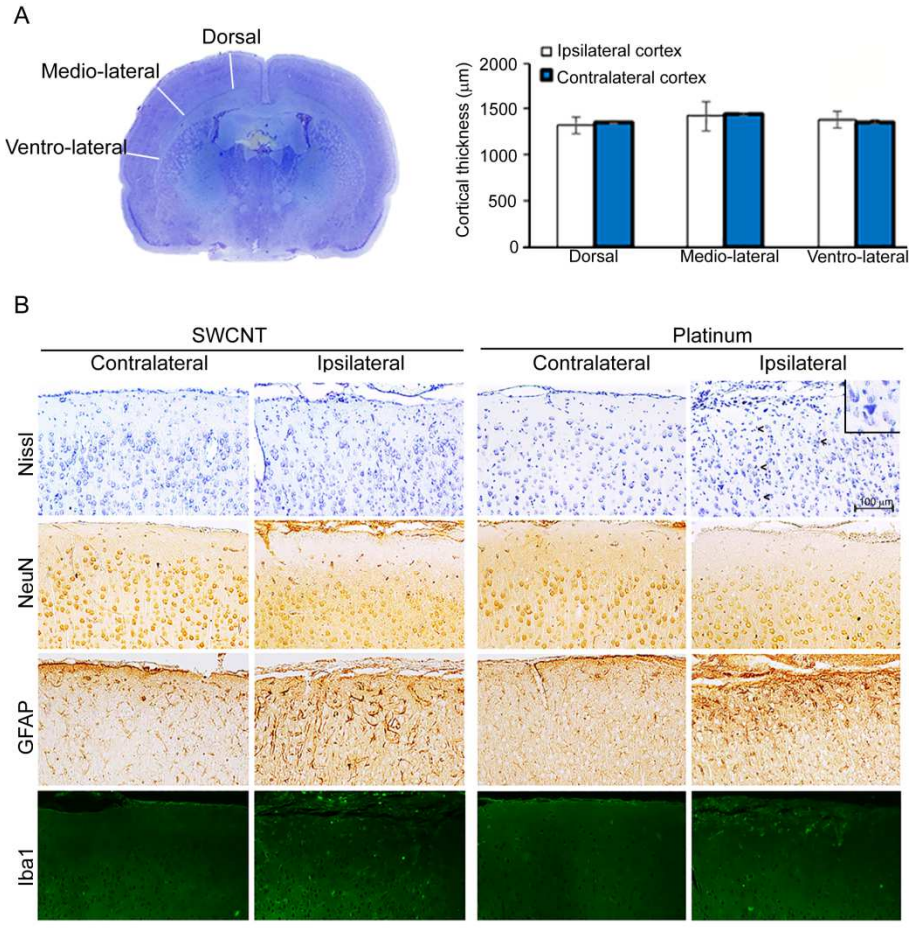

C

Percentage of nuclei with abnormal phenotype

SWCNT		Platinum	
Contralateral	Ipsilateral	Contralateral	Ipsilateral
8 +/- 3	39 +/- 16	5	72

Figure 54: Histological and immunohistochemical characterization of the cortical tissue underneath the implanted ECoG arrays. (a) On the left – a representative image of brain Nissl staining. On the right - analysis of the cortical thickness (µm) measured at three indicated levels.

There was no statistically significant difference between the cortical thickness at the three levels or between the implanted and contralateral cortex in rats with SWCNT-based arrays (Wilcoxon matched pairs test, P>0.05); (b) Nissl staining and NeuN, GFAP and Iba1 immunohistochemistry in cortical tissues of rats implanted with SWCNT-based or Pt-based arrays. Note the presence of a high number of Nissl-positive nuclei with a small diameter (5 micrometer) in the cortical parenchyma of the implanted side indicating the occurrence of inflammatory infiltration. Moreover, the extent of inflammation appeared higher in the cortical tissue of rats implanted with a Pt-based grid as compared to SWCNT-based grid. The insert in the right corner of the panel illustrates the inflammatory infiltration in the surrounding area of a picnotic neuron. Scale bar: 100 μm. (c) Percentage of neurons with a reduced or absent nuclear NeuN immunoreactivity. This condition is characteristic of damaged neurons and is identified as abnormal phenotype

4.6 ANALYSIS OF RATS BEHAVIOUR

Since the SWCNT grids were placed unilaterally (right hemisphere) below the dura mater (directly on the cortical surface, on the pia mater), it may happen that the cortical neurons underlying the grid are impaired by some mechanical pressure caused by the implanted grid. In that case, asymmetry in posture of the animal, abnormalities in muscle tone, loss of coordination, weakness, and paralysis of contralateral limbs would occur [179]. No signs of such abnormalities were seen. There were neither seizures such as facial automatism, limb clonus, clonic jerks, and generalized tonic-clonic convulsions during the whole period of testing. Before the surgery, the maximum sum of the total neurological score (Table 1A) and total general behaviour (Table 1B) was 14 (mean, n=4, SWCNT-implanted rats), which was assigned as a normal behavior . At first week after the implantation, there was a small drop down of this value, but later it returned to the value of 14 until the end of the experiment (Figure 55 (a)). Figure 55 (b) shows the body weight during the whole experiment. There was a decrease in the mean weight at w1 because two of the animals (out of four rats implanted with SWCNT devices) had some difficulties for eating. Later, the weight recuperated and subsequently increased, which was normal because of the age increase.

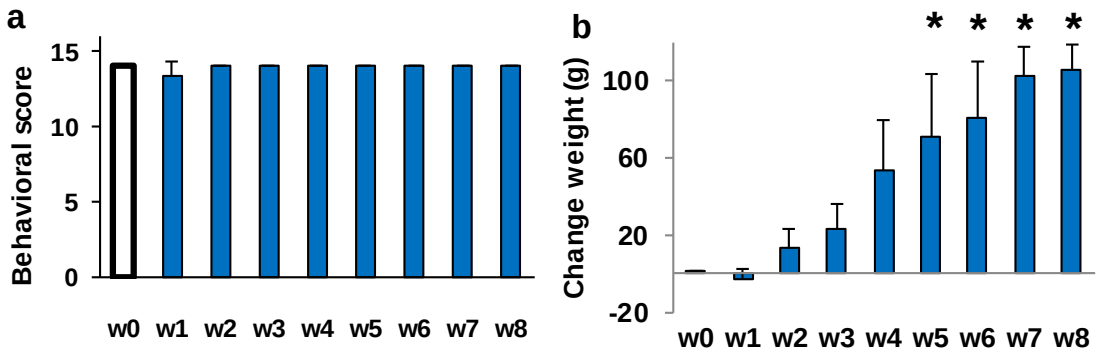

*Figure 55: Characterization of the behavioural status and body weight of rats implanted with SWCNT grids (n=4). (a) Assessment of behavioural status was performed before surgery (w0) and once per week from w1 to w8. (b) Changes in body weight measured at the same time points. * One-way repeated measures ANOVA and Dunnett post-hoc test for comparisons with body weight at w0 (n=4)*

4.7 EX-VIVO RECORDING OF SYNAPTIC EVOKED POTENTIALS

To assess the possibility of using SWCNT devices to record synaptic signals produced by selected neuronal populations in brain slices, an electrode specifically designed to this purpose was fabricated. With this device it was possible to record clear evoked synaptic volleys in slices from adult rat temporal cortex (Figure 56 (a)), which exhibited multiple waves reversibly abolished by applying tetrodotoxin (TTX, 1µM; Figure 56 (b), (c)), a selective blocker of Na+ voltage dependent channels, responsible for action potential propagation. Furthermore, the SWCNT-based electrode allowed the recording of evoked synaptic local field potentials in the CA1 region of adult rat hippocampus, which were clearly potentiated by high frequency stimulation in the CA3 region, as expected from previous studies (Figure 56 (d), (e)) [180]. All these data indicate that the SWCNT-based electrode was able to record local field potentials generated by synaptic activation due to stimulation of a population of neuronal fibres in different regions of brain slices.

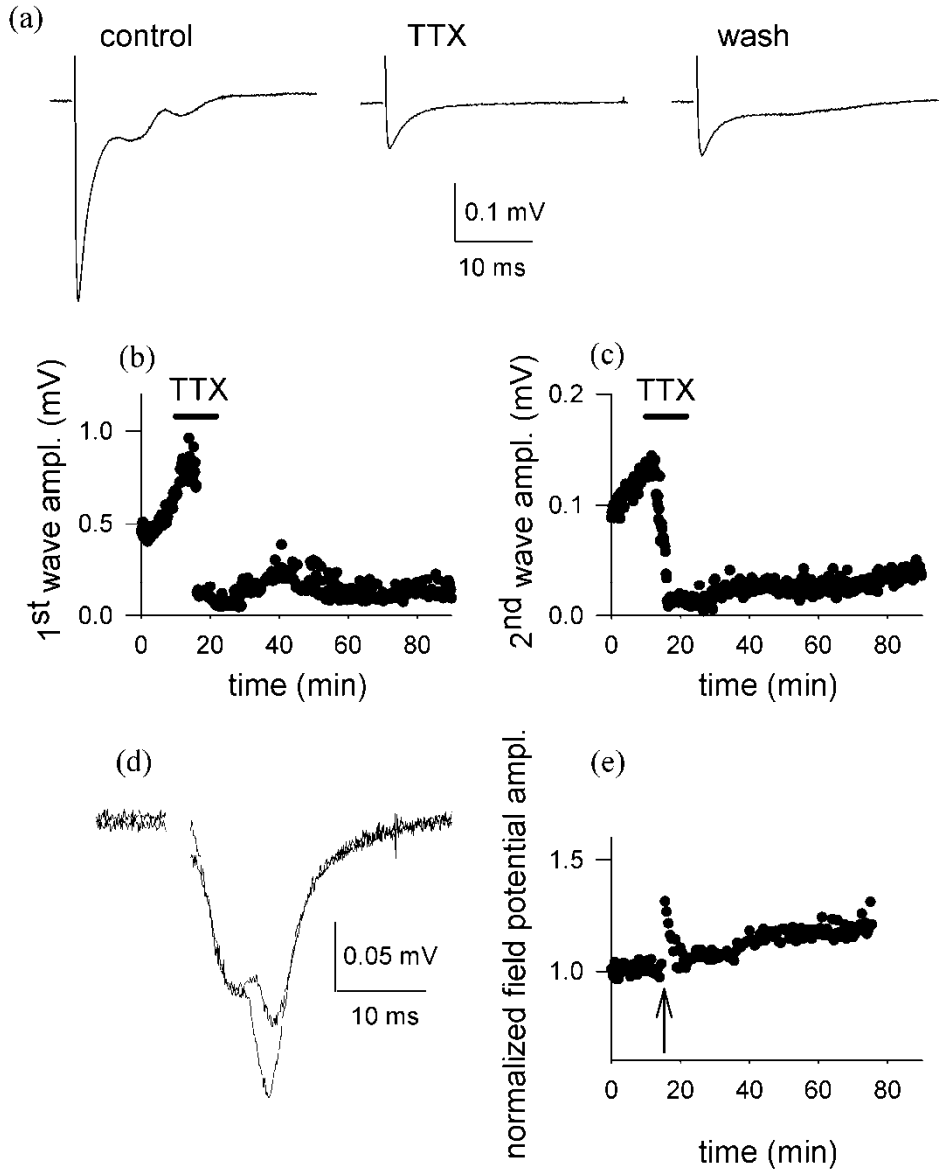

Figure 56: Evoked synaptic potentials recorded with a SWCNT-based electrode in different regions of adult rat brain slices. (a) typical traces of evoked local field potential, recorded from the temporal cortex of an adult rat in a transversal slice, before (left), during (middle) and after the application of TTX 1 μM; (b) time course of the amplitude of the first potential wave, same experiment as A. Please note the strong reduction due to TTX application, slowly reverted upon 1 hour of washout; (c) time course of the amplitude of the second potential wave, same experiments as A; (d) typical superimposed traces of local field potential recorded in the CA1 hippocampal region evoked by stimulation at the Shaffer collateral, before and after high frequency stimulation; (e) time course of the evoked local field potentials, same experiments as (d). Please note the transient potentiation induced by the high frequency stimulation (arrow), followed by a slower amplitude increase)

CHAPTER 5

CONCLUSIONS

In the present project, the ability of SWCNT/MD-PE electrode arrays to record reliable subdural ECoG in rats for a period of two months and evoked synaptic LFPs from rat's brain slices was demonstrated. First, examination of the in-vivo electrical characteristics of the SWCNT-based electrode arrays implanted subdurally on the cortex of laboratory rats in a chronic setup (eight weeks) was made in more details than in our previous study [176]. We chose to record subdural ECoG since it is a method for recording of neuronal electrical activity directly from the cortical surface that provides optimal signal-to-noise ratio and finer spatial and temporal fidelity in comparison with noninvasive standard EEG [181,182]. Furthermore, in the last years, subdural ECoG recordings have been proposed as part of BCI technology for neural motor prostheses that can enable people paralyzed by disorders such as amyotrophic lateral sclerosis, spinal cord injury or ischemic stroke to achieve successful closed-loop control of movements [182]. The fabricated SWCNT grids, having electrodes with diameter of approximately 50 μm, revealed an optimal low values of electrode/cortical tissue impedance measured in-vivo (mean 10.3 kOhm), which is much lower than theoretically expected megaohms values of impedance for electrodes with such dimensions [183]. These relatively small values means that the SWCNT may offer great promise for low-noise and high-quality ECoG recordings even with further miniaturization to micrometer or nanometer levels. The low noise levels of SWCNT electrodes should enormously facilitate the extraction of feasible ECoG features for use in any practical neurological domain and especially for BCI. Furthermore, the electrode/cortical tissue impedance and the computed ECoG parameters were stable over the entire time frame of the experiments (eight weeks), demonstrating the feasibility of such electrode arrays for

long-term use. The flexibility of the composite material is of critical importance for interfacing subdural electrode arrays with the curvilinear surface of the cerebral cortex, because the flexible substrate will decrease the mismatch between the implant and the soft tissue, thus reducing the tissue damage and the inflammation response. Both materials incorporated in the presented devices, the conductive SWCNT and the MD-PE substrate, have compliant properties to meet these requirements. Bundles made of SWCNT are extremely flexible, stretchable, and yet robust [184], while the MD-PE film substrate was chosen due to its flexibility, plasticity, excellent chemical resistance and biocompatibility. More importantly, the MD-PE-SWCNT composite has stretchable-viscoelastic properties, as demonstrated in our previous study [176]. Some investigations are available with electrode arrays placed on the cortex of the lateral brain convexity in rodents using gold electrodes [185,186] and few other studies with CNT arrays placed on the cortex of the dorsal brain convexity [187-189], but no attempts have yet been made to examine the stability and efficiency of the electrical contacts with the underlying brain tissue and the feasibility of ECoG after bending and placing the array in such a way to follow the curvilinear cortical surface of both the dorsal and lateral convexity of the brain. Our data showed, for the first time, that SWCNT arrays implanted subdurally were able to record feasible ECoG from both the surface of somatosensory cortex (upper lip region situated in the lateral brain convexity) and the parietal association cortex (situated in the dorsal brain convexity) with matching spectral characteristics. The similar overall ECoG patterns and their characteristics in both dorsal and lateral regions might be explained by the well known fact that the amplitude-frequency profile of EEG in normal subjects during quiet waking (without body movements) concerns widespead cortical territories and reflects diffuse excitability changes [190]. This matching may be disrupted by a somatosensory stimulation, by movements, or by a pathological process in one of these regions. We took much care in our experiments to not influence the normal conditions by using non-pathological rat strain (Wistar), to exclude any influence from the environment (sound isolated EEG room), and to analyze only free of movement artifacts ECoG epochs. The flexibility of cortical grids is very important especially for ECoG recordings in humans, because their gyrencephalic brain has an irregular topography with important cortical regions hidden inside the sulci, which are impossible to reach with the classical rigid

electrode arrays. Successful attempts have been made to record ECoG by copper, gold or platinum-based arrays placed intrasulcus in monkeys [191], cats [192], and humans [193]. Although our arrays were tested on rats' cortex, in which gyrification is essentially absent, this study demonstrated for the first time that the arrays can follow the curvature of the cortical surface between the dorsal and lateral convexities of the rat's brain preserving an excellent electrode-tissue contact. This approach could increase the possibility for closed-loop systems to target distant locations in the cerebral cortex [194]. Even though chronic subdural implantation of electrode arrays (mainly using metal electrodes) has been conducted previously in animals [36, 187, 195], almost nothing is known about the quality of ECoG over time. Pre-surgical ECoG monitoring of patients with drug resistant epilepsy or tumor lasts normally less than 28 days (usually one week). because of the risk of complications [196-198]. Our 2-months study on rats revealed that the relative power of high-frequency ECoG bands (alpha, beta, and gamma-1) captured with the SWCNT grids was stable and even increased from week 1 to week 8, which might be explained by the optimal and stable contact of the SWCNT electrodes with the cortical surface. The devices implanted into living organism must be biocompatible, that is, they must minimally disrupt the function of healthy tissues. Indeed, one of the key requirements for these devices is to ensure long-term use without triggering tissue reaction [145]. Opposed to penetrating electrodes, which disrupt the brain tissue and vasculature and lead to chronic inflammatory response around them, as well as to progressive neuronal degeneration at their vicinity [199], the flat (planar) ECoG electrode arrays avoid blood-brain barrier disruption and mechanical strain between the electrodes and the soft brain tissue. Although SWCNTs are the strongest material known, their bundles could potentially include graphitic debris of nanometric or even subnanometric size, which, if not surrounded by the polymer matrix, may penetrate the brain tissue. However, contrary to reported meningeal response after placement of metal grids [130], we did not observe any encapsulation or presence of NeuN positive cells in the underlying cortex, but only mild reactive gliosis (increase in the signal intensity of GFAP labeling in astrocytes). The cytoarchitectural and histological analyses of cortical layers underneath the implanted SWCNT arrays did not reveal reduction of cortex thickness neither loss of neurons, opposed to the great mechanical depression of a monkey brain due to the use of grid identical in construction

to FDA-approved electrode arrays commonly used for epilepsy monitoring [137]. We did not observed complications like those observed in the patients implanted with subdural arrays in order to help localize the ictal onset zone and eloquent cortex [196 - 198]. The results about the behavior and body weight of rats implanted with SWCNT devices gave us additional information about their biocompatibility, because if there was some damage of the sensorimotor cortex caused by the implanted device, this would lead to neurological motor deficits [179] and a decrease of sensory thresholds, that is, a decrease in ability to discriminate the properties of tactile stimuli or to identify objects by touch, which would decrease the ability of rats to handle the food pallets. We developed an original flexible mixed electrode array in which two types of electrodes, SWCNT and Pt, were embedded. The result of this comparison is affected by the fact that metal depositions are intrinsically unsuitable for extensible conductors, and indeed our physical-chemical characterization of both materials showed that, while the SWCNT tracks tended to maintain acceptable values of impedance for strains up to 70%, the Pt tracks lose their conductance at very low strains. Thus, while SWCNT devices are particularly suitable for stretchable and mouldable devices, Pt thin tracks are very fragile and cannot be strained except by extremely small amounts. However, beyond this inevitable drawback of thin metal depositions on polymeric elastic thin films, our in-vivo experiments showed that while the initial (at the first week after the implantation) electrode/cortical tissue impedance of the SWCNT electrodes in the implanted grids did not change significantly from that measured at the surgery day, the impedance of the Pt electrodes raised significantly. This might be due to presence of an initial tissue response to the implanted Pt-based arrays. The problem of the mechanical mismatch between the electrodes and the soft tissue during placement and in long-term settings is of particular importance for practice, because the rigid devices often fail due to intensive scar-tissue encapsulation induced by micro-motions between the hard materials and surrounding tissues [145,199]. As already mentioned above, the Pt traces were very fragile and they easily could be damaged when the grid was bending during implantation. In fact, the averaged in-vivo impedance of the Pt electrodes in the ECoG arrays was almost seven times greater than that of the SWCNT electrodes, that, as it is well known [147], resulted in a large noise contribution producing unacceptable SNR with the Pt electrodes. In fact, the SNR for SWCNT electrodes was twice that for Pt

electrodes. Furthermore, we observed that the spectral intensity of the ECoG captured by the SWCNT electrodes increased from the first to the last week of recording; in particular, the quantitative analysis of the spectral content of ECoG showed that the SWCNT electrodes had high F95, which demonstrated that SWCNT electrodes were able to catch high frequencies components of ECoG. High frequencies are of specific interest for control of movements by BCI, because they carry substantial information about movements [190]. The biostability analysis made after explantation of electrode arrays demonstrated that, while the SWCNT traces never lost their adhesion to the film, a delamination of the Pt traces from the MD-PE film was observed, and this shows evidence that viscoelastic surface electrodes cannot make use of Pt. The high surface area combined with the inherently outstanding conductivity and stability makes CNT and, in particular the SWCNT, a promising active nanomaterial for highly sensitive neural interfaces [200]. Moreover, we demonstrated the reliability of as-prepared SWCNT/MD-PE grids to record well-differentiated ECoG across wake-sleep cycle in a healthy Wistar rat and to capture well-characterized pathological SWDs from the cortical surface of the perioral region of a WAG/Rij rat. Although SWDs are generalized over the cortex, the cortical source driving these discharges is shown to be situated in the subgranular layers of the primary somatosensory cortex (perioral region), which is part of the cortico-thalamo-cortical interactions responsible for their appearance and generalization [201]. The time-frequency characteristics of SWDs recorded by our SWCNT-based array were coherent with those recorded by conventional metal electrodes [178,202]. Finally, we demonstrated for the first time that the SWCNT may be used as a material for creating flexible electrodes for ex-vivo recording of synaptic LFPs in brain slices. In fact, our SWCNT-based electrode was able to record evoked synaptic volleys both from the temporal cortex and the hippocampus of adult rats. In addition, we showed that it was possible to resolve well-described and expected pharmacologically or electrically-induced signal modulation in both regions. In particular, we demonstrated that a selective blocker of voltage-activated Na+ channels reversibly abolished evoked signals in the temporal cortex [203], while high frequency stimulation induced a long-term potentiation of hippocampal synaptic connections [204]. These results indicate that our SWCNT-based electrode is adequate to reliably acquire synaptic information from selected neuronal subpopulations present in brain slices. The ex-vivo

experiments served only to further demonstrate that the SWCNT is a suitable material for capturing of neuronal electrical activity and to support the in-vivo results obtained with the flat subdural ECoG arrays.

FUTURE DEVELOPMENTS

This study is, to the best of our knowledge, the first one demonstrating, by both in vivo and ex-vivo experiments, the electrical and biocompatibility properties of chronic neural interfacing of SWCNT-based electrode array and single SWCNT electrodes with rat cerebral cortex. The fabricated SWCNT-MD-PE electrode array met the specific requirements for use as a chronically implantable part of BCIs [182]. In fact, the array had appropriate mechanical properties such as softness and flexibility, relatively low electrode-tissue impedance, optimal SNR, high-quality stable ECoG and high biocompatibility. The present study demonstrates some advantages in using SWCNT-polymer based electrode arrays over array with metal electrodes. Furthermore, metal-free conductors could represent a key feature also in order to have MRI (Magnetic Resonance Imaging) compatible devices. This is particularly relevant because the MRI compatibility will allow to localize electrode sites using neuroimaging approaches, and this will be extremely useful in the epilepsy monitoring or in functional brain mapping for tumor surgery. As a future perspective, the results provide a rational basis for the use of SWCNT electrode arrays for the development of new cortical implants for opened- and closed-loop BCI systems with various clinical applications, for example for control of epilepsy and motor disturbances after stroke. The study has some limitations that will be addressed in future studies, such as the small sample size, the relatively short time frame of the experiments, and the limited properties of the EEG hardware. The most immediate improvements to the fabricated devices would be to increase the spatial resolution, trying to have as much as possible electrodes site in a restricted area and also to use active electrodes, that is electrodes able not only to passively record brain signals, but also able to electrically stimulate the brain, which is particularly important for brain computer interface applications and in epilepsy control. Another possible

future development of such devices could be the perspective of using ink-jet printing of carbon nanotubes, that could be particularly appealing for low-cost mass production of stretchable devices.

REFERENCES

1. Leibniz G.W. The monadology. Springer, 1989
2. The Biology of Thought A Neuronal Mechanism in the Generation of Thought–A New Molecular Model, Pages 109-122, 2015
3. Katz B., Miledi R. A study of synaptic transmission in the absence of nerve impulses. The Journal of physiology, 192(2), 407–436, 1967
4. https://learn.genetics.utah.edu/content/neuroscience/neurons/(Accessed December 18, 2019)
5. Hodgkin A.L. Evidence for electrical transmission in nerve Part I. The Journal of physiology, 90(2):183–210, 1937
6. Hodgkin A.L., Huxley A.F. Resting and action potentials in single nerve fibers. The Journal of physiology, 104(2):176–195, 1945
7. Hodgkin A.L., Huxley A.F. A quantitative description of membrane current and its application to conduction and excitation in nerve. The Journal of physiology, 117(4):500, 1952
8. https://step1.medbullets.com/neurology/113052/action-potential-basics (Accessed December 18, 2019)
9. Bandettini P.A., Wong E.C., Hinks R.S. et al. Time course EPI of human brain function during task activation. Magn Reson Med, 25:390, 1992
10. Kwong K.K., Belliveau J.W., Chesler D.A. et al. Dynamic magnetic resonance imaging of human brain activity during primary sensory stimulation. Proc Natl Acad Sci USA, 89:5675, 1992

11. Ogawa S., Lee T.M., Kay A.R. et al. Brain magnetic resonance imaging with contrast dependent on blood oxygenation. Proc Natl Acad Sci U S A, 87:9868, 1990

12. Lee, S.H., Jin S.H., An J. The difference in cortical activation pattern for complex motor skills: A functional near- infrared spectroscopy study. Sci Rep, 9, 14066, 2019

13. Taube W., Mouthon M., Leukel C. et al. Brain activity during observation and motor imagery of different balance tasks: An fMRI study. Cortex, Volume 64, Pages 102-114, ISSN 0010-9452, 2015

14. Veer I.M., Beckmann C.F., van Tol M.J. et al. Whole brain resting-state analysis reveals decreased functional connectivity in major depression. Frontiers in systems neuroscience, 4, 41, 2010

15. Cherry S., Phelps M. Imaging brain function with positron emission tomography, In Brain Mapping: The Methods, Toga A.W., Mazziotta J.C. (Eds), San Diego, Academic Press, 2002

16. Fox P.T., Mintun M.A., Raichle M.E. et al. A noninvasive approach to quantitative functional brain mapping with H2 (15)O and positron emission tomography. J Cereb Blood Flow Metab, 4 (3): 329 – 333, 1984

17. Wolpaw J.R., Wolpaw E.W. Brain-computer interfaces: principles and practice. 2012

18. Villringer A., Planck J., Hock C. et al. Near infrared spectroscopy (NIRS): a new tool to study hemodynamic changes during activation of brain function in human adults . Neurosci Lett 14, 154 (1–2): 101 – 104, 1993

19. Boas D.A., Dale A.M., Franceschini M.A. Diffuse optical imaging of brain activation: approaches to optimizing image sensitivity, resolution, and accuracy. NeuroImage, 23(1) : S275 – 288, 2004

20. Martinez D.L., Peng K., Lee A.J. et al. Pain Detection with fNIRS-Measured Brain Signals: A Personalized Machine Learning Approach Using the Wavelet

Transform and Bayesian Hierarchical Modeling with Dirichlet Process Priors. 8th International Conference on Affective Computing and Intelligent Interaction Workshops and Demos (ACIIW), 304-309, 2019

21. Berger H. Über das Elektrenkephalogramm des Menschen. Archiv f. Psychiatrie, 87, 527–570, 1929

22. Jasper H.H. The ten twenty electrode system of the international federation. Electroencephalogr. Clin. Neurophysiol, 10, 371–375, 1958

23. Sharbrough F., Chatrian G., Lesser R. et al. American electroencephalographic society guidelines for standard electrode position nomenclature. Electroencephalogr. Clin. Neurophysiol, 8, 200–202, 1991

24. Klem G.H., Lüders H.O., Jasper H.H. et al. The ten-twenty electrode system of the International Federation. The International Federation of Clinical Neurophysiology. Electroencephalogr Clin Neurophysiol Suppl., 52:3-6, 1999

25. Caton R. Electrical currents of the brain . J Nerv Ment Dis, 2 (4): 610, 1875

26. Freeman W.J., Rogers L.J., Holmes M.D. et al. Spatial spectral analysis of human electrocorticograms including the alpha and gamma bands . J Neurosci Methods, 95 (2): 111 – 121, 2000

27. Slutzky M.W., Jordan L.R., Krieg T. et al. Optimal spacing of surface electrode arrays for brain-machine interface applications. J Neural Eng, 7 (2): 26004, 2010

28. Freeman W.J., Holmes M.D., Burke B.C. et al. Spatial spectra of scalp EEG and EMG from awake humans. Clin Neurophysiol, 114 : 1053 – 1068, 2003

29. Ball T., Kern M., Mutschler I. et al. Signal quality of simultaneously recorded invasive and non-invasive EEG. Neuroimage, 2009

30. Staba R.J., Wilson C.L., Bragin A. et al. Quantitative analysis of high-frequency oscillations (80–500 Hz) recorded in human epileptic hippocampus and entorhinal cortex . J Neurophysiol, 88 (4): 1743 – 1752, 2002

31. Miller K., Sorensen L., Ojemann J. et al. Power-law scaling in the brain surface electric potential . PLoS Comput Biol, 5 : e1000609, 2009a

32. Loeb G.E., Walker A.E., Uematsu S. et al. Histological reaction to various conductive and dielectric films chronically implanted in the subdural space. J Biomed Mater Res, 11 (2): 195 – 210, 1977

33. Bullara L.A., Agnew W.F., Yuen T.G. et al. Evaluation of electrode array material for neural prostheses . Neurosurgery, 5 (6): 681 – 686, 1979

34. Yuen T.G., Agnew W.F., Bullara L.A. Tissue response to potential neuroprosthetic materials implanted subdurally . Biomaterials, 8 (2): 138 – 141, 1987

35. Pilcher W., Rusyniak W. Complications of epilepsy surgery . Neurosurg Clin North Am, 4 (2): 311 – 325, 1993

36. Margalit E., Weiland J., Clatterbuck R. et al. Visual and electrical evoked response recorded from subdural electrodes implanted above the visual cortex in normal dogs under two methods of anesthesia . J Neurosci Methods, 123 (2): 129 – 137, 2003

37. Chao Z.C., Nagasaka Y., Fujii N. Long-term asynchronous decoding of arm motion using electrocorticographic signals in monkeys . Front Neuroeng, 3 : 3 – 3, 2010

38. Schalk G. Can electrocorticography (ECoG) support robust and powerful brain-computer interfaces? Front Neuroeng, 3 : 9 – 9, 2010

39. Schalk G., Miller K.J., Anderson N.R. et al. Two-dimensional movement control using electrocorticographic signals in humans. Journal of neural engineering, 5(1), 75–84, 2008

40. Shadlen M.N., Newsome W.T. The variable discharge of cortical neurons: implications for connectivity, computation, and information coding. The Journal of neuroscience: the official journal of the Society for Neuroscience, 18(10), 3870–3896, 1998

41. Einevoll G.T., Pettersen K.H. Devor A. et al. Laminar Population Analysis: Estimating Firing Rates and Evoked Synaptic Activity From Multielectrode Recordings in Rat Barrel Cortex, Journal of Neurophysiology, 97:3, 2174-2190, 2007

42. Bullock T.H. Signals and signs in the nervous system: The dynamic anatomy of electrical activity is probably information-rich. Proceedings of the National Academy of Sciences, 94 (1) 1-6, 1997

43. Colebatch J.G.. Bereitschaftspotential and movement-related potentials: Origin, significance, and application in disorders of human movement. Mov. Disord., 22: 601-610, 2007

44. Waldert S., Pistohl T., Braun C. et al. A review on directional information in neural signals for brain-machine interfaces. J. Physiol. Paris, 103, 244–254, 2009

45. Zhuang J., Truccolo W., Vargas-Irwin C. et al. Decoding 3-D reach and grasp kinematics from high-frequency local field potentials in primate primary motor cortex. IEEE transactions on bio-medical engineering, 57(7), 1774–1784, 2010

46. Gaona C.M. Freudenburg Z., Breshears J. et al. Non uniform High-Gamma (60-500 Hz) Power Changes Dissociate Cognitive Task and Anatomy in Human Cortex. The Journal of neuroscience: the official journal of the Society for Neuroscience, 31. 2091-100., 2011

47. Wolpaw J.R., Birbaumer N., McFarland D.J. et al. Brain-computer interfaces for communication and control. Clin Neurophysiol., 113(6):767-91, 2002

48. Coyle S.M., Ward T.E., Markham C.M. Brain–computer interface using a simplified functional near-infrared spectroscopy system. J. Neural Eng., 4(3), 219–226, 2007

49. LaConte S.M., Peltier S.J., Hu X.P. Real-time fMRI using brain-state classification. Hum. Brain Mapp., 28(10), 1033–1044, 2007

50. Mellinger J., Schalk G., Braun C. et al. An MEG-based brain–computer interface (BCI). NeuroImage, 36(3), 581–593, 2007

51. Ramsey N.F., van de Heuvel M.P., Kho K.H. et al. Towards human BCI applications based on cognitive brain systems: an investigation of neural signals recorded from the dorsolateral prefrontal cortex. IEEE Trans. Neural Syst. Rehabil. Eng., 14(2), 214–217, 2006

52. Weiskopf N., Scharnowski F., Veit R. et al. Self regulation of local brain activity using real-time functional magnetic resonance imaging (fMRI). J. Physiol. Paris, 98(4–6), 357–373, 2004

53. Birbaumer N., Ghanayim N., Hinterberger T. et al. A spelling device for the paralysed. Nature, 398(6725), 297–298, 1999

54. Kübler A., Kotchoubey B., Hinterberger T. et al. The Thought Translation Device: a neurophysiological approach to communication in total motor paralysis. Exp. Brain Res., 124(2), 223–232, 1999

55. Millán J.R., Renkens F., Mouriño J. et al. Noninvasive brain-actuated control of a mobile robot by human EEG. IEEE Trans. Biomed. Eng., 51(6), 1026–1033, 2004

56. Pfurtscheller G., Guger C., Müller G. et al. Brain oscillations control hand orthosis in a tetraplegic. Neurosci. Lett., 292(3), 211–214, 2000

57. McFarland D.J., Krusienski D.J., Sarnacki W.A. et al. Emulation of computer mouse control with a noninvasive brain–computer interface. J. Neural Eng., 5(2), 101–110, 2008

58. Wolpaw J.R. McFarland D.J. Multichannel EEG-based brain–computer communication. Electroencephalogr. Clin. Neurophysiol., 90(6), 444–449, 1994

59. Felton E.A., Wilson J.A., Williams J.C. et al. Electrocorticographically controlled brain–computer interfaces using motor and sensory imagery in patients with temporary subdural electrode implants. Report of four cases. J. Neurosurg., 106(3), 495–500, 2007

60. Wilson J., Felton E., Garell P. et al. ECoG factors underlying multimodal control of a brain–computer interface. IEEE Trans. Neural Syst. Rehabil. Eng., 14, 246–250, 2006

61. Leuthardt E., Schalk G., Wolpav J.R. et al. A brain–computer interface using electrocorticographic signals in humans. J. Neural Eng, 1(2), 63–71, 2004
62. Loeb G.E., Walker A.E., Uematsu S. et al. Histological reaction to various conductive and dielectric films chronically implanted in the subdural space. J. Biomed. Mater. Res., 11(2), 195–210, 1977
63. Bullara L.A., Agnew W.F., Yuen T.G. et al. Evaluation of electrode array material for neural prostheses. Neurosurg, 5(6), 681–686, 1979
64. Yuen T.G., Agnew W.F., Bullara L.A. Tissue response to potential neuroprosthetic materials implanted subdurally. Biomaterials, 8(2), 138–141, 1987
65. Serruya M., Hatsopoulos N., Paninski L. et al. Instant neural control of a movement signal. Nature, 416(6877), 141–142, 2002
66. Santhanam G., Ryu S.I., Yu B.M. et al. A high-performance brain–computer interface. Nature, 442(7099), 195–198, 2006
67. Stice P., Muthuswamy J. Assessment of gliosis around moveable implants in the brain. J. Neural Eng, 6(4), 046004, 2009
68. Donoghue J., Nurmikko A., Friehs G. et al. Development of neuromotor prostheses for humans. Suppl. Clin. Neurophysiol, 57, 592–606, 2004
69. Shain W., Spataro L., Dilgen J. et al. Controlling cellular reactive responses around neural prosthetic devices using peripheral and local intervention strategies. IEEE Trans. Neural Syst. Rehabil. Eng, 11, 186– 188, 2003
70. Leuthardt E.C., Schalk G., Moran D. et al. The emerging world of motor neuroprosthetics: a neurosurgical perspective. Neurosurgery, Volume 59, Issue 1, Pages 1–14, 2006
71. Polikov V.S., Tresco P.A., Reichert W.M. Response of brain tissue to chronically implanted neural electrodes. Journal of Neuroscience Methods, 148(1):1–18, 2005
72. Brette R., Destexhe A. Handbook of Neural Activity Measurement, Cambridge University Press, 2012
73. Neher E., Sakmann B. Single channel currents recorded from membrane of denervated frog muscle fibers. Nature, 260(7):799–802, 1976
74. Sakmann B., Neher E. Single-channel recording. Springer New York, 2009

75. Li N., Tourovskaia A., Folch A. Biology on a chip: microfabrication for studying the behavior of cultured cells. Critical Reviews in Biomedical Engineering, 31(5&6), 2003
76. Wirth C., Lüscher H. Spatiotemporal evolution of excitation and inhibition in the rat barrel cortex investigated with multielectrode arrays. Journal of neurophysiology, 91(4):1635–1647, 2004
77. Prohaska O.J, Olcaytug F., Pfundner P. et al. Thin-film multiple electrode probes: Possibilities and limitations. IEEE Transactions on Biomedical Engineering, (2):223–229, 1986
78. Liu M.G., Chen X.F., He T. et al. Use of multi-electrode array recordings in studies of network synaptic plasticity in both time and space. Neuroscience bulletin, 28. 409-22. 10.1007/s12264-012-1251-5, 2012
79. Petroff O.A., Spencer D.D., Goncharova I.I. et al. A comparison of the power spectral density of scalp EEG and subjacent electrocorticograms. Clin. Neurophysiol, 127, 1108–1112, 2016
80. Towle V.L., Yoon H.A., Castelle M. et al. ECoG gamma activity during a language task: Differentiating expressive and receptive speech areas. Brain, 131, 2013–2027, 2008
81. Hill, N.J., Gupta, D., Brunner, P. et al. Recording human electrocorticographic (ECoG) signals for neuroscientific research and real-time functional cortical mapping. J. Vis. Exp, 64, e3993, 2012
82. Lycke R.J., Schendel A., Williams J.C. et al. In vivo evaluation of a μECoG array for chronic stimulation. In Proceedings of the 2014 36th Annual International Conference of the IEEE Engineering in Medicine and Biology Society, Chicago, IL, USA, 26–30, pp. 1294–1297, 2014
83. Kellis S., Sorensen L., Darvas F. et al. Multi-scale analysis of neural activity in humans: Implications formicro-scale electrocorticography. Clin. Neurophysiol, 127, 591–601, 2016
84. Schalk G., Kubanek J., Miller K. et al. Decoding two-dimensional movement trajectories using electrocorticographic signals in humans. J. Neural Eng, 4, 264, 2007

85. Shimoda K., Nagasaka Y., Chao Z.C. et al. Decoding continuous three-dimensional hand trajectories from epidural electrocorticographic signals in Japanese macaques. J. Neural Eng, 9, 036015, 2012
86. Breshears J.D., Gaona C.M., Roland, J.L. et al. Decoding motor signals from the pediatric cortex: Implications for brain-computer interfaces in children. Pediatrics, 128, e160–e168, 2011
87. Chao Z.C., Nagasaka Y., Fujii N. Long-term asynchronous decoding of arm motion using electrocorticographic signals in monkey. Front. Neuroeng., 3, 3, 2010
88. Yanagisawa T., Hirata M., Saitoh Y. et al. Real-time control of a prosthetic hand using human electrocorticography signals: Technical note. J. Neurosurg., 114, 1715–1722, 2011
89. Rubehn B., Bosman C., Oostenveld R. et al. A MEMS-based flexible multichannel ECoG-electrode array. J. Neural Eng. 6, 036003, 2009
90. Yanagisawa T., Hirata M., Saitoh Y. et al. Prosthetic arm control by paralyzed patients using electrocorticograms. Neurosci. Res., 68, e83, 2010
91. Derix J., Iljina O., Schulze-Bonhage A. et al. “Doctor” or “darling”? Decoding the communication partner from ECoG of the anterior temporal lobe during non-experimental, real-life social interaction. Front. Hum. Neurosci., 6, 251, 2012
92. Leuthardt E.C., Gaona C., Sharma M. et al. Using the electrocorticographic speech network to control a brain–computer interface in humans. J. Neural Eng., 8, 036004, 2011
93. Bleichner M., Freudenburg Z., Jansma, J. et al. Give me a sign: Decoding four complex hand gestures based on high-density ECoG. Brain Struct. Funct., 221, 203–216, 2016
94. Cook M.J., O’Brien T.J., Berkovic S.F. et al. Prediction of seizure likelihood with a long-term, implanted seizure advisory system in patients with drug-resistant epilepsy: A first-in-man study. Lancet Neurol. , 12, 563–571, 2013
95. Shokoueinejad M., Park D.W., Hwan Jung Y.H. et al. Progress in the Field of Micro-Electrocorticography Micromachines (Basel)., 10(1): 62, 2019
96. Wang W., Degenhart A.D., Collinger J.L. et al. Human motor cortical activity recorded with Micro-ECoG electrodes, during individual finger movements. In Proceedings of the 2009 Annual International Conference of the IEEE

Engineering in Medicine and Biology Society, Minneapolis, MN, USA, pp. 586–589, 2009

97. Vinjamuri R., Weber D., Degenhart, A. et al. A fuzzy logic model for hand posture control using human cortical activity recorded by micro-ECoG electrodes. In Proceedings of the 2009 Annual International Conference of the IEEE Engineering in Medicine and Biology Society, Minneapolis, MN, USA, pp. 4339–4342, 2009
98. Kellis S., Miller K., Thomson K. et al. Decoding spoken words using local field potentials recorded from the cortical surface. J. Neural Eng., 7, 056007, 2010
99. Kellis S., Miller K., Thomson K. et al. Classification of spoken words using surface local field potentials. In Proceedings of the 2010 Annual International Conference of the IEEE Engineering in Medicine and Biology, Buenos Aires, Argentina, pp. 3827–3830, 2010
100. Strumwasser F. Long-term recording from single neurons in brain of unrestrained mammals. Science, 127:469–470, 1958
101. Budai D., István H., Mészáros B. Electrochemical responses of carbon fiber microelectrodes to dopamine in vitro and in vivo. Acta Biologica Szegediensis., 54. 155-160, 2010
102. Ferguson J.E., Boldt C., Redish A.D. Creating low-impedance tetrodes by electroplating with additives. Sens. ActuatorsA Phys., 156, 388–393, 2009
103. Buzsáki G. Large-scale recording of neuronal ensembles. Nature neuroscience, 7(5):446–451, 2004
104. Nicolelis M.A.L., Dimitrov D., Carmena J.M. et al. Chronic, multisite, multielectrode recordings in macaque monkeys. Proceedings of the National Academy of Sciences, 100(19):11041– 11046, 2003
105. Wise K.D., Anderson D.J., Hetke J.F. et al. Wireless Implantable Microsystems: High-Density Electronic Interfaces to the Nervous System. Proceedings of the IEEE, 92(1):76–97, 2004
106. Campbell P.K., Jones K.E., Huber R.J. et al. A silicon-based, three-dimensional neural interface: manufacturing processes for an intracortical electrode array. IEEE Transactions on Biomedical Engineering, 38(8):758–768, 1991

107. Branner A., Stein R.B., Fernandez E. et al. Long-term stimulation and recording with a penetrating microelectrode array in cat sciatic nerve. IEEE Transactions on Biomedical Engineering, 51(1):146– 157, 2004
108. Stieglitz T., Schuettler M., Meyer J.U. et al. Micromachined, polyimide based devices for flexible neural interfaces. Biomedical Microdevices, 2(4):283–294, 2000
109. Metallo C., White R.D., Trimmer B.A. Flexible parylene-based microelectrode arrays for high resolution emg recordings in freely moving small animals. Journal of Neuroscience Methods, 195(2):176–184, 2011
110. Skousen J.L., Bridge M.J., Tresco P.A. A strategy to passively reduce neuroinflammation surrounding devices implanted chronically in brain tissue by manipulating device surface permeability. Biomaterials, 2014
111. Parikh K.S., Bradley P.A., Lannutti J.J. et al. Hydrogel–electrospun fiber mat composite coatings for neural prostheses. Frontiers in Neuroengineering, 4(2):1–8, 2011
112. Weremfo A., Carter P., Hibbert D.B. et al. Investigating the interfacial properties of electrochemically roughened platinum electrodes for neural stimulation. Langmuir, 31, 2593–2599, 2015
113. Park D.W., Schendel A.A., Mikael S. et al. Graphene-based carbon-layered electrode array technology for neural imaging and optogenetic applications. Nat. Commun., 5, 5258, 2015
114. Park D.W., Ness J.P., Brodnick S.K. et al. Electrical Neural Stimulation and Simultaneous in Vivo Monitoring with Transparent Graphene Electrode Arrays Implanted in GCaMP6f Mice. ACS Nano, 12, 148–157, 2018
115. Kwon K.Y., Sirowatka B., Weber A. et al. Opto-_ECoG array: A hybrid neural interface with transparent _ECoG electrode array and integrated LEDs for optogenetics. IEEE Trans. Biomed. Circuits Syst., 7, 593–600, 2013
116. Kunori N., Takashima I. A transparent epidural electrode array for use in conjunction with optical imaging. J. Neurosci. Methods, 251, 130–137,2015
117. Ledochowitsch P., Olivero E., Blanche T. et al. A transparent _ECoG array for simultaneous recording and optogenetic stimulation. In Proceedings of the 2011

Annual International Conference of the IEEE Engineering in Medicine and Biology Society, Boston, MA, USA, pp. 2937–2940, 2011

118. Cogan S.F., Plante T., Ehrlich J. Sputtered iridium oxide films (SIROFs) for low-impedance neural stimulation and recording electrodes. In Proceedings of the 26th Annual International Conference of the IEEE Engineering in Medicine and Biology Society, IEMBS'04, San Francisco, CA, USA, pp. 4153–4156, 2004
119. Richner T.J., Thongpang S., Brodnick S.K. et al. Optogenetic micro-electrocorticography for modulating and localizing cerebral cortex activity. J. Neural Eng., 11, 016010, 2014
120. Hwang S.W., Tao H., Kim D.H. et al. A physically transient form of silicon electronics. Science, 337, 1640–1644, 2012
121. Yu K.J., Kuzum D., Hwang S.W. et al. Bioresorbable silicon electronics for transient spatiotemporal mapping of electrical activity from the cerebral cortex. Nat. Mater., 15, 782–791, 2016
122. Leach J., Achyuta A.K.H., Murthy S.K. Bridging the divide between neuroprosthetic design, tissue engineering and neurobiology. Front. Neuroeng., 2, 18, 2010
123. Richter A., Xie Y., Schumacher A. et al. A simple implantation method for flexible, multisite microelectrodes into rat brains. Front. Neuroeng., 6, 6, 2013
124. Jorfi M., Skousen J.L., Weder C et al. Progress towards biocompatible intracortical microelectrodes for neural interfacing applications. J. Neural Eng., 12, 011001, 2014
125. Tsytsarev V., Taketani M., Schottler F. et al. A new planar multielectrode array: Recording from a rat auditory cortex. J. Neural Eng., 3, 293, 2006
126. Moshayedi P., Ng G., Kwok J.C. et al. The relationship between glial cell mechanosensitivity and foreign body reactions in the central nervous system. Biomaterial, 35, 3919–3925, 2014
127. Polikov V.S., Block M.L., Fellous J.M. et al. In vitro model of glial scarring around neuroelectrodes chronically implanted in the CNS. Biomaterials, 27, 5368–5376, 2006

128. Arulmoli J., Pathak M.M., McDonnell L.P. et al. Static stretch affects neural stem cell differentiation in an extracellular matrix-dependent manner. Sci. Rep., 5, 8499, 2015
129. Thongpang S., Richner T.J., Brodnick S.K. et al. A micro-electrocorticography platform and deployment strategies for chronic BCI applications. Clin. EEG Neurosci., 42, 259–265, 2011
130. Schendel A.A., Nonte M.W., Vokoun C. et al. The effect of micro-ECoG substrate footprint on the meningeal tissue response. J. Neural Eng., 11, 046011, 2014
131. Reddy C.G., Reddy, G.G., Kawasaki H. et al. Decoding movement-related cortical potentials from electrocorticography. Neurosurg. Focus, 27, E11, 2009
132. Schendel, A.A., Thongpang S., Brodnick S.K. et al. A cranial window imaging method for monitoring vascular growth around chronically implanted micro-ECoG devices. J. Neurosci. Methods, 218, 121–130, 2013
133. Williams J.C., Hippensteel J.A., Dilgen J. et al. Complex impedance spectroscopy for monitoring tissue responses to inserted neural implants. J. Neural Eng., 4, 410, 2007
134. Wang K., Bekar L.K., Furber K. et al. Vimentin-expressing proximal reactive astrocytes correlate with migration rather than proliferation following focal brain injury. Brain Res., 1024, 193–202, 2004
135. Schouenborg J., Garwicz M., Danielsen N. Reducing surface area while maintaining implant penetrating profile lowers the brain foreign body response to chronically implanted planar silicon microelectrode arrays. Brain Mach. Interfaces Implic. Sci. Clin. Pract. Soc., 194, 167, 2011
136. Jorfi M., Skousen J.L., Weder C. et al. Progress towards biocompatible intracortical microelectrodes for neural interfacing applications. J. Neural Eng., 12, 011001, 2014
137. Degenhart A.D, Eles J., Dum R. et al. Histological evaluation of a chronically-implanted electrocorticographic electrode grid in a non-human primate. J Neural Eng., 13(4):046019, 2016
138. Twardoch U.M. Integrity of ultramicro-stimulation electrodes determined from electrochemical measurements. J. Appl. Electrochem., 24, 835–857, 1994

139. Chestek C.A., Gilja V., Nuyujukian P. et al. Long-term stability of neural prosthetic control signals from silicon cortical arrays in rhesus macaque motor cortex. J. Neural Eng., 8, 045005, 2011
140. Kim D.H., Viventi, J., Amsden, J.J. et al. Dissolvable films of silk fibroin for ultrathin conformal bio-integrated electronics. Nat. Mater., 9, 511–517, 2010
141. Someya T., Kato Y., Sekitani T. et al. Conformable, flexible, large-area networks of pressure and thermal sensors with organic transistor active matrixes. Proc. Natl. Acad. Sci. USA, 102, 12321–12325, 2005
142. Fukushima M., Chao Z.C., Fujii N. Studying brain functions with mesoscopic measurements: advances in electyrocorticography for non-human primates. Cur. Opin. Neurobio., 32: 124-131, 2015
143. Mehring C., Nawrot M.P, de Oliveira S.C. et al. Comparing information about arm movement direction in single channels of local and epicorticalfield potentials from monkey and human motor cortex. J Physiol Paris, 98(4-6):498-506, 2005
144. Ball T., Nawrot M.P., Pistohl T. et al. Towards a brain-machine interface based on epicortical field potentials. 2004
145. Kotov J., Winter J.O., Clements I.P. et al. Nanomaterials for neural interfaces, Adv. Mater., 21, 3970-4004, 2009
146. Poole-Warren L., Lovell N., Baek S. et al. Development of bioactive conducting polymers for neural interfaces. Expert Rev. Med. Devices, 7, 35-49, 2010
147. Cogan S.F. Neural stimulation and recording electrodes. Ann. Rev. Biomed. Eng., 10, 275-309, 2008
148. Iijima S. Helical microtubules of graphitic carbon. Nature, 354, 56–58, 1991
149. Tsubokawa N. Preparation and properties of polymer-grafted carbon nanotubes and nanofibers. Polym J., 37, 637–655, 2005
150. Vaisman L., Wagner H.D., Marom G. The role of surfactants in dispersion of carbon nanotubes, Advances in Colloid and Interface Science, Volumes 128–130, Pages 37-46, 2006
151. Rahman M.J., Mieno T. Water-Dispersible Multiwalled Carbon Nanotubes Obtained from Citric-Acid-Assisted Oxygen Plasma Functionalization, Journal of Nanomaterials, 2014

152. Ru C.Q. Column buckling of multiwalled carbon nanotubes with interlayer radial displacements. Phys. Rev. B, 62, 10405-10408, 2000
153. Sekitani T., Noguchi Y., Hata K. et al. A Rubberlike Stretchable Active Matrix Using Elastic Conductors. Science, 1468-1472, 2008
154. Zhan Z., Lin R., Tran V. et al. Paper/Carbon Nanotube-Based Wearable Pressure Sensor for Physiological Signal Acquisition and Soft Robotic Skin ACS Applied Materials & Interfaces, 9 (43), 37921-37928, 2017
155. Vitale F., Summerson S.R., Aazhang B. et al. Neural Stimulation and Recording with Bidirectional, Soft Carbon Nanotube Fiber. ACS Nano, 9 (4), 4465-4474, 2015
156. Liu Z.F., Fang S., Moura A. et al. Hierarchically buckled sheath-core fibers for superelastic electronics, sensors, and muscles. Science, 400-404, 2015
157. Minev I.R., Musienko P., Hirsch A. et al. Electronic dura mater for long-term multimodal neural interfaces. Science, Vol. 347, Issue 6218, pp. 159-163,2015
158. Byrne M.T., Gun'ko Y.K. Recent Advances in Research on Carbon Nanotube–Polymer Composites. Adv. Mater., 22: 1672-1688, 2010
159. Bronikowski M.J., Willis P.A., Colbert D.T. et al. Gas-phase production of carbon single-walled nanotubes from carbon monoxide via the HiPco process: A parametric study. Journal of Vacuum Science & Technology A, 19:4, 1800-1805, 2001
160. Salvetat J.P., Kulik A.J., Bonard J.M. et al. Elastic Modulus of Ordered and Disordered Multiwalled Carbon Nanotubes. Adv. Mater., 11: 161-165, 1999
161. Walters D.A., Ericson L.M., M. Casavant J. Elastic strain of freely suspended single-wall carbon nanotube ropes. Applied Physics Letters, 74:25, 3803-3805, 1999
162. Cao Q., Hur S.H., Zhu Z.T. et al. Highly Bendable, Transparent Thin-Film Transistors That Use Carbon-Nanotube-Based Conductors and Semiconductors with Elastomeric Dielectrics. Adv. Mater., 18: 304-309, 2006
163. Schridde U., van Luijtelaar G. The role of the environment on the development of spike-wave discharges in two strains of rats. Physiol Behav., 16;84(3):379-86. 50, 2005

164. van Luijtelaar G., Sitnikova E., Luttjohann A. On the origin and suddenness of absences in genetic absence models. Clin EEG Neurosci., 42(2):83-97, 2011
165. Blumenfeld H. Cellular and network mechanisms of spike-wave seizures. Epilepsia, 46 Suppl 9:21-33. *, 2005
166. Coenen A.M., van Luijtelaar E. L. Genetic Animal Models for Absence Epilepsy: A Review of the WAG/Rij Strain of Rats. Behavior Genetics, Vol. 33, No. 6, 2003
167. Sutula T.P., Sackallares J.C., Miller J.Q., Dreifuss F.E. Intensive monitoring in refractory epilepsy. Neurology, 31: 243– 7, 1981
168. Dreifuss F.E. Role on intensive monitoring in classification. In: R Gumnit, ed. Intensive neurodiagnostic monitoring. New York: Raven Press, 13, 1987
169. Binnie C.D., Rowan A.J., Overweg J. et al. Telemetric EEG and video monitoring in epilepsy. Neurology, 31: 298– 303, 1981
170. Gotman J., Levtova V., Farine B. Graphic representation of the EEG during epileptic seizures. Electroencephalogr Clin Neurophysiol., 87: 206– 14, 1993
171. Gotman J., Marciani M.G. Electroencephalographic spiking activity, drug levels and seizure occurrence in epileptic patients. AnnNeurol., 17: 597– 603, 1985
172. Ebersole J.S. Ambulatory EEG: telemetered and cassette-recorded. In: R Gumnit, ed. Intensive neurodiagnostic monitoring. New York: Raven Press, 139– 55, 1987
173. Kaplan P.W., Lesser R.P. Non invasive EEG. In: E Wyllie, ed. The treatment of epilepsy: principles and practice. Baltimore: Williams & Wilkins. 976– 87, 1996
174. Moyanova S.G., Kortenska L.V., Mitreva R.G. et al. Multimodal assessment of neuroprotection applied to the use of MK-801 in the endothelin-1 model of transient focal brain ischemia. Brain Res., 1153, 58-67, 2007
175. Martinello K., Sciaccaluga M., Morace R. et al. Loss of constitutive functional γ-aminobutyric acid type A-B receptor crosstalk in layer 5 pyramidal neurons of human epileptic temporal cortex. Epilepsia, 59, 449-459, 2018
176. Morales P., Moyanova S., Pavone L. et al. Self-grafting carbon nanotubes on polymers for stretchable electronics. Europ. Phys. J. Plus., 113, 2018
177. Gottesmann C. Detecton of seven sleep-waking stages in the rat. Neurosci. Biobehav. Rev., 16, 31-38, 1992
178. Van Luijtelaar G., Coenen A.M.L. Two types of electrocortical paroxysms in an inbred strain of rats. Neurosci. Lett., 70, 393–397, 1986

179. Schallert T., Fleming S.M., Leasure J.L. et al. CNS plasticity and assessment of forelimb sensorimotor outcome in unilateral rat models of stroke, cortical ablation, parkinsonism and spinal cord injury. Neuropharmacol., 39, 777-787, 2000
180. Taube J.S., Schwartzkroin P.A. Mechanisms of long-term potentiation: EPSP/spike dissociation, intradendritic recordings, and glutamate sensitivity. J.Neurosci., 8, 1632-1644, 1998
181. Petroff O.A., Spencer D.D., Goncharova I,I. et al. A comparison of the power spectral density of scalp EEG and subjacent electrocorticograms. Clin. Neurophysiol., 127, 1108-1112, 2016
182. Schalk G., Leuthardt E.C. Brain-computer interfaces using electrocorticographic signals. IEEE Rev. Biomed. Eng., 4, 140-154, 2011
183. Robinson D.A. The electrical properties of metal microelectrodes. Proceed. IEEE, 56, 1065-1071, 1968
184. Kulik A., Kis A., Lukic B. et al. Mechanical Properties of Carbon Nanotubes., Fundamentals of Friction and Wear, 2007
185. Konerding W.S., Froriep U.P., Kal A. et al. New thin-film surface electrode array enables brain mapping with high spatial acuity in rodents. Sci. Rep., 8, 3825, 2018
186. Hollenberg B.A., Richards C.D., Richards R. et al. A MEMS fabricated flexible electrode array for recording surface field potentials. J.Neurosci. Meth., 153, 147-153, 2006
187. Henle C., Raab M., Cordeiro J.G. et al. First long term in vivo study on subdurally implanted micro-ECoG electrodes, manufactured with a novel laser technology. Biomed.Microdevices, 13, 59-68, 2011
188. Khodagholy D., Doublet T., Gurfinkel M. et al. Highly conformable conducting polymer electrodes for in vivo recordings. Adv. Mater., 23, H268–H272, 2011
189. Malarkey E.B, Parpura V. Applications of carbon nanotubes in neurobiology. Neurodegenerative Dis., 4, 292-299, 2007
190. Steriade M., Gloor. P., Llinás R.R. et al. Basic mechanisms of cerebral rhythmic activities, Electroenceph. Clin. Neurophysiol., 76, 1990, 481-508, 1990

191. Fukushima M., Saunders R.C., Mullarkey M. et al. An electrocorticographic electrode array for simultaneous recording from medial, lateral, and intrasulcal surface of the cortex in macaque monkeys. J.Neurosci. Meth., 233, 155–165, 2014
192. Viventi J. Flexible, foldable, actively multiplexed, high-density electrode array for mapping brain activity in vivo. Nat.Neurosci., 14, 1599-1605, 2011
193. Yanagisawa T., Hirata M., Saitoh Y. et al. Neural decoding using gyral and intrasulcal electrocorticograms. Neuroimage, 45, 1099-1106, 2008
194. Guggenmos D.J., Azin M., Barbay S. et al. Restoration of function after brain damage using a neural prosthesis. PNAS, 110, 21177-21182, 2013
195. Wang K., Fishman H.A., Dai H. et al. Neural stimulation with a carbon nanotube microelectrode array. Nano Lett., 6, 2043-2048, 2006
196. Lee W.S., Lee J.K., Lee S.A. et al. Complications and results of subdural grid electrode implantation in epilepsy surgery. Surg Neurol., 54(5):346–351, 2000
197. Hamer H.M., Morris H.H., Mascha E.J. et al. Complications of invasive video-EEG monitoring with subdural grid electrodes. Neurology, 58:97–103, 2002
198. Fong J.S., Alexopoulos A.V., Bingaman W.E. et al. Pathologic findings associated with invasive EEG monitoring for medically intractable epilepsy. Am J Clin Pathol., 2012
199. Fattahi P., Yang G., Kin G. et al. A Review of organic and inorganic biomaterials for neural interfaces. Adv. Mater., 26, 1846–1885, 2014
200. Bareket-Keren. L,. Hanein Y. Carbon nanotube-based multi electrode arrays for neuronal interfacing: progress and prospects. Front. Neural Circuits, 6,122, 2013
201. Meeren H.K.M., Pijn J.P.M., van Luijtelaar E.L.J.M. et al. Cortical focus drives widespread corticothalamic networks during spontaneous absence seizures in rats. The J. Neuroscience, 22, 1480-1495, 2002
202. Midzianovskaia I.S., Kuznetsova G.D., Coenen A.M.L. et al. Electrophysiological and pharmacological characteristics of two types of spike-wave discharges in WAG/Rij rats. Brain Res., 911, 62-70, 2011
203. Melnikova D.I., Khotimchenko Y.S., Magarlamov T.Y. Addressing the issue of tetrodotoxintargeting. Mar Drugs., 16, 2018
204. Herring B.E., Nicoll R.A. Long-Term Potentiation: From CaMKII to AMPA Receptor Trafficking. Annu. Rev. Physiol., 78, 351-365, 2016